PROTEIN COMPOSITION AND SUBCELLULAR LOCALIZATION OF THE *DE NOVO* LIPOGENIC METABOLON

APPROVED BY SUPERVISORY COMMITTEE

_____

JAY D. HORTON, M.D.

_____

RUSSELL A. DEBOSE-BOYD, Ph.D.

_____

DAVID W. RUSSELL, Ph.D.

_____

KOSAKU UYEDA, Ph.D.

DEDICATION

To Christie, Cole, Reid, Mom, and Dad

For your constant support and enthusiasm through my academic career

PROTEIN COMPOSITION AND SUBCELLULAR LOCALIZATION OF THE *DE NOVO* LIPOGENIC METABOLON

by

WILLIAM BENNION MCKEAN, JR.

DISSERTATION

Presented to the Faculty of the Graduate School of Biomedical Sciences

The University of Texas Southwestern Medical Center at Dallas

In Partial Fulfillment of the Requirements

For the Degree of

DOCTOR OF PHILOSOPHY

The University of Texas Southwestern Medical Center at Dallas

Dallas, Texas

May, 2016

ACKNOWLEDGEMENTS

Throughout my life I have been surrounded by people dedicated to promoting my happiness and success. My experiences during graduate school have proven no exception, and I would be remiss if I did not express gratitude to everyone involved.

First, I must thank my wife Christie for her love and commitment to our family and my education. She constantly creates an environment of encouragement and optimism. Her selflessness and determination are an inspiration to me, as is her dedication to our sons. Our small family brings me all the happiness in the world.

I am also deeply appreciative for my parents, Bill and Diane. Their care, support, wisdom, and sacrifice continue to shape my daily life. They have always been my heroes, and I strive every day to be more like them. In addition, I am lucky to have wonderful siblings – Jonathan, James, Anna, Stephen, Michael, and Kathryn. Their accomplishments and character are each an example to me.

I could not have hoped for a better research mentor than Dr. Jay Horton. His enthusiasm and curiosity for his work are contagious, and well reflected in all the laboratory members he trains. He has taught me the importance of thoroughness, clarity, and persistence in my laboratory experiments and data. I feel extremely fortunate for his guidance and preparation as I enter a career in scientific research. I have also been lucky to have worked so closely with Dr. Chai-Wan Kim. I admire his work ethic, novel scientific ideas, and careful planning – they are wonderful representations of the spirit of the department and our laboratory.

Several other members of our laboratory have been essential in my training. Dr. Young-Ah Moon has been a wonderful help in planning projects and interpreting results, and her insight regularly provided clarity during my thesis preparation. Also, Norma Anderson has been the model example of organization and efficiency, and harbored a work environment that helped streamline my experiments. In addition, Tuyet Dang was always willing to sacrifice her time and efforts to help me with questions or procedures.

I am also appreciative of Judy Sanchez and Katie Lim for their maintenance of laboratory mouse and rat colonies. Furthermore, my thanks to Lisa Beatty for her assistance with cell culture, Angela Carroll and Linda Donnelly for their in-house antibody preparation, and Dr. Karen Rothberg for helping me with immunocytochemistry and confocal microscopy.

Finally, I give my heartfelt appreciation to the remaining members of my thesis committee – Drs. Russell Debose-Boyd, David Russell, and Kosaku Uyeda – for their prompt and thorough feedback. Their critical review of my projects and dissertation were wonderful examples of professional collaboration and academic rigor.

PROTEIN COMPOSITION AND SUBCELLULAR LOCALIZATION OF THE *DE NOVO* LIPOGENIC METABOLON

WILLIAM BENNION MCKEAN, JR., Ph.D.

The University of Texas Southwestern Medical Center at Dallas, 2016

JAY D. HORTON, M.D.

Fatty acids are the major components of triglycerides, phospholipids, and sphingolipids. Production of palmitate, the most abundant saturated fatty acid, involves the stepwise actions of three enzymes: ATP citrate lyase, acetyl-CoA carboxylase, and fatty acid synthase. Canonically each enzyme catalyzes discrete reactions, and it is thought that they localize diffusely in cellular cytoplasm separate from one another. If true, transfer of metabolic intermediates must occur through passive diffusion from one lipogenic enzyme to another. Such a model proposes an extremely inefficient and potentially hazardous method of palmitate production.

We demonstrated that two related proteins – designated MIG12 and Spot 14 – modulate fatty acid synthesis and triglyceride production by regulating the polymerization and activity of acetyl-CoA

carboxylase. To better characterize the relationship between these three proteins, biochemical properties of purified recombinant MIG12, Spot 14, and MIG12:Spot 14 heterodimer were assayed in combination with acetyl-CoA carboxylase. We found that Spot 14 abrogates the ability of MIG12 to polymerize and activate acetyl-CoA carboxylase. Co-immunoprecipitation studies using Spot 14 in rat liver revealed Spot 14 exists in a complex with fatty acid synthase and acetyl-CoA carboxylase. MIG12 and Spot 14 co-immunoprecipitation also revealed that ATP citrate lyase was in association with the complex, suggesting that these proteins can function as scaffolds for the three enzymes required for palmitate synthesis.

Studies of the subcellular localization of these lipogenic proteins corroborated a functional interaction between these proteins. Confocal images of MIG12 and acetyl-CoA carboxylase in primary hepatocytes show filamentous structures that are immunofluorescent along junctions between the endoplasmic reticulum and mitochondria. Under high carbohydrate dietary conditions in which lipogenesis is stimulated, these structures expand to include fatty acid synthase, ATP citrate lyase, and Spot 14. They also co-localize around lipid droplets – storage organelles for excess triglycerides. Finally, the structural integrity of this lipogenic complex is shown to require microtubules. Blockade of microtubule formation inhibits proper formation of acetyl-CoA carboxylase structure and decreases total fatty acid synthesis in cells.

Combined, these findings support the existence of a functional metabolon complex which facilitates the efficient channeling of fatty acid synthesis intermediates through an enzyme cascade that results in the production of palmitate at functionally relevant locations within the cell.

TABLE OF CONTENTS

PRIOR PUBLICATIONS

Colbert, C. L., Kim, C.W., Moon, Y.A., Henry, L., Palnitkar, M., **McKean, W.B.**, Fitzgerald, K., Deisenhofer, J., Horton, J.D., and Kwon, H.J. Crystal structure of Spot 14, a modulator of fatty acid synthesis. *Proc. Natl. Acad. Sci. U. S. A.* **107,** 18820–18825 (2010)

FIGURES

TABLES

ABBREVIATIONS

ACC	Acetyl-CoA carboxylase isoform
ACL	ATP citrate lyase
AGPAT	1-acylglycerol-3-phosphate O-acyltransferase
AMPK	AMP-activated protein kinase
BiFC	Bimolecular Fluorescence Complementation
DG	Diglyceride
DGAT	Diglyceride acyltransferase
ELOVL	Elongation of very long chain fatty acids
ER	Endoplasmic reticulum
FAS	Fatty acid synthase
GPAT	Glycerol-3-phosphate acyltransferase
IEF	Isoelectric focusing
LD	Lipid droplet
MAM	Mitochondrial associated membrane
MAP	Microtubule associated protein
MIG12	Mid1-interacting G12-like protein
MT	Microtubule
PAP	Phosphatidic acid phosphatase
PCC	Pearson's correlation coefficient
PFK	Phosphofructokinase
SCD	Stearoyl-CoA desaturase
S14	Spot 14

THRSP	Thyroid hormone responsive protein
TG	Triglyceride

CHAPTER ONE: INTRODUCTION

Glucose is an essential carbohydrate that provides energy to cells through its breakdown during glycolysis, oxidation in the citric acid cycle, and respiration. Once cellular energy needs have been met, excess glucose is converted into triglycerides for long term storage. Overconsumption of carbohydrates causes the pathologic accumulation of triglycerides, which, in turn, can lead to obesity, diabetes, high blood pressure, heart disease, and strokes. According to the National Health and Nutrition Examination Survey (NHANES), over 30% of citizens of the United States are obese and at risk for its comorbidities.[1] This estimate increases to as much as 50% among certain ethnic groups. Fat buildup can also extend from the adipose tissue to the liver, a condition known as non-alcoholic fatty liver disease (NAFLD). Though initial stages are often benign, simple hepatic steatosis can progress to steatohepatitis, cirrhosis and hepatocellular carcinoma.[2] It is estimated that up to one-third of all adults in developed countries exhibit some stage of NAFLD.[3] In addition, the prevalence of NAFLD appears to be increasing in both adult and pediatric populations, particularly with the expansion of the Western-style diet.

De novo production of fatty acids and triglycerides occurs primarily in the liver. Glucose is transported into the hepatocyte by the GLUT2 protein – a low-affinity transmembrane receptor that becomes active in the presence of high concentrations of its ligand. Once in the cytosol, glucose is either converted to glycogen and stored, or is sequentially catabolized into pyruvate though glycolysis. Pyruvate, in turn, diffuses through the outer membrane of the mitochondria via voltage-gated ion channels, and through the inner membrane via the action of the multimeric mitochondria pyruvate carrier (MPC).[4] While in the mitochondrial matrix, pyruvate is processed though the tricarboxylic acid (TCA) cycle to generate reduced coenzymes for use during

oxidative phosphorylation. When sufficient ATP has been produced in the cisternae, however, oxidative phosphorylation halts. To compensate for the mitochondrial influx of pyruvate, citrate, an intermediate in the TCA cycle, is shuttled out of the matrix by the cotransporter tricarboxylate carrier.[5]

Cytosolic citrate is the starting point for *de novo* production of fatty acids in hepatocytes. The first enzyme in this cascade is ATP citrate lyase (ACL). It catalyzes the conversion of citrate to acetyl-CoA with cofactors coenzyme A and ATP, and releases oxaloacetate and ADP as byproducts.[6] The active ACL is a homotetramer, and each individual polypeptide consists of approximately 1100 amino acids.[7,8] Hepatic expression of ACL is primarily under the influence of the transcription factor sterol regulatory element-binding protein (SREBP) isoforms 1a and 1c.[9] Once expressed, protein activity is further regulated via the PI3K/Akt pathway. Three residues on ACL are phosphorylated and these post-translational modifications stabilize the active homotetramer form to increase activity.[10–12] Precise mechanisms through which this occurs have not been completely elucidated; however, one of the modifications, acetylation, has also been shown to positively regulate ACL in HEK 293T cells. Lin and colleagues[13] have shown that under high glucose conditions, ACL becomes acetylated on at least three residues. This increases both resistance to ubiquitination and production of intracellular phospholipids.

Acetyl-CoA carboxylase (ACC) is the second enzyme in the fatty acid biosynthetic pathway. ACC is the most highly regulated and first committed step in fatty acid synthesis. ACC is expressed primarily in highly lipogenic tissues such as liver and adipose.[14] In these tissues, ACC regulates the transfer of a carboxyl group to acetyl-CoA through the use of a biotin cofactor and ATP.[15] This produces the two-carbon building block malonyl-CoA. ACC itself is a ~2300 amino acids in length, and is divided into three functional domains. Because of its size,

ACC's full crystal structure has not been solved. However, several reports of individual domain crystal structures have provided valuable information about the mechanics of ACC function.[16–20] Initially, bicarbonate ions are coupled to ACC's biotin cofactor in the N-terminal biotin carboxylase (BC) domain. The biotin cofactor itself is anchored to ACC slightly downstream of this reaction site in the biotin carboxylase carrier protein (BCCP) domain. The biotin arm swings to the C-terminal end of ACC where bicarbonate is added to acetyl-CoA in the carboxyltransferase (CT) domain. Several factors influence this enzymatic activity. ACC, like ACL, is transcriptionally induced by SREBP-1c.[21] A glucose responsive transcription factor, carbohydrate response element-binding protein (ChREBP), also independently promotes ACC transcription.[22,23] In addition to transcriptional regulation, ACC activity is modified by post-translational modifications. AMP-activated protein kinase (AMPK) phosphorylates ACC at several locations and dramatically reduces its activity.[24,25] Finally, polymerization of ACC directly enhances activity increasing the formation of malonyl-CoA. At basal levels, ACC exists almost exclusively as an inactive dimer in solution. Upon stimulation, ACC forms higher-order oligomers (i.e. tetramers, octamers, etc.) that display an exponential increase in activity. Citrate can promote polymerization; however concentrations effective in eliciting significant polymerization are well above normal physiologic levels.[26,27] Also of note is the fact that ACC has two isoforms – ACC1 and ACC2.[28] Both have similar sequences and carry out the same reaction. ACC2, however, is more enriched in striated muscle and heart.[29] Moreover, ACC2 has been associated with the mitochondrial membrane and thought to produce malonyl-CoA to inhibit CPT1 – and thus beta-oxidation – by reducing fatty acid import into the mitochondria.[14]

Recently, we showed a small protein – Mid1-interacting G12-like protein (MIG12) – dramatically increases the polymerization and activity of ACC1, even in the absence of citrate.[30]

MIG12 was initially identified as a microtubule stabilizing protein during midline and neural tube formation in embryogenesis.[31,32] It was initially identified as a gene regulated by SREBPs in microarray experiments.[33] These microarrays identified genes that were upregulated in SREBP transgenic mice and downregulated in mice that lack active SREBPs as a result of deleting SCAP, a protein required for SREBP activation. In addition to SREBP, MIG12 is also transcriptionally regulated by ChREBP.[34] MIG12 has a ubiquitous tissue distribution, and exists in solution as a dimer.[30] MIG12 binds to ACC and is incorporated into its oligomers, thus facilitating the polymerization and enhancing the activity of ACC. MIG12 overexpression in livers of mice not only increases ACC activity but also total fatty acid synthesis and hepatic triglyceride content.[30]

Interestingly, MIG12 shows sequence homology with only one other protein – thyroid hormone responsive protein (THRSP), or Spot 14 (S14).[35] S14 was identified by comparing two-dimensional electrophoretic liver protein profiles between euthyroid and thyroidectomized rats.[36] These experiments indicated that S14 is strongly induced by the thyroid hormone T_3. Like MIG12 and ACC, S14 expression is enhanced by ChREBP and SREBP-1c.[23,33,37] Like MIG12 and ACC, S14 exists as a homodimer in solution.[38] Nonetheless, despite these similarities, and despite sharing a 32% identity with MIG12, S14 does not induce polymerization or activation of ACC.[35] S14 does, however, bind to MIG12 and form a heterodimer when the two are co-transfected in cell culture.[35] The formation of this heterodimer abrogates MIG12's effect on ACC, as overexpression of S14 in cultured cells decreases ACC polymer size and activity in the presence of MIG12. Similarly, siRNA knockdown of S14 in mouse liver promotes formation of higher-order ACC oligomers and increases the *in vitro* activity of partially purified ACC. S14 knockdown, however, *decreases* total fatty acid biosynthesis in mouse liver.

This result contradicts the effects of S14 on MIG12 and ACC, but supports the possibility that S14 interacts with additional proteins involved in hepatic lipogenesis.

The third and final enzyme in the conversion of citrate to palmitate is fatty acid synthase (FAS). Like ACC, FAS is extremely large and consists of several functional domains. Six domains, in fact, facilitate the sequential addition of seven malonyl-CoA units to an acetyl-CoA primer. This multi-step process, which requires the coenzyme NADPH, culminates in the formation of palmitate, an abundant 16-carbon saturated fatty acid.[39] The crystal structure of the mammalian homologue has been solved to a resolution of 3.2 Å, and suggests that active FAS exists as a head-to-head homodimer intertwined about the middle of its monomers.[40] Several post-translational modifications can disrupt the functional quaternary structure of FAS, including threonine and serine phosphorylation.[41,42] Though the exact kinase that facilitates this inactivation is unknown, AMPK has been tentatively linked as an intermediate in the process. While certain tyrosine phosphorylations have been promoted as stimulatory to FAS activity, these studies examine aberrant FAS expression in cancer models rather than normal physiologic states.[43,44] Preliminary reports suggest that acetylation may also inhibit active FAS formation.[45]

Following the production of palmitate by FAS, double bonds are introduced into the saturated 16:0 fatty acid carbon chain by stearoyl desaturases (SCDs), the most prominent of which is SCD1.[46] Palmitate can also be elongated two carbons through the activity of elongation of very long chain fatty acid 6 (ELOVL6).[47] The combination of these two enzyme classes produces a wide variety of saturated and monounsaturated fatty acids including stearate (18:0), palmitoleate (16:1) and oleate (18:1). For energy storage, these fatty acids are then conjugated to glycerol backbones through the sequential activity of acyltransferases and lipases. In the liver, glycerol-3-phosphate acyltransferase 1 (GPAT1), which is located on the

mitochondrial membrane, coordinates the binding of fatty acids to the sn-1 position on glycerol-3-phosphate to form lysophosphatidic acids.[48] 1-acylglycerol-3-phosphate O-acyltransferase (AGPAT) then promotes binding of a second fatty acid to the sn-2 position. Dephosphorylation by phosphatidic acid phosphatase (PAP) primes phosphatidic acids for conjugation to fatty acids at the sn-3 position. Subsequent acyltransferase activity by diglyceride acyltransferase (DGAT) transforms diglycerides into mature triglycerides.

Despite our current understanding of the complexity and regulation for each step of fatty acid biosynthesis, significant questions remain unanswered. For example, there is no data to suggest that ACL, ACC, and FAS interact in any functional manner. Indeed, using microscopy and subcellular fractionation, these three enzymes have been shown to exist loosely and independently in the cytoplasm. Such subcellular localizations suggest that the reaction product of each step must passively diffuse through the cell and find the next enzyme in the lipogenic cascade. This model is not only inefficient, but also potentially hazardous, as it would require extremely high and potentially toxic levels of metabolic intermediates to generate palmitate. For instance, in gastric carcinoma cell lines, increasing levels of citrate in culture medium leads to a proportionate increase in caspase signaling, as well as a significant decrease in cell viability.[49] Excessive uptake and abnormally high intracellular citrate, then, can induce apoptotic cascades. Also, disproportionate amounts of malonyl-CoA can promote cell death. In MCF7 cells, inhibition of FAS by C75 or cerulenin reduces clonigenicity by 70% and increases apoptosis in more than 85% of cells. When these same cells are also treated with TOFA, an inhibitor of ACC, blockade of malonyl-CoA synthesis decreases apoptosis to 50%.[50] One possible solution to this problem is that there is a physical association between ACL, ACC, and FAS to streamline palmitate production and prevent toxic accumulation of intermediates.

Another discrepancy in the cytosolic location of ACL, ACC, and FAS exists. Once palmitate has been produced, desaturation and elongation by SCD1 and ELOVL6 occur. However, neither of these enzymes localize to the cytoplasm, but are both integral proteins in the endoplasmic reticulum (ER).[51,52] The next enzyme in hepatic triglyceride synthesis, GPAT1, localizes to yet another organelle – the mitochondria. Studies by Gonzales-Baró and colleagues[53] show that radiolabeled recombinant GPAT1 expressed using *in vitro* transcription-translation incorporates directly into mitochondria purified from rat liver. Subcellular fractionation of liver cytosol using sucrose gradients confirms that the most active endogenous GPAT1 fraction is bound to the outer mitochondrial membrane. Moreover, subsequent enzymes in triglyceride synthesis are not associated with the mitochondria. Rather, AGPAT, PAP, and DGAT isoforms exist exclusively in the ER. Truly efficient triglyceride synthesis cannot occur if palmitate produced in the cytosol is metabolized only after passive diffusion between the ER and mitochondria. Therefore, a putative lipogenic complex of ACL, ACC, and FAS should associate at an interface between the ER and mitochondria.

Enzymatic complexes formed at specific subcellular locations to streamline glucose metabolism have been described previously. In 1987, Paul Srere at UT Southwestern found that instead of completely solubilizing mitochondrial structure, gentle disruption enhanced the coupled reaction rates of citrate synthase and malate dehydrogenase by more than 125%.[54] Srere proposed a model wherein particles bound to the inner leaflet of the mitochondria coordinated the activities of most TCA cycle enzymes. He termed this non-covalent quaternary aggregate a metabolon. Since then, other metabolons have been characterized. For example, investigators Kurganov and Lyubarev proposed a similar model of protein interactions could be extended to glycolytic enzymes.[55]

In addition to multiple enzymes, metabolons often have structural proteins that maintain integrity and appropriate orientation. For instance, sedimentation experiments have shown that the majority of glycolytic enzymes bind microtubule networks, and that this crosslinking increases rates of activity.[56,57] Indeed, sequential binding of purified phosphofructokinase (PFK) and aldolase to stable microtubules promotes the maintenance of active PFK conformers and production of fructose-1,6-bisphosphate.[58]

Given such precedent, my hypothesis was that enzymes and proteins involved in fatty acid biosynthesis associate to form a functional complex that streamlines palmitate, and ultimately triglyceride, production. To investigate this hypothesis I proposed the following three aims.

AIM 1. Identify physical interactions between ACC, FAS, ACL, MIG12, and S14 and determine their effects on individual enzymatic function. Preliminary studies have already indicated binding occurs between MIG12, S14, and ACC and has functional consequences on malonyl-CoA synthesis. Here, recombinant MIG12:S14 heterodimers were purified and combined *in vitro* with ACC. Biochemical assays showed S14 abrogates the ability of MIG12 to facilitate ACC polymerization and activity by sequestering monomers and preventing homodimer formation. These findings explained the variation of heterodimer levels and lipogenesis found in different species. Studies using fusion proteins also proved that, in addition to ACC, S14 binds FAS in hepatocytes. Similarly, co-immunoprecipitation of ACL by recombinant S14 and MIG12 was shown following transient expression in CHO-K1 cells. By extension, knockdown of MIG12 or S14 influences the ability of purified recombinant ACL to produce acetyl-CoA. All of these functional interactions will be linked to a multimeric complex

common to ACC, FAS, ACL, MIG12 and S14 using 2-dimensional gel electrophoresis of native liver proteins.

AIM 2. Pinpoint the subcellular location of any interacting lipogenic proteins and establish whether the ER or mitochondria are involved. Using primary rat hepatocytes that are responsive to insulin and carbohydrate signaling, formation of filamentous aggregates immunoresponsive to both ACC and MIG12 were visualized using confocal microscopy. These structures co-localize with markers for both the ER and mitochondria, and are recruited to specialized junctions between the two. Normal physiologic responsiveness to AMPK and ChREBP is shown by disrupting ACC filaments with AICAR and low glucose concentrations. By culturing with high concentrations of glucose, insulin, and T_3, endogenous expression patterns of ACC, as well as FAS and ACL, expand to incorporate the majority of ER structures within hepatocytes. After prolonged incubation, co-localization of these three lipogenic enzymes about the ER extends to surround lipid droplets formed to store excess triglycerides.

AIM 3. Evaluate whether the cytoskeleton helps maintain integrity and function of this putative lipogenic metabolon. Specifically, I determine whether microtubules have a positive or negative effect on *de novo* production of palmitate from citrate. Clear images of microtubules overlapping ACC, FAS, and ACL structures along the ER are shown in primary hepatocytes. Experiments that disrupt these microtubules using nocodazole, also demonstrate that ACC structure becomes similarly compromised. Furthermore, by incubating native liver proteins with stable populations of microtubules, physical binding between the two is shown. Finally, *de novo* fatty acid synthesis is inhibited by blocking microtubule polymerization with nocodazole in hepatocytes.

Thus, subcellular co-localizations and physical interactions between ACC, MIG12, S14, FAS, ACL, and microtubules are demonstrated. This complex, or lipogenic metabolon, provides for the first time a functional niche wherein palmitate can be efficiently produced and quickly transferred to desaturases, elongases, and acyltransferases for packaging in triglycerides.

CHAPTER TWO: NOVEL INTERACTIONS OF MIG12 AND S14 WITH ACC

The model of a heterogeneous complex that coordinates the activity of multiple lipogenic enzymes has not been shown previously. However, simpler homogenous systems are essential for fatty acid synthesis. For instance, ACL, ACC, and FAS must each self-associate to form an enzymatic oligomer in order to be active. These oligomers can bind transiently with other modulatory proteins such as kinases, phosphatases, and acetyl transferases. Nonetheless, few permanent interactions of ACL, ACC, and FAS with cognate binding partners have been described. In fact, the only protein that has been thoroughly shown to complex with a lipogenic enzyme is MIG12. As previously described, MIG12 binds to ACC and induces its polymerization and MIG12 is physically incorporated into the active ACC polymer remaining associated with it during maximal catalytic activity.[30] Along with binding between MIG12 and ACC, additional proteins modulate MIG12's effect on ACC's activity. For example, MIG12's effect on ACC polymerization and activity can be abrogated by the thyroid hormone responsive protein S14.[35] Specifically, S14 binds to and can form a heterodimer with MIG12 *in vivo*, which ameliorate MIG12's affinity for ACC. Titrating increasing amounts of S14 causes a proportional decrease in endogenous ACC polymerization and activity when co-transfected with MIG12 in CHO-K1 cells. Similarly, when S14 is knocked down in mouse livers, there is increased ACC polymerization and activity. Further investigation, then, of biochemical interactions between MIG12, S14, and ACC will further our understanding of protein-protein interactions in fatty acid biosynthesis and, by extension, the possibility of the existence of a lipogenic metabolon.

Acetyl-CoA Carboxylase Central Unknown Deletion Mutants

Immunoprecipitation studies using MIG12 and deletion mutants of ACC1 have suggested that the binding site of MIG12 is likely within the central unknown (CU) domain of ACC1 (**unpublished observations**). Also, the stoichiometric ratio for this interaction has been estimated to be 1:1.[30] To further define this interaction, I prepared baculovirus constructs expressing two forms of His-tagged ACC1: full-length wild-type ACC1 and a deletion mutant lacking the CU domain (Δ900-1000). Both recombinant proteins were expressed in insect Sf9 cells and purified using immobilized Ni-NTA metal affinity chromatography (IMAC) **[Figure 2-1a].** Equal volumes of the purified full-length ACC1 and the Δ900-1000 mutant were separated using SDS-PAGE, and immunoblot analysis was performed to determine the relative concentration of non-degraded product for each. Using the Odyssey Infrared Imaging System to quantitate protein band intensity, I determined that the concentration of the Δ900-1000 mutant was exactly 25 percent of the concentration of full-length ACC1 **[Figure 2-1b].**

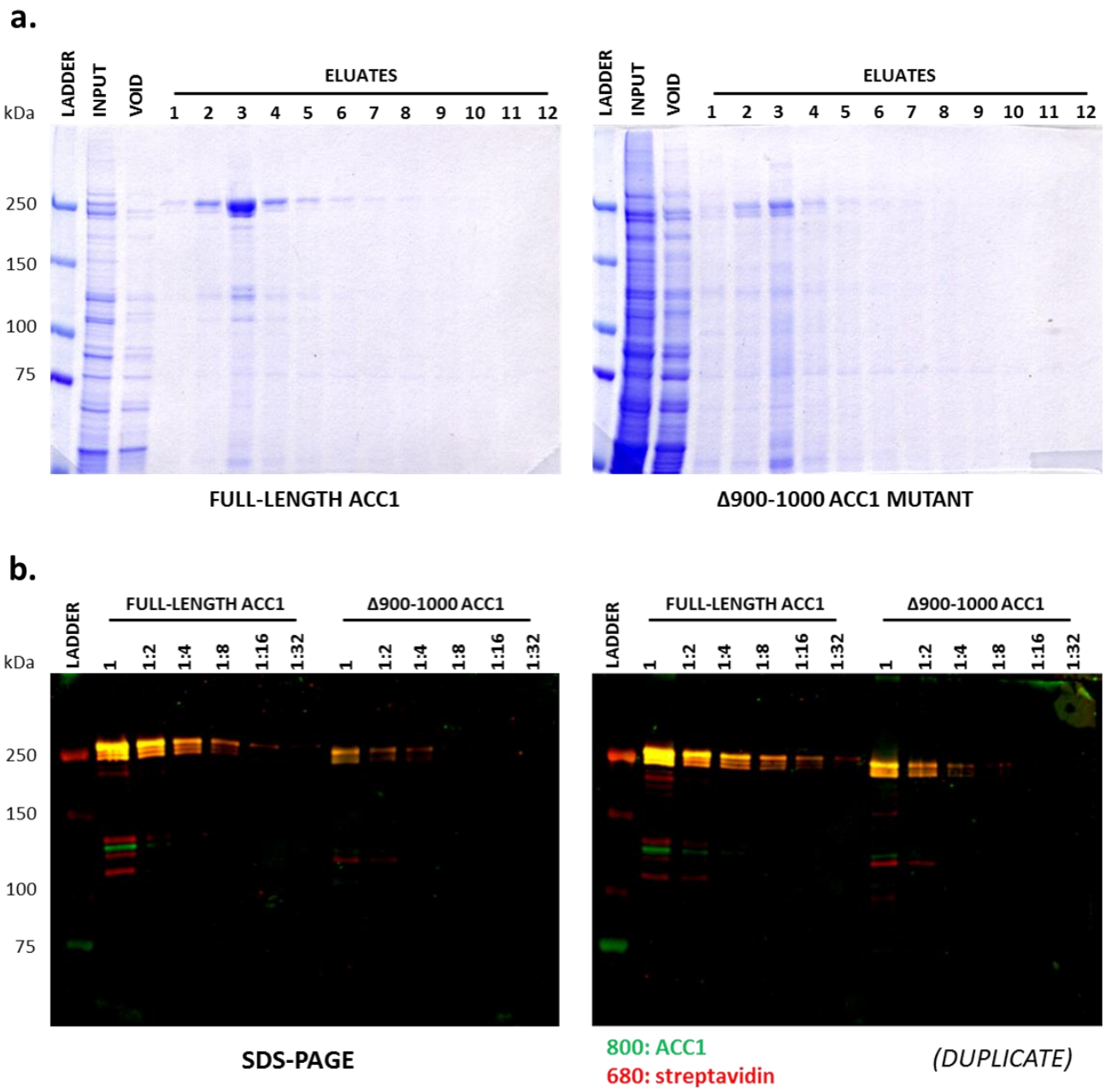

FIGURE 2-1. **Purification and quantitation of recombinant full-length and Δ900-1000 ACC1.**
(A) Equal volumes of *sf-9* clarified cytosol (INPUT), Ni-NTA column flow through (VOID), and consecutive Ni-NTA eluates for both forms of ACC1 were loaded on 5.5% polyacrylamide gels and separated by SDS-PAGE. Gels were stained with Imperial Protein Stain and visualized by washing in distilled water. *(B)* Equal volumes of purified recombinant full-length ACC1 and the Δ900-1000 mutant were serially diluted, denatured, and separated using SDS-PAGE on 5.5% polyacrylamide gels. Antibodies against ACC1 (green) or streptavidin (red) were used to detect the presence of purified protein. Intensity of each band was determined with Odyssey Imaging Software and averaged over all dilutions.

To test the effect of MIG12 on ACC lacking the CU domain, purified recombinant MIG12 was combined with wild-type ACC1 or the Δ900-1000 mutant and incubated under activating conditions. As expected, MIG12 induced significant polymerization of full-length ACC1. Furthermore, the Δ900-1000 mutant showed complete polymerization on BN-PAGE, even in the absence of MIG12 protein **[Figure 2-2a]**. This level of polymerization, however, does not correlate with *in vitro* activity rates of the Δ900-1000 mutant. Indeed, while ACC1 activity proportionally increased when incubated with MIG12 and/or increasing amounts of citrate, Δ900-1000 ACC1 showed absolutely no activity under any conditions **[Figure 2-2b]**. These data suggest that the higher order oligomers formed by the Δ900-1000 mutant are actually abnormal protein aggregates incapable of normal enzymatic function. More importantly, however, it validates the necessity of the CU domain for proper folding and function of ACC activity.

a.

	FULL-LENGTH ACC1						Δ900-1000 ACC1					
citrate (mM)	0			10			0			10		
MIG12 (μg)	0	1	5	0	1	5	0	1	5	0	1	5
LANE	1	2	3	4	5	6	7	8	9	10	11	12

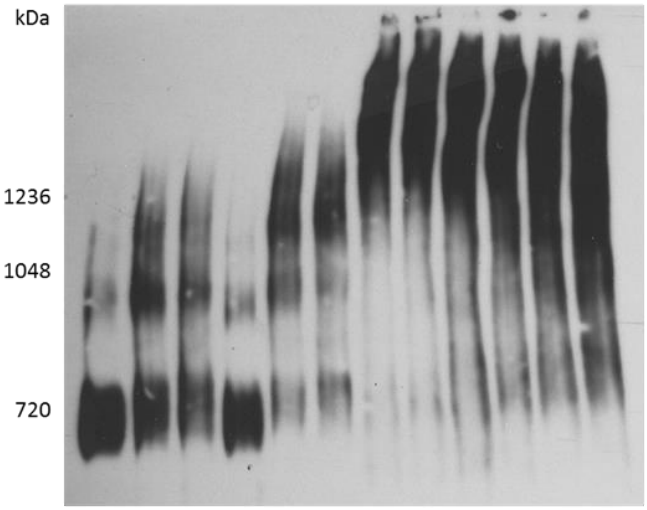

2°: α-ACC1
BN-PAGE

b.

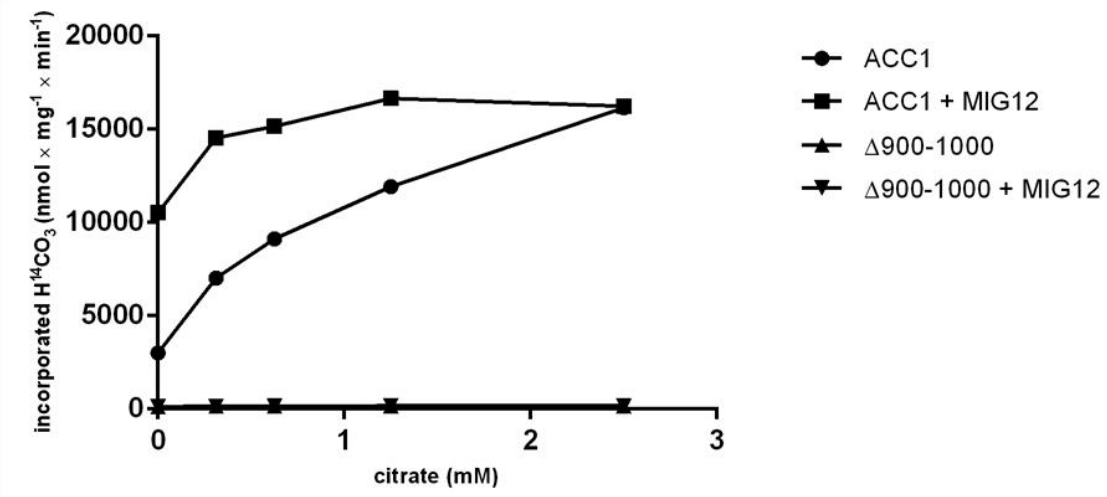

FIGURE 2-2. Effect of MIG12 on the polymerization and activity of full-length and Δ900-1000 ACC1.

(A) Purified recombinant full-length or Δ900-1000 ACC1 (6 μg) was incubated at 37 °C for 15 minutes with increasing amounts of purified recombinant MIG12 in the presence or absence of 10 mM citrate. Samples were then separated using BN-PAGE and analyzed using immunoblots against ACC1. *(B)* Purified recombinant full-length or Δ900-1000 ACC1 (0.5 μg) was incubated with 2 μg of MIG12 or BSA in the presence of increasing amounts of citrate, and incorporation of $H^{14}CO_3$ was measured as described in *Methods*. Each data point represents the mean of three separate measurements, with error reported as ±SEM.

Interspecies and Tissue Variability of MIG12 Function

Physiologic induction of ACC polymerization not only requires full-length protein but homodimeric MIG12 as well. Indeed, maximal induction of ACC activity and fatty acid biosynthesis are dependent upon total levels of MIG12. To investigate whether a loss of MIG12 decreases ACC activity and total fatty acid biosynthesis *in vivo*, mice possessing a germline deletion of *Mig12* were generated. Immunoblot analysis confirms a complete absence of MIG12 protein in knockout mouse liver, even when fasted or refed on a high carbohydrate/fat-free diet **[Figure 2-3a]**. The germline deletion of MIG12 has no effects on the growth and development. Unexpectedly, the deletion of MIG12 also had no effect on either the polymerization or activity of ACC in mouse liver **[Figure 2-3b,c]**. By extension, hepatic rates of fatty acid biosynthesis and total liver triglycerides remain unchanged in MIG12 KO mice when compared to wild-type mice **[Figure 2-3d]**.

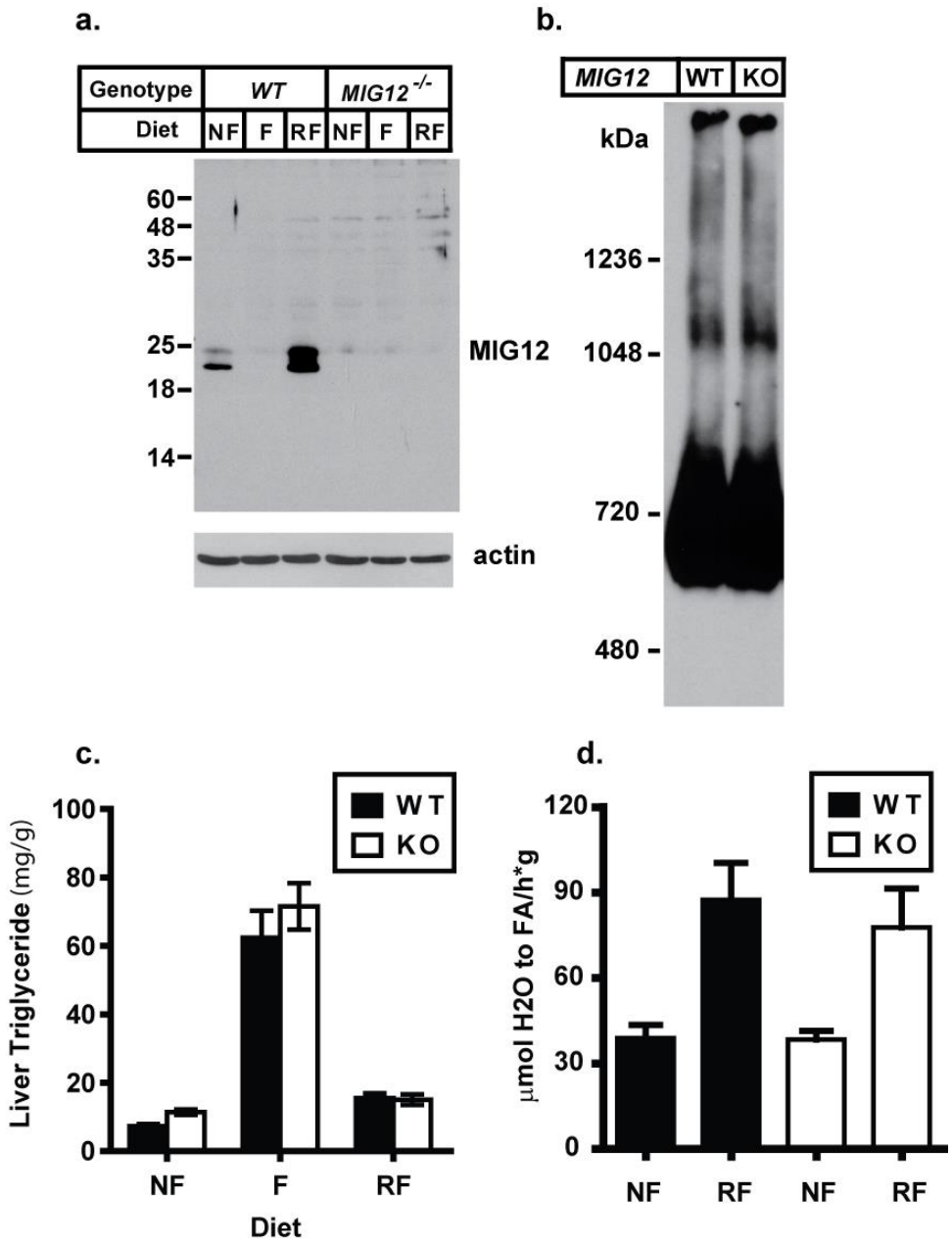

FIGURE 2-3. ***Mig12*** **germ-line knockout mice show no variation in hepatic ACC1 polymerization, fatty acid synthesis rates, or triglyceride production.**

(A) Equal amounts of total protein between the livers of fasted (F), *ad libitum* CHOW fed (NF), or FFD refed (RF) C57BL/6 wild-type or *Mig12*$^{-/-}$ mice were separated using SDS-PAGE. Immunoblots against MIG12 were prepared following protein transfer to nitrocellulose membranes. *(B)* MIG12 immunoblot of mouse liver cytosol from C57BL/6 wild-type and *Mig12*$^{-/-}$ mice separated using BN-PAGE. *(C)* Total liver triglycerides in various dietary states of C57BL/6 wild-type and *Mig12*$^{-/-}$ mice. *(D)* Hepatic fatty acid synthesis rates as measured by $^{3}H_2O$ incorporation into newly formed fatty acids in C57BL/6 wild-type and *Mig12*$^{-/-}$ mice. *Ad libitum* CHOW fed mice and fasted and FFD refed mice are represented.

These findings are different than those previous reports by Aipoalani and colleagues[59] who showed knockdown of MIG12 in rat primary hepatocytes reduces *de novo* fatty acid biosynthesis and triglyceride production. To further investigate this discrepancy, MIG12 siRNA was transfected into rat primary hepatocytes. Under these conditions, fatty acid biosynthesis is indeed significantly attenuated following MIG12 knockdown **[Figure 2-4c]**. In addition, total ACC polymerization is reduced in rat primary hepatocytes treated with MIG12 siRNA, suggesting that ACC activity levels are also decreased **[Figure 2-4b]**. Importantly, knockdown of MIG12 has no effect on the protein levels of ACC or other lipogenic enzymes **[Figure 2-4a]**.

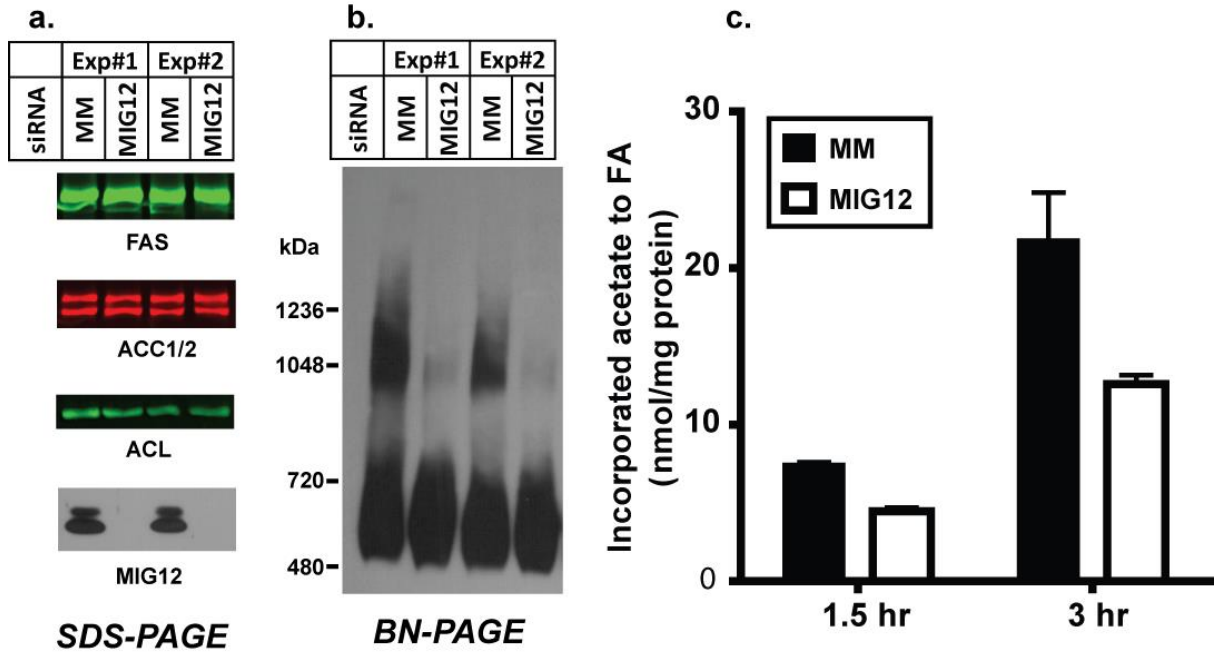

Figure 2-4. Knockdown of MIG12 using siRNA in rat primary hepatocytes reduces ACC polymerization and fatty acid synthesis.
Rat primary hepatocytes were transfected with mismatch (MM) or MIG12 siRNA and incubated for 45 hours as described in *Methods.* *(A)* Cell lysates (20 μg) from siRNA treated rat primary hepatocytes was separated using SDS-PAGE on 4-15% polyacrylamide gels and analyzed using immunoblots against FAS, streptavidin, ACL, and MIG12. *(B)* Non-denatured cell lysates (30 μg) of siRNA treated rat primary hepatocytes were separated using BN-PAGE with 3.5-10% polyacrylamide gradient gels and stained with rabbit polyclonal antibodies against ACC1. *(C)* Fatty acid synthesis in siRNA treated rat primary hepatocytes was measured using ^{14}C-acetate incorporation. Incubation with ^{14}C-acetate was performed in hepatocyte cultures for 1 hour and 45 minutes at 37 °C and 5% CO_2.

It appears that MIG12 has little influence on ACC in mouse liver, while significantly promoting its activity in rat hepatocytes. Interestingly, as mentioned previously, knockdown of S14 in mouse livers increases ACC polymerization and activity.[35] This effect could presumably result from decreasing the amount of S14 available for heterodimer formation and thereby increasing the total proportion of MIG12 that exists as a homodimer. To investigate whether MIG12:S14 heterodimer formation might account for the contradictory effects of MIG12 reduction in mice and rats, total liver protein from both species was separated using BN-PAGE. Immunoblot analysis of MIG12 and S14 confirms that a significant difference in MIG12:S14 heterodimer levels exist between rat and mouse tissues. Indeed, while approximately half of rat MIG12 protein is homodimeric **[Figure 2-5a, lane R]**, essentially all of mouse MIG12 exists as a heterodimer with S14 **[Figure 2-5a, lane M]**. S14 appears primarily homodimeric in both mouse and rat liver tissues **[Figure 2-5b, lanes R and M]**. To further investigate this finding, equal amounts of mouse and rat liver cytosol were separated using SDS-PAGE, and total hepatic protein levels of MIG12 and S14 compared between species. Despite equal levels of MIG12 in mouse and rat liver **[Figure 2-5a, lanes R and M]**, S14 protein levels are approximately 10-fold higher in mice than rats **[Figure 2-5b, lanes R and M]**. These protein ratios permit for a stable population of MIG12 homodimer in rats, while pushing the majority of the equilibrium toward MIG12:S14 heterodimer formation in mice. Furthermore, these data reinforce previous findings in knockout mice that show that germ-line deletion of *Spot 14* causes a significant increase in hepatic lipogenesis rates.[60] In this model, the absence of S14 protein in the liver frees MIG12 from its heterodimeric form and promotes ACC polymerization and activity.

MIG12, S14, and MIG12:S14 heterodimer levels were also investigated in other mammalian species. Liver tissue cytosol from vervet monkeys and baboons were separated

using SDS-PAGE and then analyzed using MIG12 and S14 immunoblots. Vervet monkey samples were taken from animals fed *ad libitum* on a CHOW diet or a 0.2% cholesterol diet. Baboon samples were taken from animals that were fasted or fed *ad libitum* on a CHOW diet. While data from vervet monkeys is largely uninformative **[Figure 2-5a,b, lanes V1 and V2]**, data from baboons indicates that total S14 levels and MIG12:S14 oligomer formation is increased under fasting conditions **[Figure 2-5b, lanes B1 and B2]**. MIG12, however, maintains normal insulin responsiveness and total protein levels decrease when fasted **[Figure 2-5a, lanes B1 and B2]**. These results provide yet an additional species-specific method for MIG12 regulation, and highlight the complications of comparing fatty acid synthesis between model species.

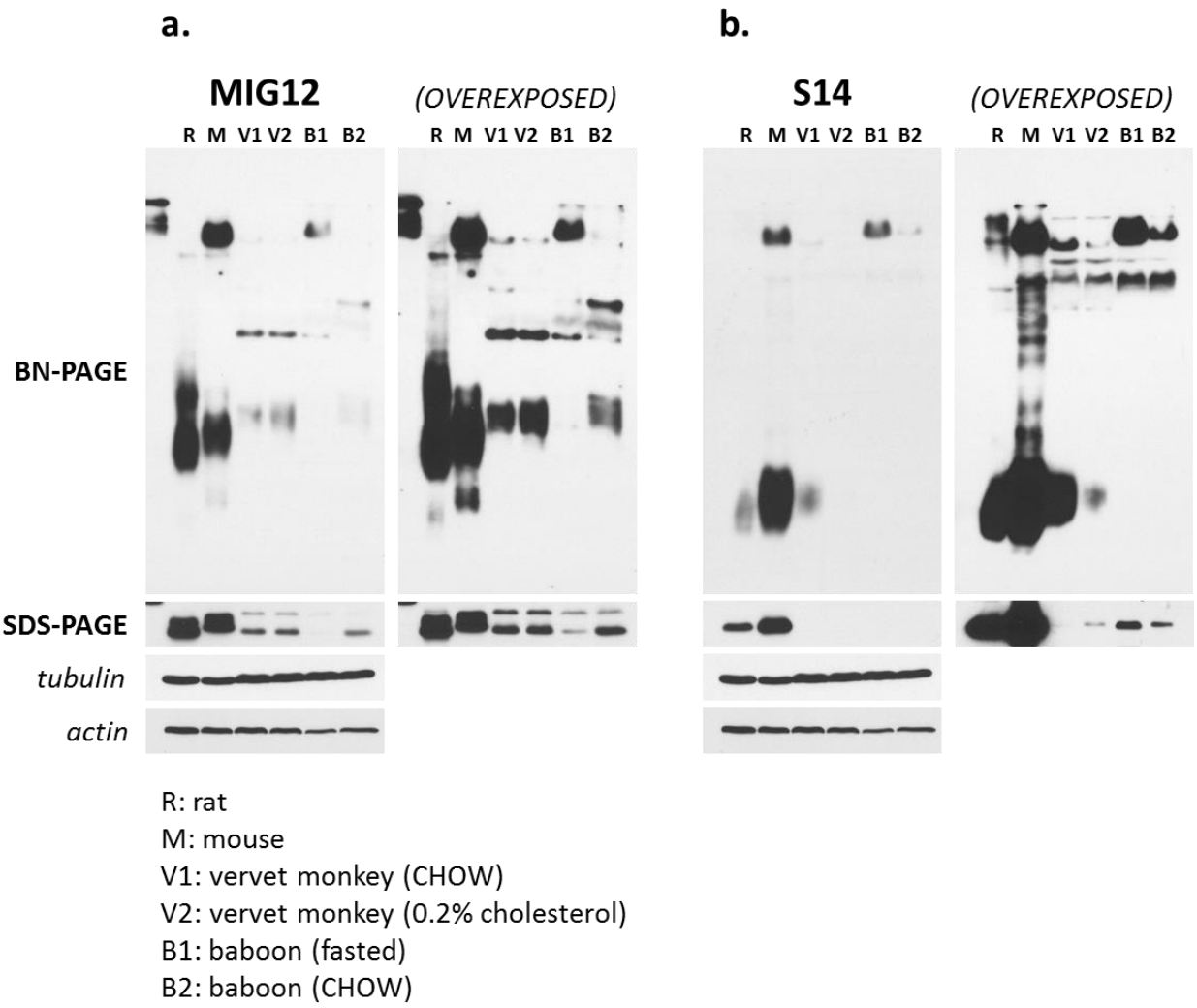

Figure 2-5. Protein levels and polymerization status of MIG12 and S14 in rat, mouse, vervet monkey, and baboon liver tissue.
(A) MIG12 immunoblot of rat, mouse, vervet monkey, and baboon liver cytosol separated using BN-PAGE (30 μg) with 14% polyacrylamide gels and SDS-PAGE (20 μg) with 4-15% polyacrylamide gradient gels. Rats and mice were fasted for 12 hours and refed on a FFD diet for 24 hours, while vervet monkeys and baboons were fed as indicated. Film was exposed to immunoblots for 1 second prior to development, or overexposed for 1 minute. *(B)* S14 immunoblots of experiments described in *(A)*. Membranes were not stripped for these exposures; rather, fresh SDS-PAGE and BN-PAGE experiments were performed using the same samples.

Because of these interspecies variations, I confirmed that the mouse was a valid species to model pathology of lipogenesis in humans. To do this, ACC1 polymerization was tested in the presence of human and mouse homologues of recombinant MIG12 and S14. Equal amounts of constructs expressing hMIG12, mMIG12, hS14, or mS14 were transiently transfected singly or together in CHO-K1 cells. Constructs expressing ACC1 were also transfected alone or with the aforementioned homologues. Non-denatured cell lysates were then separated using BN-PAGE, and the effect of MIG12 and S14 homologues on heterodimer formation and exogenous ACC1 polymerization determined. Reassuringly, no visible difference in MIG12:S14 heterodimer formation exists between mouse and human protein **[Figure 2-6, lanes 6 and 7]**. Interspecies results are also similar between MIG12's ability and S14's inability to induce ACC1 polymerization **[Figure 2-6, lanes 9-12]**. ACC1 polymerization in the presence of heterodimer, however, appears significantly increased when compared to MIG12 alone **[Figure 2-6, lanes 13 and 14]**. This is likely due to an overall increase in hMIG12 or mMIG12 construct expression when co-transfected with S14 homologues and ACC1. Indeed, protein levels for both MIG12 and S14 are increased when analyzed with BN-PAGE, and MIG12 homodimers are still abundantly present despite MIG12:S14 heterodimer formation **[Figure 2-6, lanes 6 and 7]**.

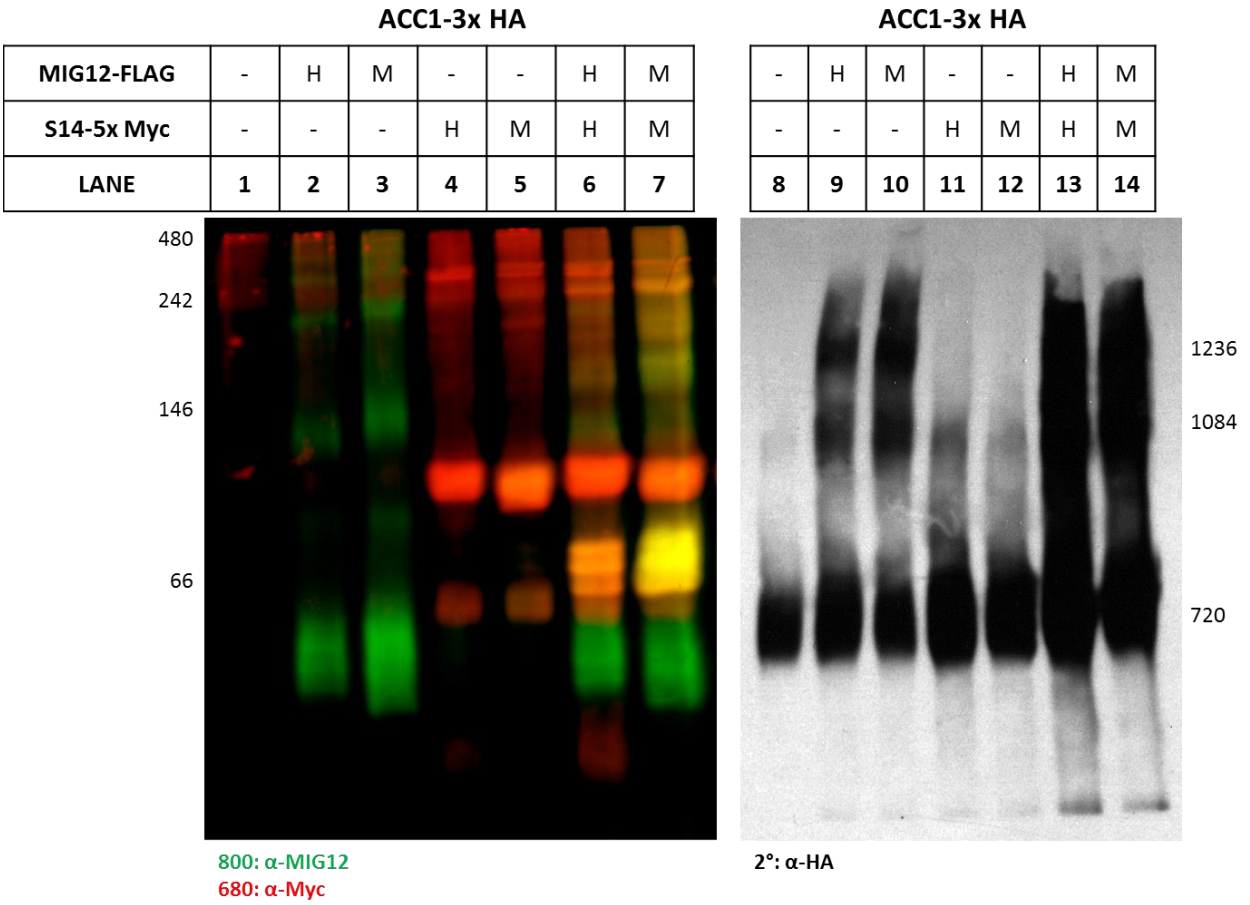

Figure 2-6. Human and mouse homologues of MIG12 and S14 show no difference between heterodimer formation and effects on ACC1 polymerization.
CHO-K1 cells were co-transfected with constructs expressing ACC1-3x HA (1 μg) alone or in combination with constructs expressing human MIG12-FLAG (hMIG12, 0.5 μg), mouse MIG12-FLAG (mMIG12, 0.5 μg), human S14-5x Myc (hS14, 0.5 μg), and/or mouse S14-5x Myc (mS14, 0.5 μg). CHO-K1 cells were cultured for 24 hours and cell cytosol collected after lysis and centrifugation. Equal amounts of total protein (40 μg) were separated using BN-PAGE with 14% polyacrylamide gels for MIG12 and S14 analysis and 3.5-10% polyacrylamide gradient gels for ACC1 analysis. Immunoblots were performed with polyclonal antibodies against MIG12 and HA, or with monoclonal antibodies against Myc. Note the presence of epitope tags shifts the molecular weight of S14 homodimer higher than MIG12 homodimer. MIG12:S14 heterodimer still lies intermediate between these two species.

To confirm whether the formation of MIG12:S14 heterodimer *in vivo* could account for the lack of phenotype in *Mig12* knockout livers, various tissues from *Mig12* knockout mice were harvested and assayed for rates of fatty acid synthesis as measured by tritiated water. While S14 is found mostly in lipogenic organs like the liver, adipose tissue, and mammary glands, MIG12 is expressed more ubiquitously in all tissues **[Figure 2-7a]**. [61,62] Therefore, *Mig12* deletion should have a more pronounced effect in tissues lacking S14 and thus the MIG12:S14 heterodimer. In lung, which has a very high ratio of MIG12 to S14 protein, heterodimer formation is entirely absent **[Figure 2-7b]**. This is also reflected by enhanced ACC1 polymerization. In wild-type and *Mig12* knockout mouse liver tissue, ACC1 polymerization is absent. In wild-type mouse lung tissue, however, polymerization of ACC1 is present. Furthermore, knockout of MIG12 protein eliminates ACC1 polymerization in the lung **[Figure 2-7c]**. Consistent with these data, organs like the lung and ovaries show a significant decrease in total fatty acid synthesis in *Mig12* knockout mice when compared to wild-type controls **[Figure 2-7d]**. Cholesterol synthesis, however, remains unchanged through all tissues regardless of genotype.

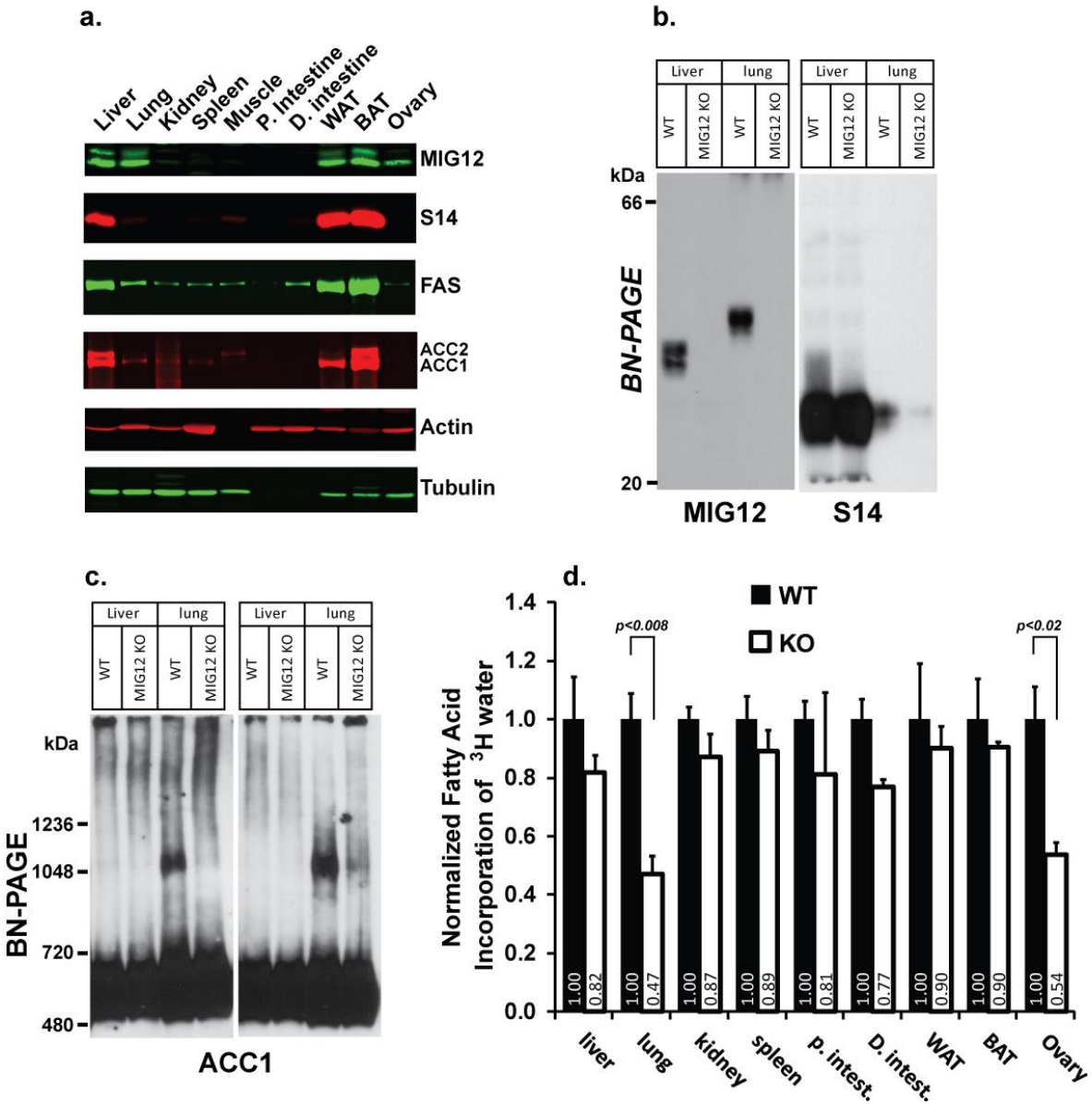

Figure 2-7. Effect of Mig12 knockout on ACC1 polymerization and fatty acid synthesis in various mouse tissues.

Female C57BL/6 mice (wild-type or *Mig12* knockout) were fasted for 12 hours and refed on a high carbohydrate/fat-free diet for one week. *(A)* Immunoblots of pooled cytosolic protein (30 μg) from various tissues in wild-type mice were performed after separation using SDS-PAGE. Rabbit polyclonal antibodies against MIG12, S14, and FAS, monoclonal antibodies against tubulin and actin, and streptavidin were used. *(B)* BN-PAGE separation of wild-type and *Mig12* knockout liver and lung tissue (30 μg) using 14% polyacrylamide gels. Immunoblots were generated using rabbit polyclonal MIG12 and S14 antibodies. *(C)* BN-PAGE separation of samples prepared in *(B)* using 3.5-10% polyacrylamide gradient gels and rabbit polyclonal antibodies to detect polymerization. *(D) In vivo* fatty acid synthesis rates were determined from various tissues in wild-type and *Mig12* knockout mice using incorporation of ^3H_2O.

Recombinant MIG12:S14 Heterodimer

The above results suggested that heterodimer formation of MIG12 and S14 is important for physiologic maintenance of ACC activity and fatty acid biosynthesis. To confirm that MIG12:S14 heterodimerization is not an artifact induced by cell lysis or tissue homogenization, constructs for use in bimolecular fluorescence complementation (BiFC) were prepared. In BiFC, proteins are co-expressed with either the N-terminal (VN) or C-terminal (VC) half of the YFP Venus. If the proteins are indeed binding partners, the Venus halves fuse upon close proximity and emit a fluorescent signal. Co-transfection of separate MIG12 constructs fused to separate halves of Venus induces fluorescence, indicating that MIG12 homodimer is actively formed in cells **[Figure 2-8a]**. Similar results are seen for S14 homodimer formation **[Figure 2-8b]**. Furthermore, when MIG12-VN and S14-VC (or alternatively MIG12-VC and S14-VN) are co-expressed in CHO-K1 cells, Venus signal is strongly emitted **[Figure 2-8c,d]**. These results support the conclusion that MIG12 and S14 form a heterodimer under normal physiologic conditions.

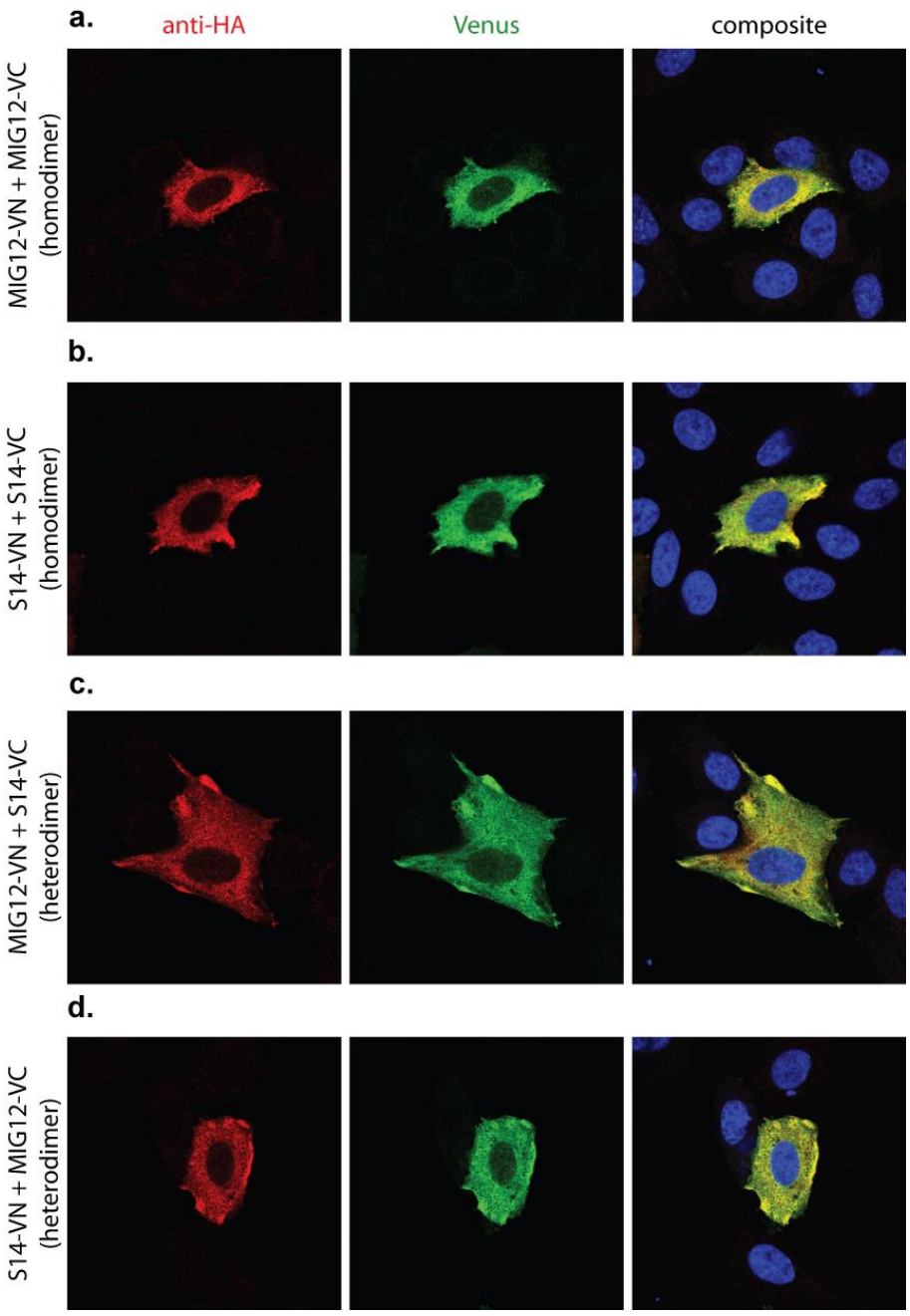

Figure 2-8. Bimolecular Fluorescence Complementation (BiFC) of MIG12 and S14 constructs.

Constructs expressing MIG12-VN155, MIG12-VC155, S14-VN155, and/or S14-VC155 (0.5 µg each) were co-transfected into CHO-K1 cells. Fusion proteins produced from VN155 constructs were detected using anti-HA mouse primary and Alexa Fluor 568 secondary antibodies (red). Homodimer and heterodimer formations are visible as a reconstituted Venus signal (green). Overlap between signals is shown in yellow. *(A)* Formation of MIG12 homodimer using MIG12-VN and MIG12-VC transfected constructs. *(B)* Formation of S14 homodimer using S14-VN and S14-VC transfected constructs. *(C-D)* Formation of MIG12:S14 heterodimer using either MIG12-VN and S14-VC *(C)* or S14-VN and MIG12-VC *(D)* transfected constructs.

To further investigate the effect of MIG12:S14 heterodimers on ACC polymerization and activity, recombinant MIG12:S14 heterodimer was produced and purified from insect *sf-9* cells. FLAG-tagged MIG12 protein and His-tagged S14 protein were co-expressed and subjected to sequential affinity chromatography. More specifically, insect cell lysates expressing both proteins were treated first with Ni-NTA resin to purify S14 homodimers and MIG12:S14 heterodimers. Eluates from these columns were then incubated with anti-FLAG M2 affinity gel to isolate only the heterodimeric species. Affinity tags were cleaved with thrombin and removed following purification, and the MIG12:S14 heterodimer compared to recombinant MIG12 and S14 homodimers using SDS-PAGE and BN-PAGE. Quantification of protein bands following SDS-PAGE and coomassie staining suggested that MIG12 and S14 exist in a 1:1 stoichiometric ratio when bound together prior to purification. Coomassie staining also indicated that purified recombinant MIG12:S14 heterodimers, MIG12 homodimers, and S14 homodimers were free of any contaminating protein species **[Figure 2-9a]**. Immunoblot analysis of MIG12 and S14 following separation using BN-PAGE indicated the size of MIG12:S14 heterodimer is consistent with a species intermediate between MIG12 homodimers and S14 homodimers. These data also suggest that oligomers of recombinant S14 normally present in homogeneous mixtures are restricted largely to dimer sizes when MIG12 binds. Interestingly, independently mixing recombinant MIG12 with recombinant S14 after purification does not generate MIG12:S14 heterodimers suggesting that their interaction is formed during translation **[Figure 2-9b]**.

When incubated with purified recombinant ACC1, MIG12:S14 heterodimers fail to induce polymerization. Separation of this mixture by FPLC generates an ACC1 polymerization pattern that is identical to that seen after incubation with S14 homodimers or BSA alone. In contrast, recombinant MIG12 homodimers induce a sharp increase in ACC1 complex size and

forces earlier elution from Sepharose 6 columns **[Figure 2-9d]**. As expected, immunoblots of MIG12 and S14 indicate that, after incubation, purified recombinant MIG12 elutes together in high molecular weight fractions with ACC1 oligomers, whereas S14 and MIG12:S14 heterodimer do not **[Figure 2-9e]**. These data also suggest that, like S14 homodimers, purified recombinant MIG12:S14 heterodimers do not bind to, nor are they incorporated into ACC1 polymers.

By extension, *in vitro* activity of ACC1 in the presence of citrate is completely unaffected by increasing concentrations of MIG12:S14 heterodimers or S14 homodimers. Under these same conditions, however, MIG12 significantly enhances the incorporation of ^{14}C-labeled bicarbonate to malonyl-CoA. Furthermore, simultaneously incubating MIG12 and S14 homodimers with ACC1 has the same effect on polymerization and activity as MIG12 homodimers alone **[Figure 2-9c]**. This data is in accordance with the finding that MIG12:S14 heterodimers do not form when recombinant MIG12 and S14 homodimers are mixed together after purification, and suggests that production of MIG12:S14 heterodimers requires intact cellular machinery. Such a conclusion is also supported by the finding that combining separate CHO-K1 cell lysates that express MIG12 or S14 does not result in heterodimer formation.

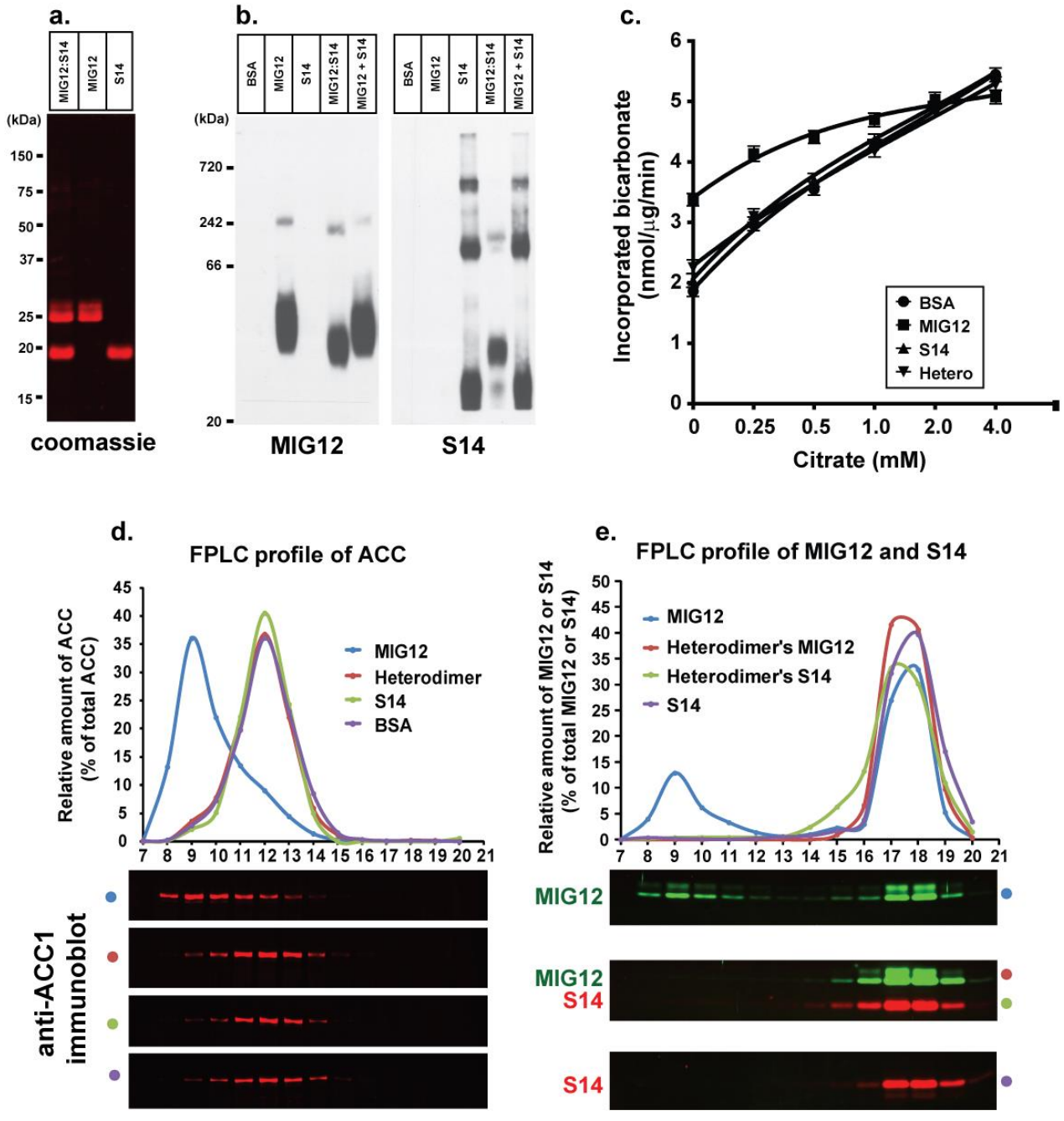
a.
MIG12:S14
MIG12
S14
(kDa)
150
75
50
37
25
20
15
coomassie
b.
BSA
MIG12
S14
MIG12:S14
MIG12 + S14
(kDa)
720
242
66
20
MIG12
S14
c.
Incorporated bicarbonate (nmol/μg/min)
Citrate (mM)
BSA
MIG12
S14
Hetero
d.
FPLC profile of ACC
Relative amount of ACC (% of total ACC)
MIG12
Heterodimer
S14
BSA
anti-ACC1 immunoblot
e.
FPLC profile of MIG12 and S14
Relative amount of MIG12 or S14 (% of total MIG12 or S14)
MIG12
Heterodimer's MIG12
Heterodimer's S14
S14
MIG12
MIG12
S14
S14

Figure 2-9. Recombinant MIG12:S14 heterodimer has no effect on ACC1 polymerization or activity.

(A) Purified recombinant MIG12:S14 heterodimers, MIG12, and S14 were separated by SDS-PAGE and visualized by coomassie staining. *(B)* BSA, MIG12, S14, and MIG12:S14 heterodimers, or mixed equivalent amounts of MIG12 and S14 homodimers, were separated on 14% BN-PAGE gel. MIG12 and S14 proteins were visualized by immunoblot analysis using anti-MIG12 and S14 antibodies. *(C)* Recombinant ACC1 (0.5 μg) and 0.125 μg of BSA, recombinant MIG12, S14, or MIG12:S14 heterodimers were incubated in the presence of various concentrations of citrate, after which ACC activity was measured. *(D)* Recombinant ACC1 (40 μg) was mixed with 5 μg of MIG12, 10 μg of MIG12:S14 heterodimer, 5 μg of S14, or 5 μg of BSA and incubated at RT for 5 minutes. These mixtures were separated by FPLC using superpose 6 columns, and the fractions from 7 to 20 ml were subjected to immunoblot analysis using anti-ACC1 antibodies. Relative ACC amount was calculated using the LI-COR scanning system as described in **Figure 3**. Blue dot: ACC1 mixture with MIG12; red dot: with heterodimer; green dot: with S14; purple dot: with BSA. *(E)* Fraction samples obtained from FPLC in *(D)* were analyzed by immunoblotting with antibodies against MIG12 and S14. Relative amounts of MIG12 and S14 were calculated by scanning each bands' intensity as described above. Blue dot: MIG12 immunoblot from ACC1 with MIG12; red dot: MIG12 immunoblot from ACC1 with heterodimer; green dot: S14 immunoblot from ACC1 with heterodimer; purple dot: S14 immunoblot from ACC1 with S14.

MIG12 immunoblots of these samples at high molecular weights indicate that, under native conditions, small amounts of heterodimeric MIG12 bind to ACC1 oligomers minimally induce polymerization **[Figure 2-10a,b]**. Weak signals observed in overexposed immunoblots suggests that the same may be true of heterodimeric S14 **[Figure 2-10c]**. Furthermore, these same MIG12:S14 heterodimers appear to slightly induce ACC1 activity *in vitro*. Though they do not activate ACC1 to the same extent as homodimeric MIG12, ^{14}C-acetate incorporation is significantly higher than incubation with S14 homodimer or BSA alone **[Figure 2-10d]**. It is possible that these findings are the result of MIG12:S14 heterodimer instability. More specifically, under higher temperatures or prolonged storage, MIG12 and S14 might dissociate and reform homodimers. Newly generated MIG12 homodimers, then, could account for the slight induction in ACC1 polymerization and activity observed.

To determine whether these observations are the effect of dynamic heterodimer disassociation followed by unwanted MIG12 homodimer reformation, MIG12:S14 heterodimer was incubated at 4 °C and 37 °C for increasing amounts of time and then visualized by immunoblot after BN-PAGE. Surprisingly, the results indicate that purified recombinant heterodimer is very stable and will not recombine during incubation with ACC1 **[Figure 2-10e,f]**. It is possible, then, that residual ACC1 polymerization and activity is the effect of higher order MIG12:S14 oligomers that inefficiently link ACC1 dimers. Indeed, such a mechanism has been suggested in studies involving ACC2 and heterodimer interaction.[63]

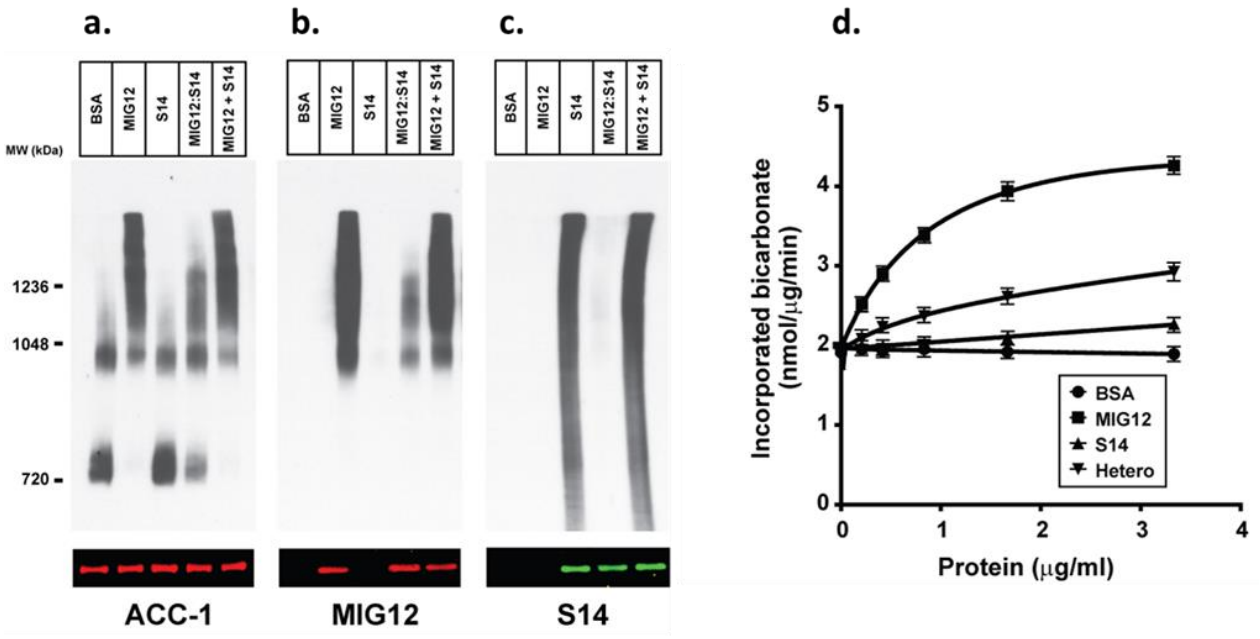

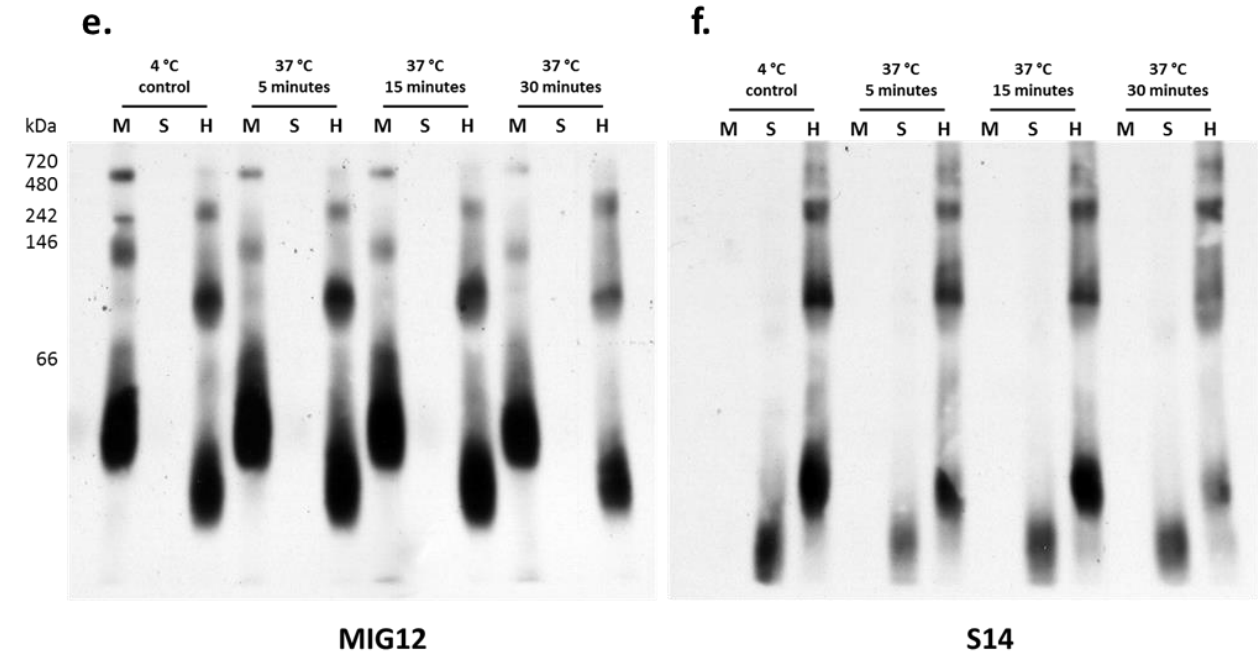

M: MIG12
S: S14
H: MIG12:S14 Heterodimer

Figure 2-10. Aberrant induction of ACC1 polymerization and activity by MIG12:S14 heterodimer is not the result of thermal or temporal instability.
(A-C) Purified recombinant ACC1 (40 μg) was incubated with recombinant MIG12 (5 μg), S14 (5 μg), or MIG12:S14 heterodimer (10 μg). Mixtures were incubated for 15 minutes at 37 °C and separated using BN-PAGE with 3.5-10% polyacrylamide gradient gels. SDS-PAGE separation was also performed for each experiment to confirm equal protein levels between samples. Immunoblots were performed using rabbit polyclonal antibodies against ACC1 *(A)*, MIG12 *(B)*, and S14 *(C)*. *(D)* Purified ACC1 (0.5 μg) was incubated with 0.125 μg of BSA, recombinant MIG12, S14, or MIG12:S14 heterodimer at 37 °C for 15 minutes, after which activity was measured by $H^{14}CO_3^-$ incorporation. *(E-F)* Purified recombinant MIG12:S14 heterodimer was incubated by itself at 4 °C and 37 °C for 5 to 30 minutes. Samples were then separated using BN-PAGE with 14% polyacrylamide gels. Immunoblots were performed using rabbit polyclonal antibodies against MIG12 *(E)* and S14 *(F)*.

Summary

Based on these data, regulation of hepatic fatty acid synthesis requires the action of heterocomplexes involving at least three proteins – ACC, MIG12, and S14. Robust polymerization and activation of ACC occurs through a physical incorporation of MIG12 homodimers. This binding is presumed to occur, at least in part, on the central domain of ACC. *In vitro* assays also indicate this domain is required for normal ACC folding and function **[Figures 2-1 and 2-2]**. Differences in the ability of MIG12 to increase ACC activity can be seen between rat and mouse species **[Figure 2-3 and 2-4]**. Such discrepancies can be attributed to expression levels of S14, a small protein which binds and sequesters endogenous MIG12 **[Figure 2-5]**. Indeed, when total S14 is high, MIG12 equilibrium shifts from a functional homodimer to an inactive heterodimer. This is evidenced by tissue-specific native protein conformation and malonyl-CoA synthesis rates in *Mig12* knockout mice **[Figure 2-7]**. Recombinant MIG12:S14 heterodimer can be recapitulated following transient expression in cell culture and can also be purified from *sf-9* cells as a stable species **[Figure 2-8 and 2-9]**. Incubating purified MIG12:S14 heterodimer with recombinant ACC confirms observations in mouse and rat tissue – specifically that MIG12 can only induce polymerization and activity as a homodimer.

CHAPTER THREE: EVIDENCE OF HIGHER-ORDER COMPLEX FORMATION BETWEEN REGULATORS OF FATTY ACID SYNTHESIS

While S14 clearly abrogates MIG12's activation of ACC1, its effect on lipogenesis is less clear. For instance, although knockdown of S14 in mouse liver increases ACC activity as described, hepatic fatty acid biosynthesis is decreased in this model.[35] Though counterintuitive, this finding suggests that S14 exerts positive regulation through a component of lipogenesis separate from ACC action. Consistent with this, lipogenic rates are decreased in mouse mammary glands when S14 is deleted.[64] Because MIG12 expression is extremely low in these tissues, such data suggests that S14 alone can exert a positive influence on fatty acid synthesis. It also supports a model wherein additional proteins and enzymes interact with S14, MIG12, and ACC in multimeric complexes for more efficient regulation of fatty acid synthesis. Indeed, the aforementioned complexes between MIG12 and ACC1 or MIG12 and S14 could serve as a foundation for the formation of these metabolons.

Immunoprecipitation of Spot 14 Protein

To identify additional proteins that might bind to and influence lipogenic enzymes, affinity columns were prepared with polyclonal S14 rabbit IgG or preimmune rabbit IgG. Liver cytosol from mice fasted and refed on a high carbohydrate, fat-free diet was then incubated with these columns. Bound proteins were washed, eluted, normalized, and separated using SDS-PAGE. To determine differences between column eluates and to permit subsequent mass spectrographic analysis of band identity, protein profiles were visualized on gels after silver staining. Unfortunately, multiple attempts revealed no difference between the gel stain patterns of S14 and premature IgG bound species **[Figure 3-1a,b]**. This could be attributed to significant nonspecific binding of total liver protein to control affinity columns, as well as relatively weak

binding of S14 to antibodies. To correct for these limitations, S14-FLAG was overexpressed in rat primary hepatocytes using an adenovirus, and the cell lysate clarified using an anti-FLAG agarose column. This preparation showed strong immunoprecipitation of abundant S14 protein, as well as significant differences between protein profiles of S14 and β-gal adenovirus infected controls **[Figure 3-1c,d]**. Among the more significant products that co-immunoprecipitate with S14 were ACC2, an isozyme of ACC1, and FAS, the third and final enzyme in *de novo* fatty acid biosynthesis **[Table 3-1]**. ACC1 also immunoprecipitates with S14, consistent with previous findings in CHO-K1 cells.[35]

Table 3-1. Co-immunoprecipitation products of S14-FLAG in rat primary hepatocytes.

Protein	Peptide Spectrum Matches
fatty acid synthase	1331
acetyl-CoA carboxylase 1	1115
acetyl-CoA carboxylase 2	353
tubulin alpha-1c	949
tubulin alpha-1a	886
tubulin beta-5	757
DnaK-type molecular chaperone	1164

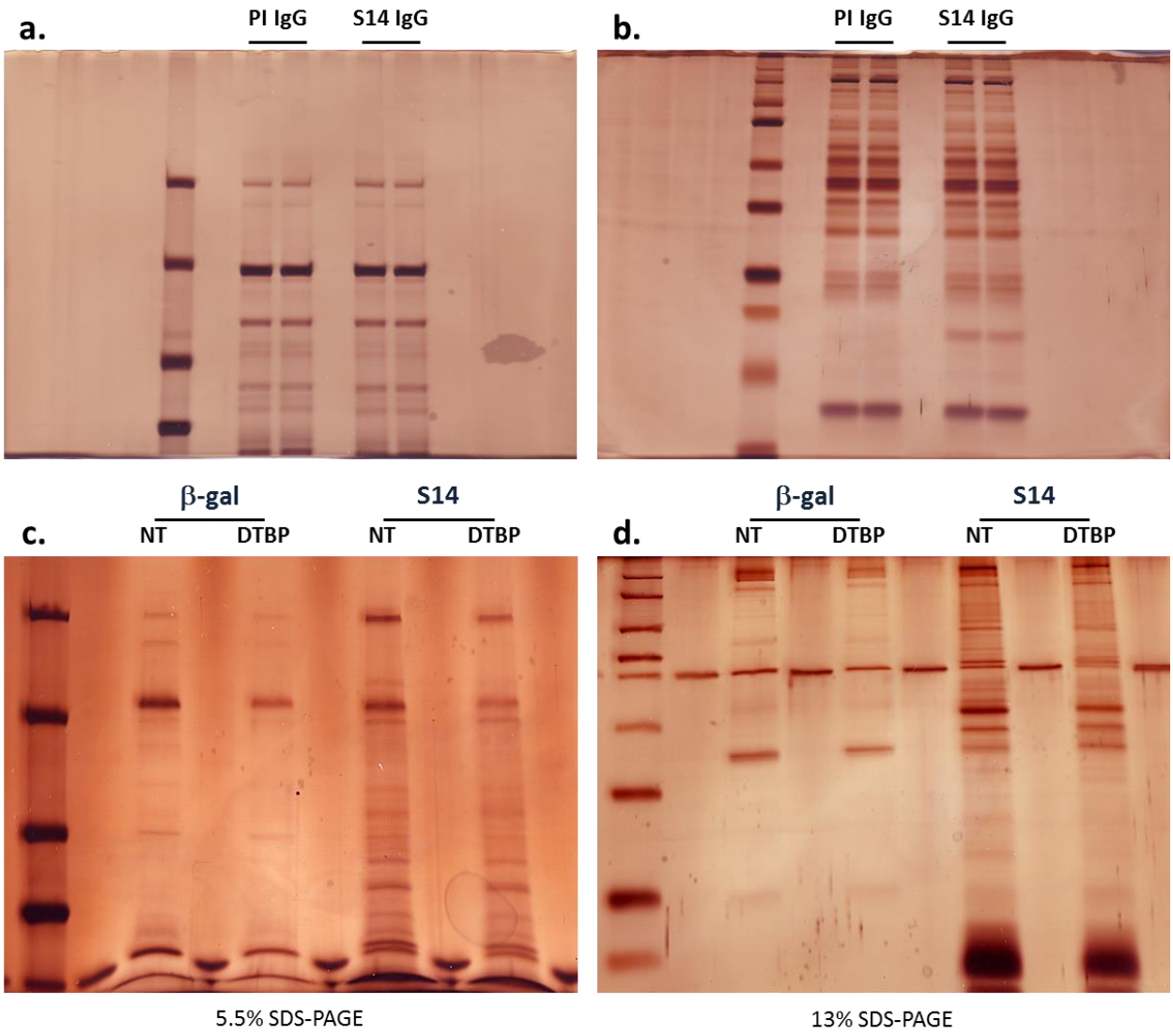

Figure 3-1. Silver stains of S14 co-immunoprecipitation products in mouse liver cytosol and rat primary hepatocytes.

(A, B) Liver cytosol from FFD fed mice was precleared with pre-immune IgG. Samples were loaded on conjugated agarose columns with either preimmune or S14 IgG and rotated for 6 hours at 4 °C. Columns were washed and eluates separated using SDS-PAGE with 5.5% *(A)* or 13% *(B)* polyacrylamide gels. Gels were then visualized by silver staining. *(C, D)* Rat primary hepatocytes were infected with β-gal or S14 adenovirus and incubated at 37 °C in 5% CO_2. Cells were either treated with DMSO or the crosslinker DTBP, and then harvested and lysed. Samples were incubated with anti-FLAG M2 affinity gel, washed, and eluted. Eluates were separated and visualized as in *(A)* and *(B)*.

Purification and Activity of Fatty Acid Synthase

Given these data, it is possible that S14 regulates lipogenic activity by altering FAS activity. To test this possibility, *in vitro* activity of FAS was measured in combination with purified S14 homodimers. First, baculovirus constructs containing a full-length human homologue of FAS in sequence with a cleavable N-terminal hexahistidine (His_6) tag were prepared. Next, purified full-length recombinant FAS was produced by expressing the FAS baculovirus in Sf9 cells. After incubating for three days at 27 °C, insect cell cultures were collected, dounced, and clarified, and the cytosol incubated with Ni-NTA resin for IMAC purification. Thrombin cleavage of the His_6-tag caused protein instability and precipitation, so elution was performed by the addition of 300 mM imidazole. Purified FAS was extremely viscous immediately after elution. This viscosity, however, quickly disappeared once fractions were combined. Also, because imidazole has an inhibitory effect on FAS activity, eluates were immediately desalted with PD-10 columns. Coomassie staining of the purification scheme for recombinant FAS indicate that the majority of protein is captured by IMAC, and little contamination exists following elution **[Figure 3-2a]**.

In addition to recombinant FAS, partially purified FAS was prepared for these *in vitro* assays. Mouse livers were homogenized in phosphate buffer (pH 7.5) containing 250 mM sucrose. Lysates were then centrifuged to remove gross cellular debris and supernatants clarified by ultracentrifugation. Proteins were precipitated by the addition of ammonium sulfate, after which pellets were dissolved and further purified by the sequential addition of 7.5% and 15% PEG8000. PEG8000 pellets (15%) containing partially purified FAS were washed and resuspended in 100 mM Tris-Cl buffer.

After purification, recombinant or partially purified FAS protein was incubated with increasing amounts of S14 homodimers and its activity measured using colorimetric spectrophotometry. More specifically, the rate of oxidation of NADPH, an FAS coenzyme, was assayed by monitoring the decrease in absorbance at 340 nm. Despite immunoprecipitation with FAS, addition of S14 to reaction mixtures had no effect on the activity of either recombinant or partially purified FAS **[Figure 3-2b]**. Interestingly, activity levels of partially purified FAS were significantly higher than those of recombinant FAS. This difference is even more pronounced when considering that FAS in partially purified fractions is significantly less than the total protein amounts used to calculate activity. These data suggest the possibility that certain proteins which co-purify with FAS during PEG8000 treatment may positively regulate FAS activity. It is also possible that inhibitory post-translational modifications that are absent on partially purified FAS are present on recombinant FAS due to *sf-9* culture conditions.

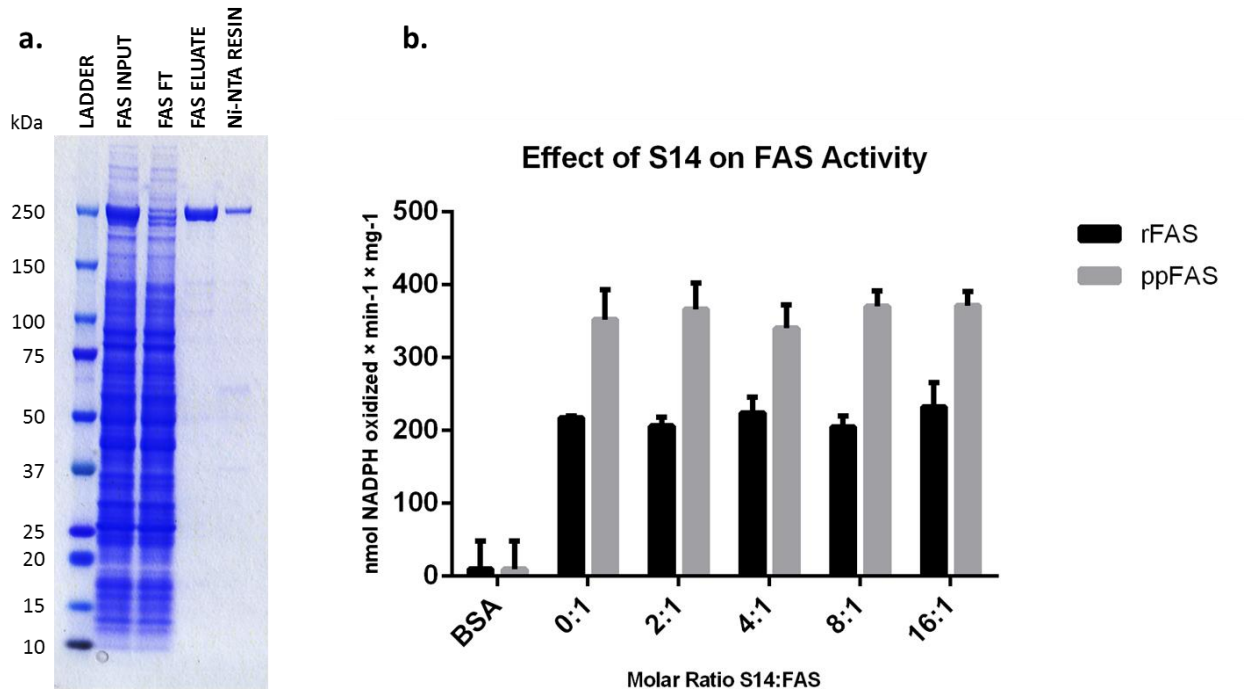

Figure 3-2. Recombinant S14 has no effect on the activity of partially purified or recombinant FAS.
(A) Recombinant human FAS was purified following expression in *sf-9* insect cells. Cytosol from dounced cells was incubated with Ni-NTA resin for 2 hours at 4 °C. Ni-NTA columns were washed with 1x DPBS and 50 mM imidazole, and proteins eluted with 300 mM imidazole in 1x DPBS. *(B)* Increasing amounts of recombinant S14 were incubated with 4 μg of partially purified or recombinant FAS. Oxidation of NADPH in reaction mixtures was observed colorimetrically at 340 nm as described in *Methods*. Kinetics proceeded until rates became non-linear. Triplicate measurements were taken and error is reported as SEM.

I was skeptical of these findings, however, because these data depict FAS activity rates significantly lower than what has been previously reported. Indeed, several studies estimate oxidation values between 1500 and 2000 nmol NADPH min^{-1} mg^{-1} for both partially purified and recombinant FAS.[65–67] Interestingly, early reports of FAS purification have also established that temperature and buffer conditions can influence FAS lability. More specifically, FAS that is stored at temperatures below 20 °C and separated using sucrose density gradient centrifugation is found more exclusively in an inactive monomeric 9 S fraction than its native 13 S homodimer.[68] Also, purified FAS stored under oxidizing conditions or solutions of low ionic strength dissociates over time and loses a significant percentage of its enzymatic activity.[67,69] These same

reports provide protocol through which dissociated FAS can be regenerated into an active form. Long-term incubation of FAS at room temperature, combined with high concentrations of reducing reagent and buffer (i.e. 1-10 mM DTT and >50 mM sodium phosphate) has been shown to dramatically increase the activity of partially purified or recombinant protein.[67–69]

To test these findings and determine whether inactivity could contribute to my negative results with S14, partially purified and recombinant FAS was incubated at room temperature in 250 mM phosphate buffer (pH 7.0), 10% glycerol, 1 mM EDTA, and 1 mM DTT for one hour. Specific activity of FAS protein alone was then measured as previously described. Unfortunately, under these conditions oxidation of NADPH is still remarkably low **[Figure 3-3]**. While regenerated FAS does show a significant increase in activity compared to untreated FAS, enzymatic rates remain at only ~25% of reported values. It is uncertain, then, why such low activity rates are seen in these experiments. It is possible that longer incubation or more reducing conditions are needed to restore FAS dimeric structure. It is also possible that during IMAC or PEG treatment, necessary cationic cofactors are stripped from the FAS complex, rendering it less active. Indeed, it may be recalled that during purification of recombinant FAS, eluates are initially incredibly viscous. This may represent an aggregation from instability in protein structure induced by overly harsh purification conditions.

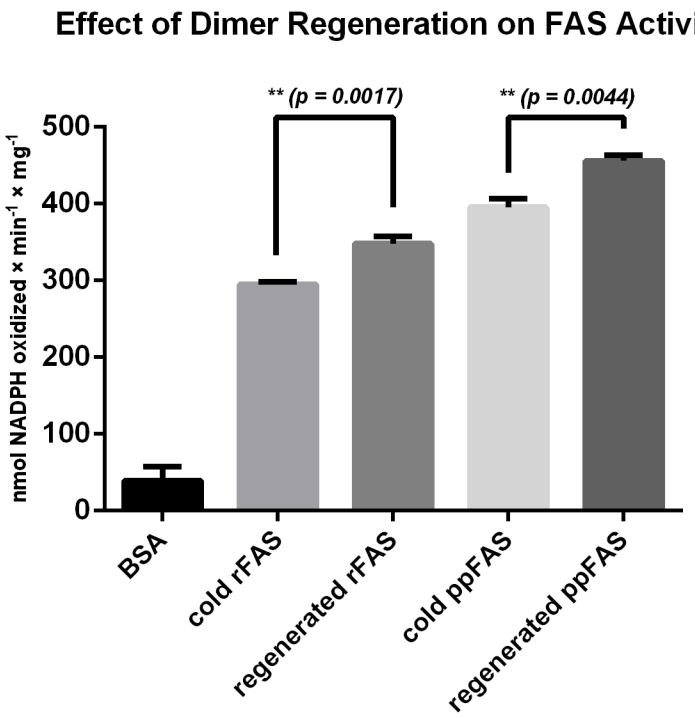

Figure 3-3. Regeneration of FAS homodimer only slightly increases activity.
BSA, recombinant FAS, or partially purified FAS (4 μg) were kept at 4 °C and 50 mM phosphate or incubated with 250 mM phosphate, 10% glycerol, 1 mM EDTA, and 1 mM DTT for 1 hour at 37 °C. Proteins were then combined with reaction mixtures and oxidation of NADPH measured colorimetrically as described in *Methods*. Kinetics proceeded until rates became non-linear. Quadruple measurements were taken and error is reported as SEM.

Co-immunoprecipitation of Lipogenic Proteins

In order to further investigate the interaction between S14, FAS, and ACC1, as well as their potential roles in the formation of a multimeric lipogenic complex, new antibodies against FAS were needed. To generate a new FAS antibody, GST-fusion products of a ~60 kDa fragment of FAS (fFAS) were expressed in BL21 cells and purified using glutathione affinity resin, after which the epitope tag was cleaved and removed from solution **[Figure 3-4a]**. Purified recombinant fFAS was injected into rabbits to generate polyclonal antibodies. Serum samples from rabbits were subsequently screened for efficacy in immunoblot and immunoprecipitation, and the best collections were purified using IgG affinity columns.

Once purified, rabbit polyclonal antibodies against FAS were used to co-immunoprecipitate endogenous proteins in liver cytosol from *ad libitum* CHOW and FFD refed mice. Pre-cleared cytosol was incubated for 2 hours with anti-FAS antibodies and then conjugated to protein A/G agarose. Bound resin was washed with 1x DPBS, and immunoprecipitation products eluted by boiling in 2x SDS buffer. Samples were then separated using SDS-PAGE with 5.5% and 13% polyacrylamide gels, and immunoblots prepared against known lipogenic proteins. In these experiments, FAS pulls down ACC1 in CHOW fed mice **[Figure 3-4b, lane 10]**. This data likely represent direct binding between FAS and ACC1 instead of an indirect association, because no other immunoblot shows strong co-immunoprecipitation with FAS. Interestingly, less FAS and ACC1 are co-immunoprecipitated in FFD refed mouse samples despite an increase in overall expression of these two enzymes **[Figure 3-4b, lanes 1-4, 9-12]**. It should also be noted that despite increased clearance of MIG12 and tubulin from FFD supernatants post-incubation, neither are present in FFD immunoprecipitation pellets **[Figure 3-4b, lanes 5-8, 9-12]**. These discrepancies illustrate a reproducible finding when working with refed mouse or rat liver cytosol – an autonomous aggregation of lipogenic proteins. These accumulations of FAS, ACC, MIG12, and tubulin co-precipitate independent of conjugated protein A/G agarose. The disappearance of these proteins from FFD pellet immunoblots, then, is likely from solubilization during washing steps. While this autonomous aggregation might be an artifact of homogenization or buffer conditions, it might also represent a native tendency for FAS, ACC, MIG12, and tubulin to functionally interact on a quaternary level.

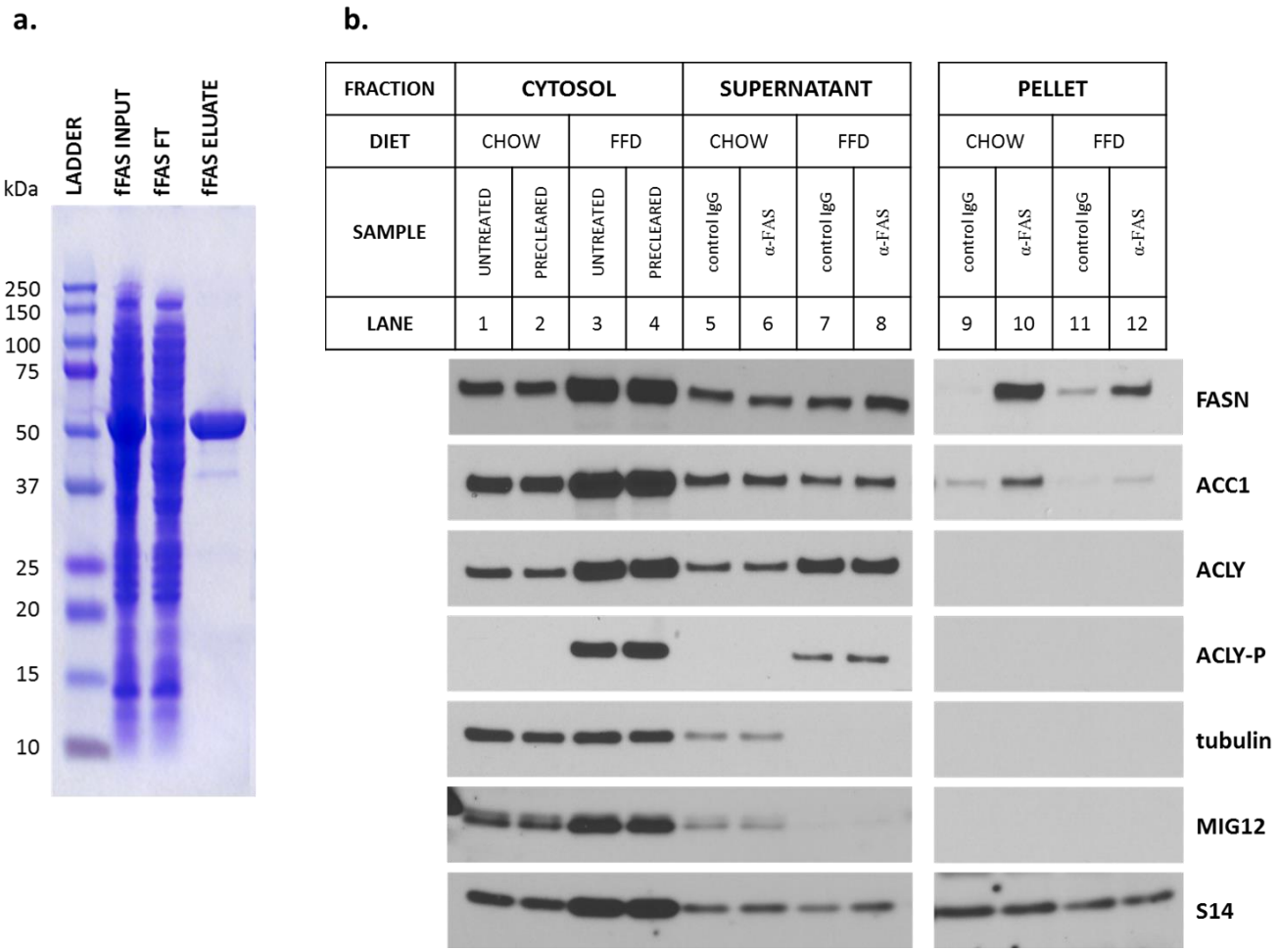

Figure 3-4. Preparation of α-FAS polyclonal antibody and co-immunoprecipitation in mouse liver cytosol.
(A) A 60 kDa FAS-GST fusion peptide was expressed in BL21 cells overnight at 4 °C. Bacterial pellets were then treated with 1x lysozyme and incubated on ice for 30 minutes, following which slurries were sonicated 5x at 40% power. Following centrifugation, supernatants were incubated with 3 mL immobilized glutathione and incubated at 4 °C for 2 hours. Columns were washed and recombinant proteins eluted with 10 mM glutathione in 50 mM Tris-Cl (pH 8.0). *(B)* Mouse livers from CHOW and FFD fed mice were homogenized and centrifuged as described in *Methods*. Cytosolic supernatants were incubated with 10 µg of control IgG or α-FAS antibodies and rotated at 4 °C for 2 hours. 50 µL protein A/G agarose was then added to each sample to conjugate antibodies and co-immunoprecipitation products. Resin was washed and eluted by boiling in 200 µL 2x SDS buffer. 40 µg total protein or equivalent was loaded for cytosol and supernatant fractions, and 20 µL eluate for pellets. Samples were separated using SDS-PAGE and immunoblots performed with rabbit polyclonal antibodies.

In addition to FAS and ACC1, co-immunoprecipitation of S14 in rat primary hepatocytes shows association with ACC2. Since endogenous immunoprecipitation suggests ACC1 and FAS directly bind, these data indicate ACC1 and ACC2 may physically interact as well. While this supposition may not be surprising given the sequence homology between ACC1 and ACC2, early reports proposed little interaction between the two due to different subcellular localization.[14,70] Furthermore, the role of either isozyme has been implicated in separate pathways – ACC1 acts in fatty acid production while ACC2 presumably functions to inhibit beta-oxidation.[14] ACC1 and ACC2, then, may have a more intimate relationship than previously suspected. To investigate this hypothesis, constructs expressing tagged ACC1-3x HA and ACC2-6x Myc were co-transfected into CHO-K1 cells and immunoprecipitated with either anti-HA or anti-Myc resin. Immunoblots of the resin eluates reveal that exogenous ACC2 can indeed precipitate ACC1, and vice versa **[Figure 3-5, lane 12]**. Interestingly, co-expression of ACC1 and ACC2 reduces total ACC1 levels significantly compared to single transfection of ACC1 alone **[Figure 3-5, lanes 2 and 4]**. This accounts for the relatively small amount of ACC1 bound to ACC2 after immunoprecipitation.

	INPUT				SUPE				PELLET			
ACC1-3x HA (µg)	0	2	0	2	0	2	0	2	0	2	0	2
ACC2-6x Myc (µg)	0	0	2	2	0	0	2	2	0	0	2	2
LANE	**1**	**2**	**3**	**4**	**5**	**6**	**7**	**8**	**9**	**10**	**11**	**12**

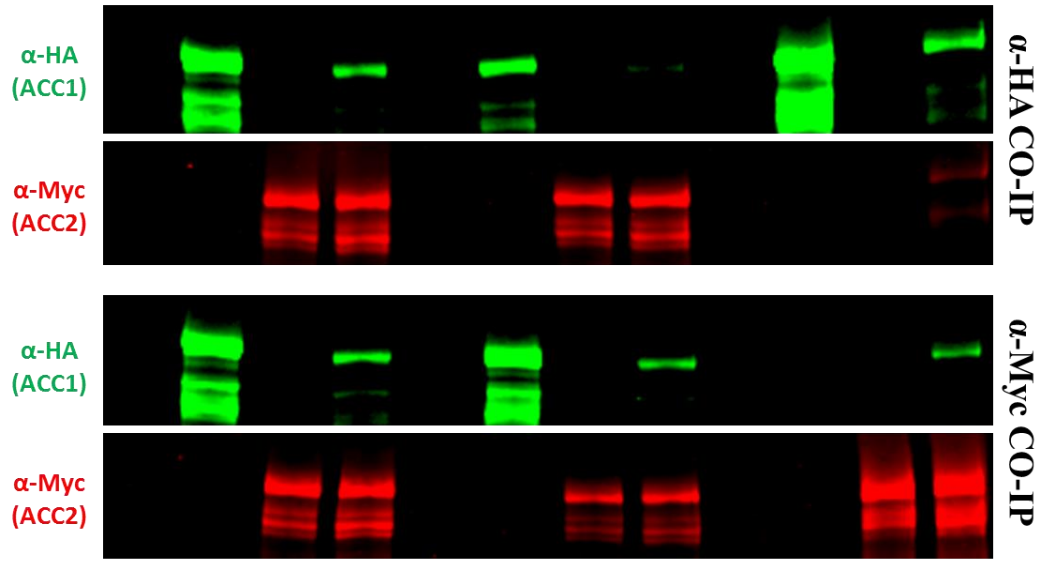

Figure 3-5. ACC1 co-immunoprecipitates with ACC2 following transient overexpression in CHO-K1 cells.
CHO-K1 cells were transfected singly or in combination with constructs expressing ACC1-3x HA (2 µg) and ACC1-6x Myc (2 µg). Cells were cultured for 24 hours at 37 °C and 8.8% CO_2, following which cells were lysed in a HEPES and sucrose buffer by passing through a 22-gauge needle. Samples were centrifuged, precleared with protein A/G agarose, and incubated with 20 µL anti-HA or anti-Myc resin. Proteins were eluted after washing by boiling in 2x SDS buffer and separated on 5.5% polyacrylamide gels using SDS-PAGE.

In addition to ACC and FAS, MIG12 and S14 interact with the first enzyme in fatty acid biosynthesis, ACL. When MIG12 (2 μg), S14 (8 μg), and ACL (6 μg) are transiently overexpressed in CHO-K1 cells, both MIG12 and S14 immunoprecipitate ACL from cell lysates **[Figure 3-6, lanes 9 and 10]**. In the converse experiment, ACL immunoprecipitates MIG12 and S14 under these same conditions. It should be noted that unequal amounts of each construct were transfected in order to have equal protein expression. Interestingly, these data suggest that MIG12 and ACL show higher affinity than S14 and ACL. While this might be due to direct and variable binding between ACL and MIG12 or S14, it could also be the result of indirect interaction between species. For example, while MIG12 and S14 both co-immunoprecipitate with ACC, MIG12 does so with much greater affinity than S14. This might be due to the fact that the interaction with MIG12 is direct and the interaction with S14 is indirect through other proteins in the complex. The ACL IP results, then, might be from direct association of MIG12 or S14 with ACC, and indirect association with ACL through ACC in the putative lipogenic complex.

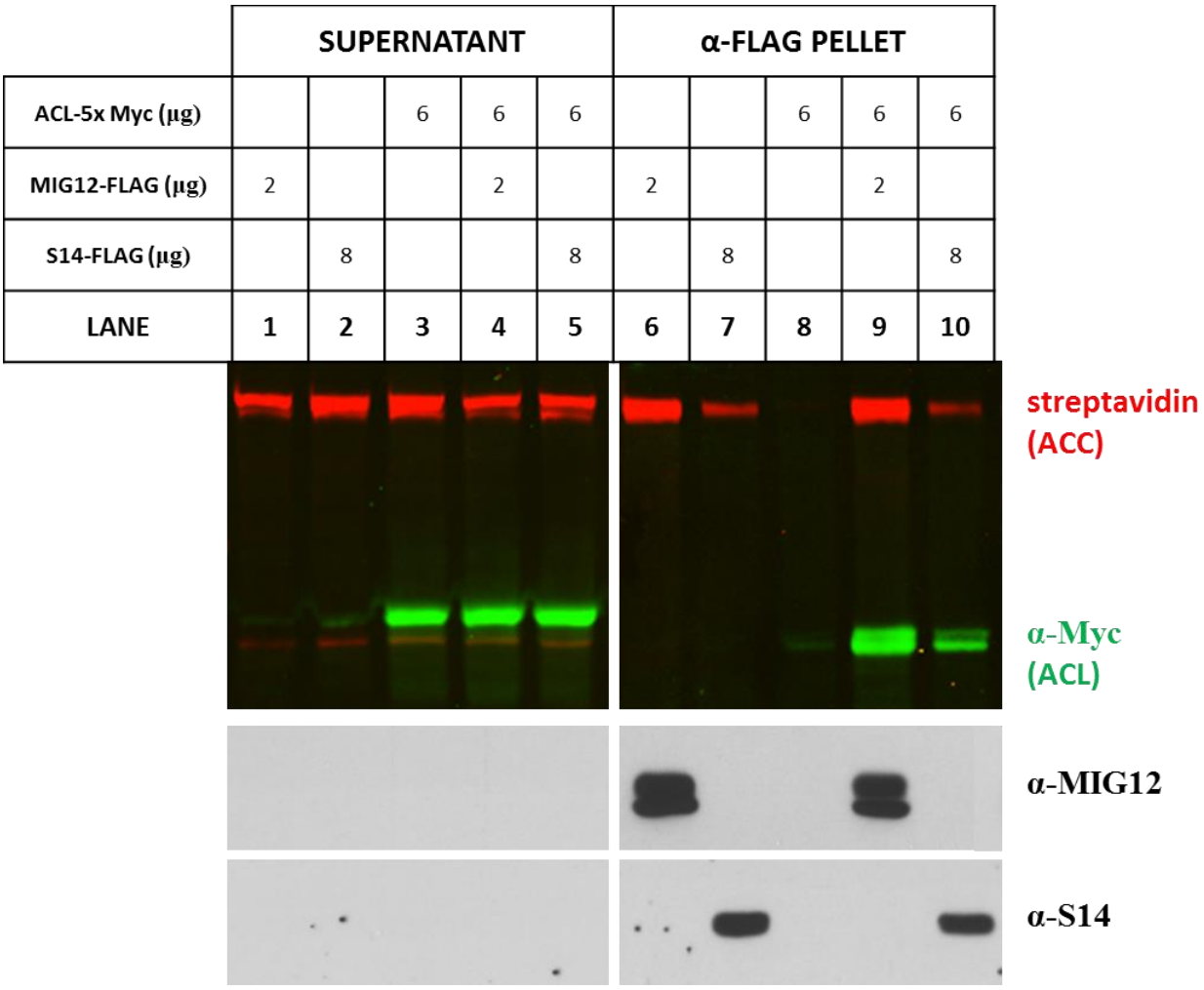

Figure 3-6. ACL co-immunoprecipitates with MIG12 and S14 following transient overexpression in CHO-K1 cells.
Constructs expressing tagged ACL-5x Myc (6 µg), MIG12-FLAG (2 µg), or S14-FLAG (8 µg) were transfected singly or in combination to CHO-K1 cells. Cells were cultured for 24 hours at 37 °C and 8.8% CO_2. Cells were lysed in a digitonin buffer by passing through an insulin needle. Lysates were centrifuged and precleared using protein A/G agarose. Cytosolic supernatants were incubated with 50 µL of anti-FLAG M2 affinity gel at 4 °C for 2 hours, following which samples were washed and boiled in 100 µL 2x SDS buffer. 20 µL of each sample was separated using SDS-PAGE on 5.5% and 13% polyacrylamide gels.

Purification and Activity of ATP Citrate Lyase

To further investigate the effects of physical binding between ACL and MIG12 or S14, ACL activity was measured in the presence of MIG12, S14, or MIG12:S14 heterodimer. Like FAS, a baculovirus was prepared expressing N-terminal hexahistidine tagged human ACL. Recombinant ACL-His_6 was grown in *sf-9* insect cells for three days at 27 °C. Cytosol from insect cell lysates was subjected to IMAC for 2 hours at 4 °C using Ni-NTA resin. After DPBS washes, ACL protein was eluted with 300 mM imidazole and quickly desalted with PD-10 columns. Coomassie staining of IMAC purification shows extremely high yield and purity in recombinant ACL eluates, though some potential degradation products are present **[Figure 3-7a]**. Purified ACL was then incubated with recombinant MIG12, S14, or MIG12:S14 heterodimer in the presence of NADH and ACL enzymatic rates determined colorimetrically. Like FAS activity assays, the oxidation of NADPH is proportional to the activity level of ACL. Unlike FAS activity assays, however, the rate of absorbance change at 340 nm is not directly associated with ACL function. More specifically, NADH is not a required coenzyme for ACL activity, but is required for the metabolism of a byproduct of ACL reactions – oxaloacetate. Thus, by combining malate dehydrogenase and NADH with each assay sample, ACL function can be measured indirectly. Surprisingly, despite direct interaction between ACL and MIG12 or S14, supplementation of reaction mixtures with these recombinant proteins has absolutely no effect on the activity of ACL **[Figure 3-7b]**. ACL enzyme rates remain constant even when molar ratios of MIG12, S14, or heterodimer are increased 100-fold.

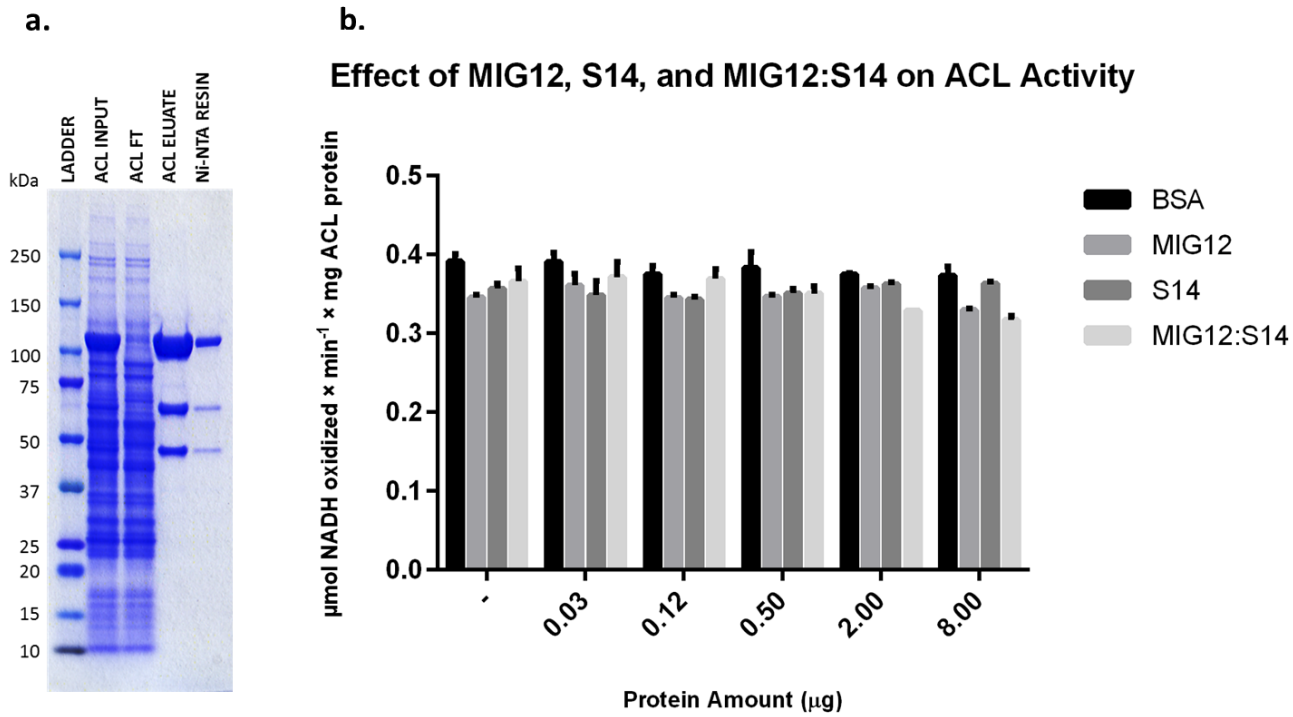

Figure 3-7. Recombinant MIG12, S14, and MIG12:S14 heterodimer do not affect the activity of recombinant ACL *in vitro*.
(A) Human recombinant ACL-His_6 was expressed in *sf-9* insect cells using a baculovirus vector. Insect cell pellets were dounced and clarified, after which cytosolic supernatants were incubated with Ni-NTA resin for 2 hours at 4 °C. ACL protein was washed, eluted with 300 mM imidazole, and desalted to remove imidazole. *(B)* Recombinant ACL protein (0.5 µg) was incubated with increasing concentrations of recombinant MIG12, S14, or MIG12:S14 heterodimer at room temperature and in the presence of 0.14 mM NADH. Decreases in absorbance at 340 nm were normalized to control wells and total ACL concentration. Duplicate measurements were taken and error is reported as SEM.

Despite the presence of minor degradation products, no complications in the process of ACL purification were encountered. However, if some undetected compromise in ACL structure occurs during IMAC, it may explain these negative data. For instance, certain buffer compositions or storage conditions may cause dissociation of active ACL homotetramer. As previously described, such is the case for partially purified or recombinant FAS homodimer. This possibility, however, is unlikely given reports that ACL activity is stable over a wide range of temperatures and pH, particularly when phosphate buffer is used.[71] A more plausible scenario is that recombinant ACL is not properly phosphorylated in *sf-9* cells, a post-translational

modification necessary for stability and increased enzymatic activity.[11,12] In mouse and rat livers, ACL becomes phosphorylated under conditions that promote lipogenesis, like high carbohydrate/fat-free diets **[Figure 3-4b, lanes 1-4]**. Unfortunately, culture conditions in *sf-9* cells lack insulin and glucose levels to signal this change. Inasmuch as multiple enzymes have been reported to phosphorylate and modulate ACL activity, kinase assays to increase activity of recombinant ACL after purification are beyond the scope of this thesis.[12,72,73] A simpler approach to verify the effect of MIG12, S14, and MIG12:S14 heterodimer on ACL is to perform *in vitro* activity assays using endogenous proteins. Therefore, rat primary hepatocytes were isolated and cultured in the presence of high glucose and insulin concentrations. Hepatocytes were treated with mismatched, MIG12, or S14 siRNA, and partially purified fractions of MIG12 and S14 prepared using PEG8000. These fractions were then combined together with ACL, malate dehydrogenase, and NADH, and oxidation rates at 340 nm measured. Under these conditions, knockdown of MIG12 significantly increases overall ACL activity relative to mismatch and S14 siRNA samples **[Figure 3-8]**. Furthermore, knockdown of both MIG12 and S14 restores NADH oxidation rates to mismatch control levels. It is possible, then, that MIG12 and S14 do regulate ACL activity. This relationship, however, likely requires cellular factors that have not yet been identified.

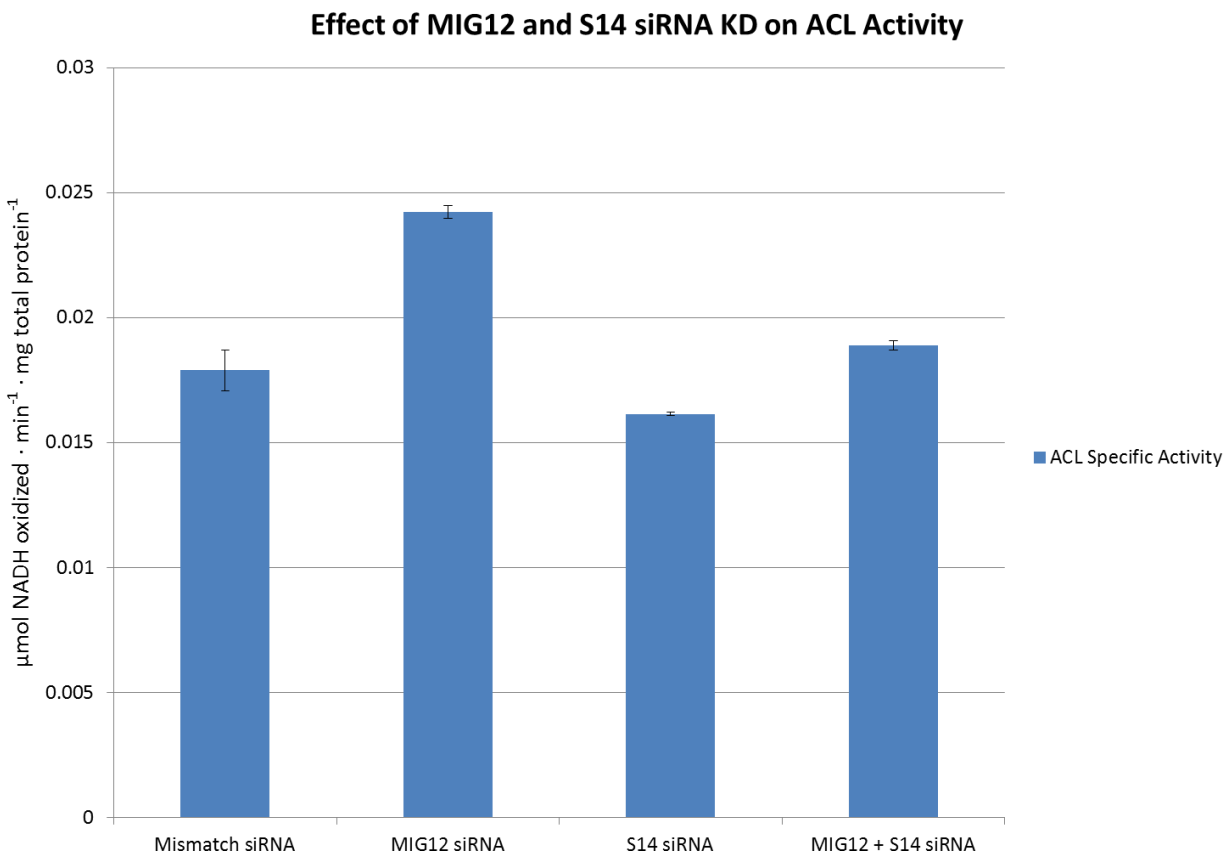

Figure 3-8. Knockdown of MIG12 and S14 using siRNA in rat primary hepatocytes modulates ACL activity.
Rat primary hepatocytes were treated with siRNA against MIG12 or S14 at 37 °C and 5% CO_2. 15% PEG8000 fractions containing MIG12 and S14 were prepared from hepatocyte cell lysates and combined with ACL and reaction buffer containing NADH and malate dehydrogenase. Activity was determined by oxidation of NADH and measured by absorbance changes at 340 nm. Triplicate measurements were taken and error is reported as SEM.

2-Dimensional Electrophoresis of Lipogenic Proteins

These biochemical data support a model wherein ACC1, ACC2, FAS, ACL, MIG12, and S14 combine in cells to form large functional complexes. However, immunoprecipitation results fail to capture all of these components together. This is likely due to more delicate quaternary interactions between extremely large enzymatic oligomers. To reconcile that some degree of association exists between each of the putative complex members, 2-dimensional gel electrophoresis was performed on denatured and native mouse liver cytosol. 2-dimensional gel

electrophoresis separates proteins first by their isoelectric point (pI) and then by their size. If ACC1, ACC2, FAS, ACL, MIG12, and S14 do exist in a large complex together, all members of that aggregate should contribute to an average pI that is disparate from that of each individual protein. Comparing protein profiles between denatured and native samples, then, might identify such change.

Livers from mice fasted and refed on a high carbohydrate and fat free diet were collected and homogenized in a non-reducing buffer. Lysates were clarified and 240 μg of total cytosolic protein used for each sample. Native liver cytosol was left untreated, while denatured samples were mixed with a cocktail of urea (7 M), thiourea (2 M), CHAPS (4%), and DTT (40 mM). Both samples were then mixed with IPG ampholytes with a pH range of 3-10 for 30 minutes on ice. Isoelectric focusing (IEF) gels were combined with respective samples in individual strip holders, and rehydration and separation performed overnight. Following IEF, each strip was loaded on a polyacrylamide gel and subjected to SDS-PAGE. Results indicate that under native conditions, ACC, FAS, ACL, MIG12, and S14 do show a shift in their isoelectric point and co-localize along an average pH **[Figure 3-9].** Denatured protein samples, on the other hand, remain separate from one another and migrate to discrete and previously characterized pI values.

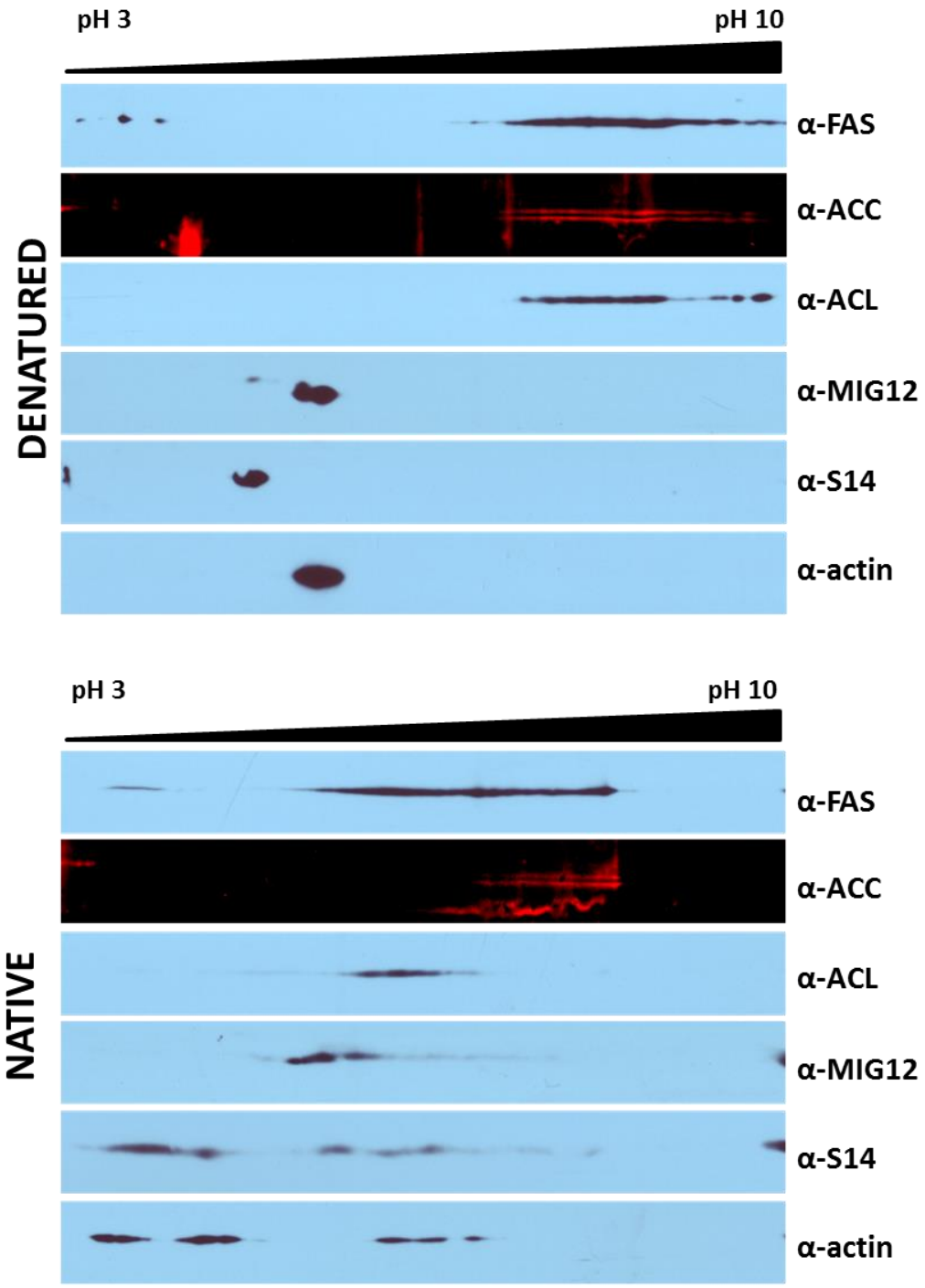

Figure 3-9. **2-dimensional gel electrophoresis of native and denatured lipogenic proteins from mouse liver cytosol.**
Refed mouse liver cytosol (240 µg) was incubated with 4.5 µL IPG buffer (pH 3-10) and 95.5 µL of native or denaturing rehydration buffer. Samples were incubated on ice for 30 minutes and separated overnight at 15 °C using 13 cm immobiline DryStrip gels (pH 3-10). Gels were then separated using SDS-PAGE with 4-15% polyacrylamide gels and immunoblots performed with antibodies as indicated.

Summary

Although knockdown of S14 in mouse liver increases ACC activity as expected, it simultaneously decreases total hepatic fatty acid biosynthesis. Such a discrepancy indicates that S14 influences other components that regulate lipogenesis. Indeed, when overexpressed in rat primary hepatocytes, S14 immunoprecipitates with endogenous FAS and both ACC isozymes **[Figure 3-1]**. *In vitro* activity of recombinant or endogenous FAS protein is not modulated by S14; however, this may be due to a loss of native structure or other interacting proteins during purification **[Figure 3-2]**. Alternatively, additional unidentified proteins might be required for S14 modulation of FAS activity, or S14 may function purely as a structural protein that stablizies the entire lipogenic complex. In addition to FAS, S14 and MIG12 bind to exogenous ACL when overexpressed in cultured cells **[Figure 3-7]**. Like FAS, these interactions appear to have no influence on ACL activity when recombinant proteins are used **[Figure 3-8]**. However, knockdown of MIG12 or S14 in mouse livers does appear to influence ACL activity, indicating that endogenous conformations or modifications are essential to lipogenic complex formation **[Figure 3-9]**. Consistent with a model involving all enzymes in fatty acid synthesis, endogenous FAS immunoprecipitates ACC1, and both ACC isozymes can form a heterocomplex when transiently co-transfected **[Figures 3-5 and 3-6]**. Taken together, these data suggest that FAS, ACC, ACL, MIG12 and S14 form a massive quaternary structure that regulates palmitate synthesis in liver cells.

CHAPTER FOUR: SUBCELLULAR LOCALIZATION OF THE PUTATIVE LIPOGENIC METABOLON

In order to create a complex that streamlines fatty acid biosynthesis, individual components must also show subcellular co-localization consistent with such function. Lipogenic enzymes have canonically been considered to exist exclusively in the cytoplasm. Subsequent steps in triglyceride production, however, localize to different organelles. For instance, once FAS has produced palmitate, the 16:0 fatty acid undergoes desaturation and elongation prior to incorporation into triglyerides or phospholipids. Desaturases such as SCD1 and the elongase ELOVL6 are integral membrane proteins in the ER.[47,52] In addition, enzymes involved in the terminal processing of triglycerides (i.e. PAP, AGPAT, DGAT) localize to the ER as well.[74] For efficient production of triglycerides from excess glucose, soluble factors like FAS, ACC, and ACL might localize to the immobile desaturases, elongases, lipases, and acyltransferases on the ER to improve the efficiency of synthesis.

Several previous reports have suggested that fatty acid synthesis occurs along the ER. For instance, liver lysates from rats refed on FFD show an increase in ACC activity in microsomal fractions compared to fasted rat livers.[75] To determine whether these assumptions and previous reports are valid, immunofluorescence of lipogenic enzymes and proteins was performed. Historically ACC1, FAS, and ACL have been shown to be localized in the cytoplasm using immunofluorescence and cell fractionation studies. Most experiments, however, were performed using immortalized cell culture lines. Such lines have been consistently shown to not respond to insulin signaling, which upregulates SREBP-1c and significantly enhances the production of fatty acids. For instance, Huh-7 cell lysates show significantly lower lipogenic protein levels compared to refed mouse and rat liver cytosol

[Figure 4-1, lanes 1-3]. Furthermore, incubation of Huh-7 cells with high concentrations of glucose, insulin, T_3, or exogenous fatty acids has no effect on lipogenic protein levels **[Figure 4-1, lanes 6-8]**. Therefore, to establish whether ACC1, FAS, and ACL are exclusively cytosolic in the presence of physiologic insulin signaling, rat primary hepatocytes were used for immunofluorescence. In contrast to immortalized cells, primary hepatocytes retain sensitivity to insulin signaling and provide a template very similar to the cellular environment in a living rat.

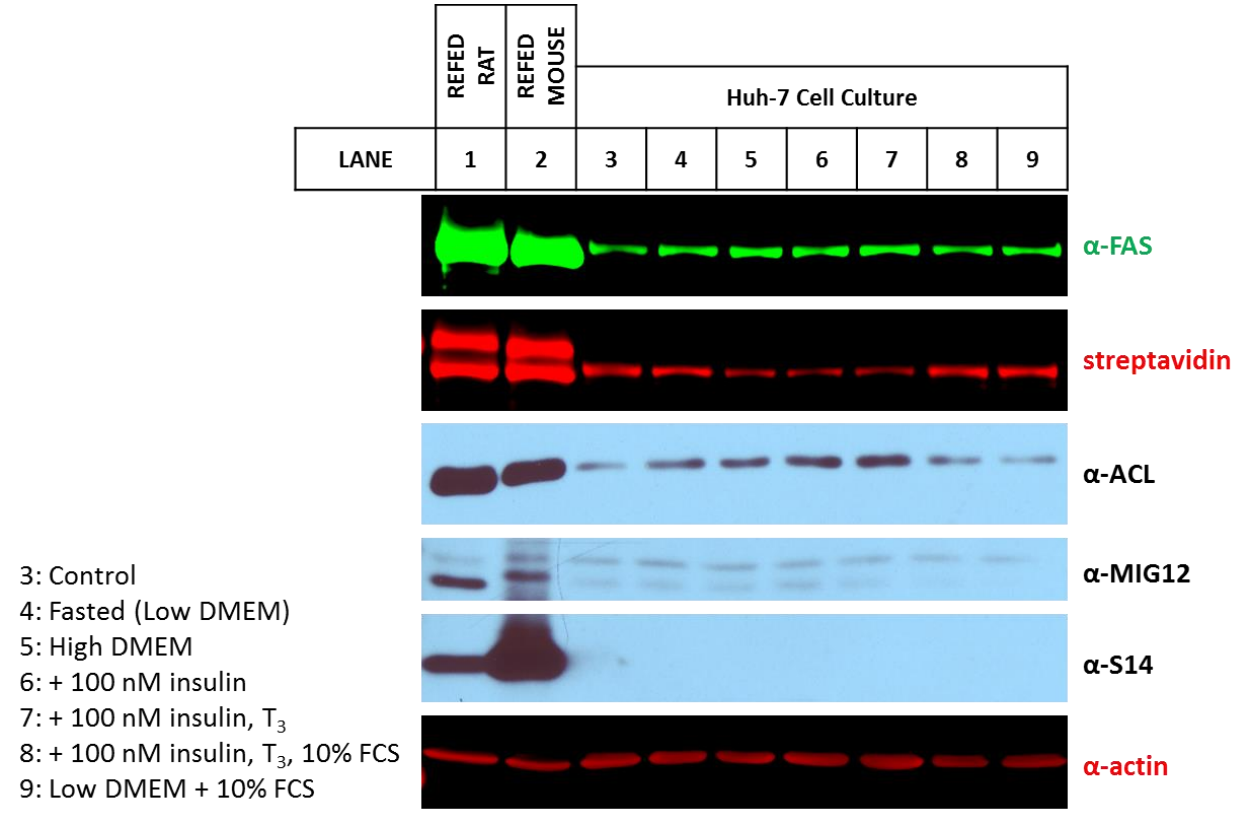

Figure 4-1. Lipogenic protein expression in cultured Huh-7 cells is not induced by glucose or insulin.
FFD refed rat and mouse liver cytosol (30 μg) or cytosol from Huh-7 cells (30 μg) treated with varying levels of glucose, insulin, T_3, and FCS was separated by SDS-PAGE using 5.5% and 13% polyacrylamide gels. Immunoblots were performed using antibodies as shown.

Subcellular ACC Filament Formation

To generate hepatocytes, livers of Sprague-Dawley rats between 1-3 months of age were perfused and digested with medium containing collagenase and dispase. Cells were then collected and sequentially centrifuged to remove contaminants, after which they were plated on glass coverslips at 37 °C and 5% CO_2. Once cultured, cells were fixed in 4% PFA alone or in combination with ice-cold 100% methanol. Blocking of fixed cells was performed at room temperature, but primary and secondary antibody incubation was performed at 37 °C for 30 minutes to allow for higher antigen selectivity as well as decreased sample background. Coverslips were mounted to slides in mounting media mixed with DAPI to visualize nuclei.

When hepatocytes from CHOW fed rats are stained with antibodies against ACC1, a unique subcellular pattern is visible. In addition to some cytosolic localization, ACC1 also localizes to numerous filamentous structures throughout hepatocytes **[Figure 4-2]**. These structures also co-localize with MIG12, but not FAS or ACL. It is likely that ACC1 filaments represent large polymeric aggregates that are bound to activating dimers of MIG12. These filaments co-localize perfectly with the endoplasmic reticulum, indicating a departure from the traditional assumption that ACC1 is exclusively cytosolic. They do not show localization to Golgi apparati, lysosomes, endosomes, or nuclei. ACC1 filaments do surround nuclei, but this signal also corresponds to perinuclear ER structures. Also, there is a possibility of overlap between ACC1 filaments and mitochondrial or cytoskeletal markers, but these data are less certain. It should be noted that fixation conditions had a significant influence on the immunofluorescent patterns seen and the efficacy of antibodies used. Fixation using 4% PFA in PBS buffer produced the most intense and numerous ACC1 filaments following immunofluorescence. Fixation using HBS buffer provided similar, though less specific, results,

while fixation with TBS significantly reduced immunofluorescence in all cells. Whether excess filament formation in PBS buffer has anything to do with phosphate ions or ACC1 phosphorylation remains to be determined.

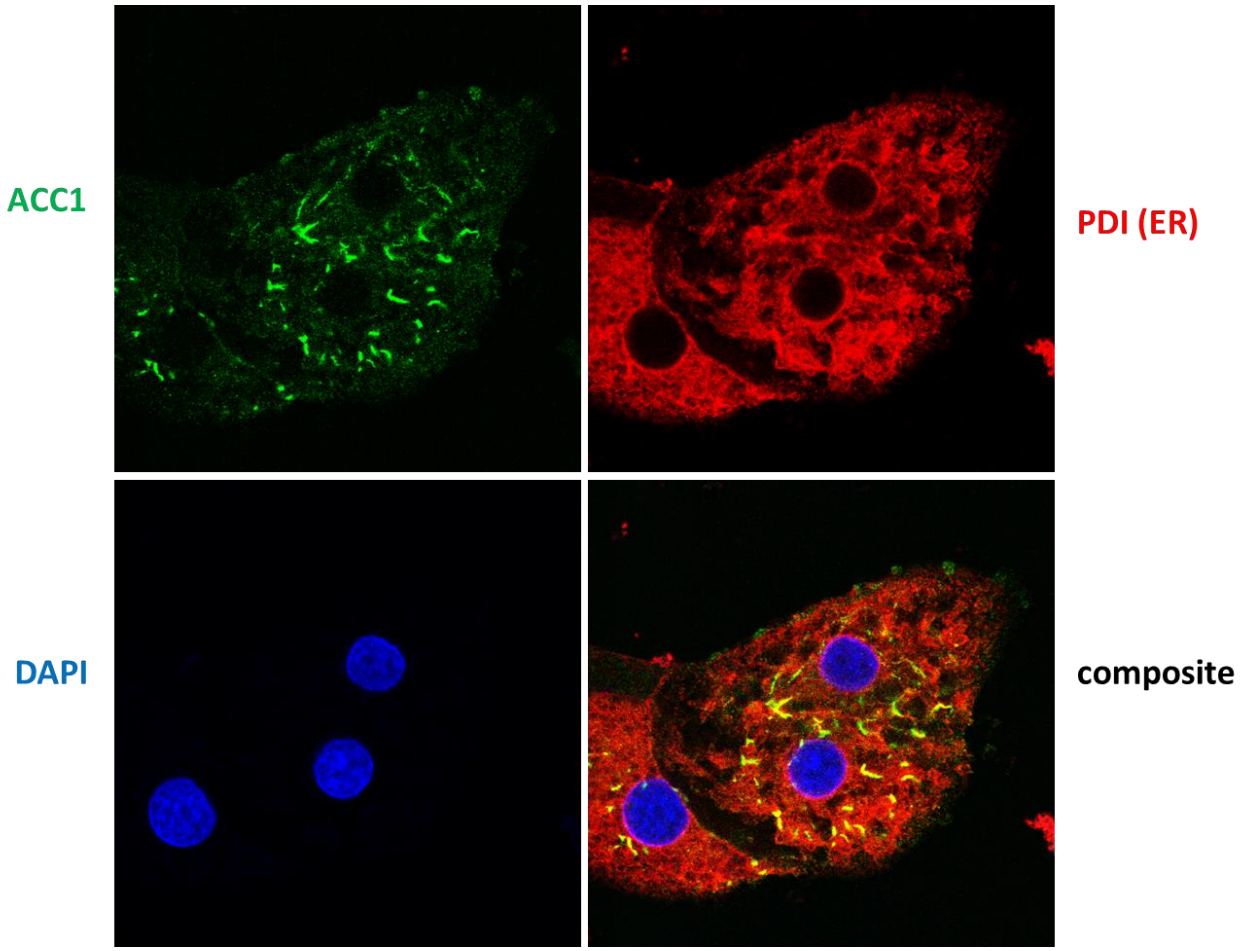

Figure 4-2. Immunofluorescence of rat primary hepatocytes shows ACC1 forms filamentous structures that co-localize with the endoplasmic reticulum.
Primary hepatocytes from CHOW fed rats were isolated and cultured on coverslips for 8 hours in complete M199, after which cells were fixed in 4% PFA/PBS and 100% MeOH. Samples were rehydrated and blocked in BSA and goat serum, and primary and secondary antibody incubation was performed at 37 °C for 30 minutes. Coverslips were mounted on slides using DAPI mounting media and sealed with nail polish. Immunofluorescence was visualized using a Leica SP5 confocal microscope.

The filaments with ACC1 and MIG12 may represent native cellular structures with a physiologic function, or they may simply be non-specific artifacts of hepatocyte isolation and fixation. To help clarify these possibilities, I tested whether these ACC1 filaments were responsive to carbohydrate and insulin signaling. After isolation and plating, hepatocyte culture was replaced with a low glucose medium lacking insulin or maintained on complete M199. Low glucose medium was also supplemented with 0.5 mM AICAR to induce ACC phosphorylation and inactivation. When rat primary hepatocytes are fed in this manner, ACC filaments disappear within 1.5 hours **[Figure 4-3]**. MIG12 signals that co-localize with these filaments also vanish. These results indicate subcellular ACC filaments are sensitive to signaling through SREBP-1c, ChREBP, and/or AMPK. This disappearance also indicates that preexisting ACC1 filaments might be depolymerized into stable dimers in the absence of active insulin and carbohydrate signaling. Alternatively, ACC1 filaments might be ubiquitinated and targeted for destruction through phosphorylation by AMPK. Indeed, phosphorylation has been shown as a prerequisite for ubiquitination in other protein systems.[76]

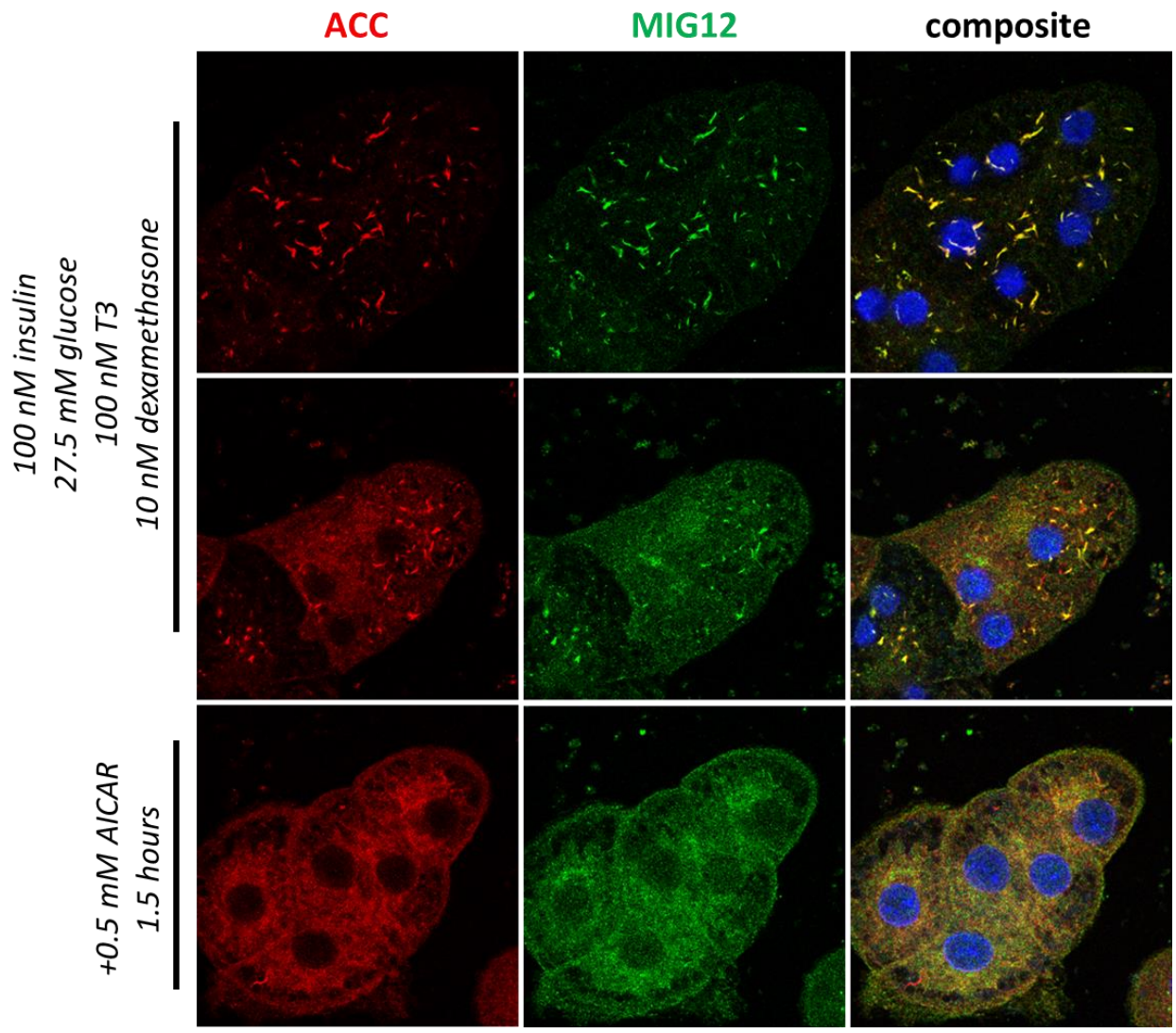

Figure 4-3. Effect of low glucose and AICAR on ACC and MIG12 filament formation. Primary hepatocytes from CHOW fed rats were isolated and cultured for 6.5 hours in complete M199. For AICAR treatment, medium was replaced with incomplete M199 supplemented with 0.5 mM AICAR. Experimental and control cells were incubated at 37 °C and 5% CO_2 for 1.5 hours. Cells were then fixed with 4% PFA/PBS, quenched with 10% glycine, and permeabilized with 0.2% IGEPAL. Blocking was performed at room temperature, after which cells were stained with primary antibodies for two hours and secondary antibodies for one hour. Mounting and confocal microscopy proceeded as described in *Methods*.

Subcellular Localization of Lipogenic Enzymes

As mentioned before, FAS and ACL do not localize to filaments immunoreactive to ACC and MIG12. Instead, when FAS and ACL are stained in hepatocytes isolated from CHOW fed rats, their subcellular localization remains largely cytosolic. Such dietary conditions, however, may not provide sufficient insulin signaling for putative lipogenic metabolon formation. Consequently, rats were fasted for 24 hours and refed for 48 hours on a high carbohydrate/fat-free diet, after which primary hepatocytes were prepared from intact livers. FAS and ACL immunofluorescence in these hepatocytes are recruited to ER networks throughout the cell **[Figure 4-4]**. Under these same conditions ACC1 localization is dramatically expanded as well, incorporating most of the visible ER and not just filamentous islands. Such strong and ubiquitous co-localization of ACL, ACC, and FAS with ER organelles efficiently links palmitate production and subsequent transfer to desaturases or elongases. However, such strong and ubiquitous co-localization can also be problematic for analysis. More specifically, in images that show a merge between large sections of two channels, immunofluorescent pixels that are not associated can appear to overlap. This is particularly true when optical or digital image resolution is low. To correct for this and verify FAS, ACL, and ACC1 do indeed massively co-localize with the ER, quantitative correlation analysis was performed on these data.[77] Background was subtracted from each image, and normalized Manders' and correlative Pearson's coefficients generated using the ImageJ plugin Co-localization Threshold. Normalized Manders' coefficients measure the total pixel overlap between two channels (represented as tM1 and tM2) and are reported as a percentage between 0 and 1. Pearson's correlation coefficients (PCC), on the other hand, represent the amount of signal between both channels that shows a

relationship between intensities. These values range from -1, or total exclusivity, to +1, or complete association.

Quantitative analysis results reinforce data observed with confocal microscopy – FAS, ACL, and ACC are highly correlated with the ER. FAS, ACL, and ACC signals each have normalized Manders' coefficients of 90% or higher when compared to ER signal **[Table 4-1]**. Furthermore, Pearson's correlation coefficients indicate strong positive connections between the intensities of these overlaps – PCC values are 0.6713 ± 0.0289, 0.7326 ± 0.0215, and 0.5400 ± 0.0184 for association of ER with FAS, ACL, and ACC, respectively.

Also of note is a unique subcellular pattern for both ACL and S14 when primary hepatocytes are isolated from FFD fed rats. In a significant proportion of cells, both show co-localization to the nucleus. These findings have been reported previously – ACL is thought to function as a source of nuclear acetyl-CoA for histone modification and gene regulation, while S14 is proposed to interact directly with transcription factors and regulate lipogenic gene expression.[78–80]

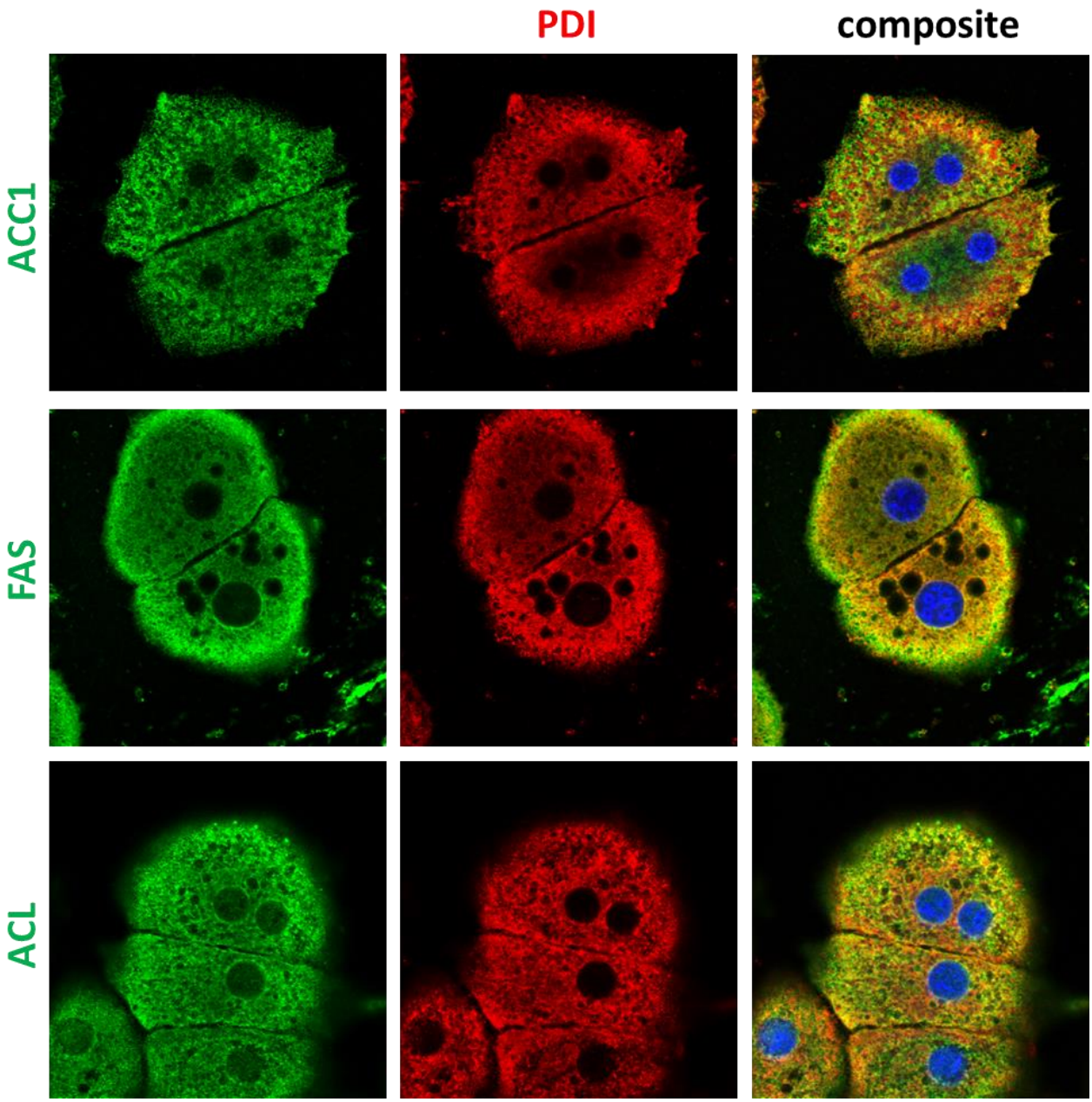

Figure 4-4. ACL, ACC, and FAS co-localize to the endoplasmic reticulum in primary hepatocytes isolated from rats refed on FFD.
Primary hepatocytes from rats fasted for 24 hours and refed on FFD for 48 hours were plated in complete M199 and incubated for 4 hours at 37 °C and 5% CO_2. Cells were fixed with 4% PFA/PBS and 100% MeOH. Following rehydration and blocking at room temperature, hepatocytes were stained with indicated primary and secondary antibodies for 30 minutes at 37 °C. Mounting and confocal microscopy were performed as described in *Methods*.

Table 4-1. Pearson's and Manders' coefficients for association of lipogenic enzymes with the ER.

	PCC	SEM	tM1	SEM	tM2	SEM
ACC	0.5400	±0.0184	0.9536	±0.0129	0.9598	0.0091
FAS	0.6713	±0.0289	0.9515	±0.0044	0.9295	0.0248
ACL	0.7326	±0.0215	0.9647	±0.0025	0.9595	0.0088

Though lipogenic enzymes and ER marker show clear co-localization, this relationship does not prove that overlap occurs between ACC, FAS, and ACL. To confirm the immunoprecipitation results observed in **Chapter 3** and establish that these subcellular reticular patterns represent a complex between ACC, FAS, and ACL, hepatocytes were co-stained with antibodies against lipogenic enzymes **[Figure 4-5]**. Immunofluorescence data reveals a significant amount of signal that overlaps between ACC and FAS or ACC and ACL. The pattern of overlap is consistent with ER marker staining seen in **Figure 4-4**; indeed, subcellular areas with less reticular structures appear to show less overlap between ACC and FAS or ACC and ACL. Also, under these conditions it appears that ACC is more specific to ER patterns than FAS or ACL, which stain more diffusely through hepatocytes. This may indicate a requirement for ACC to be recruited along the ER prior to FAS or ACL targeting. Such a conclusion would be consistent with findings that hepatocytes from CHOW fed rats show ACC filament staining along the ER, but cytoplasmic patterns of FAS and ACL.

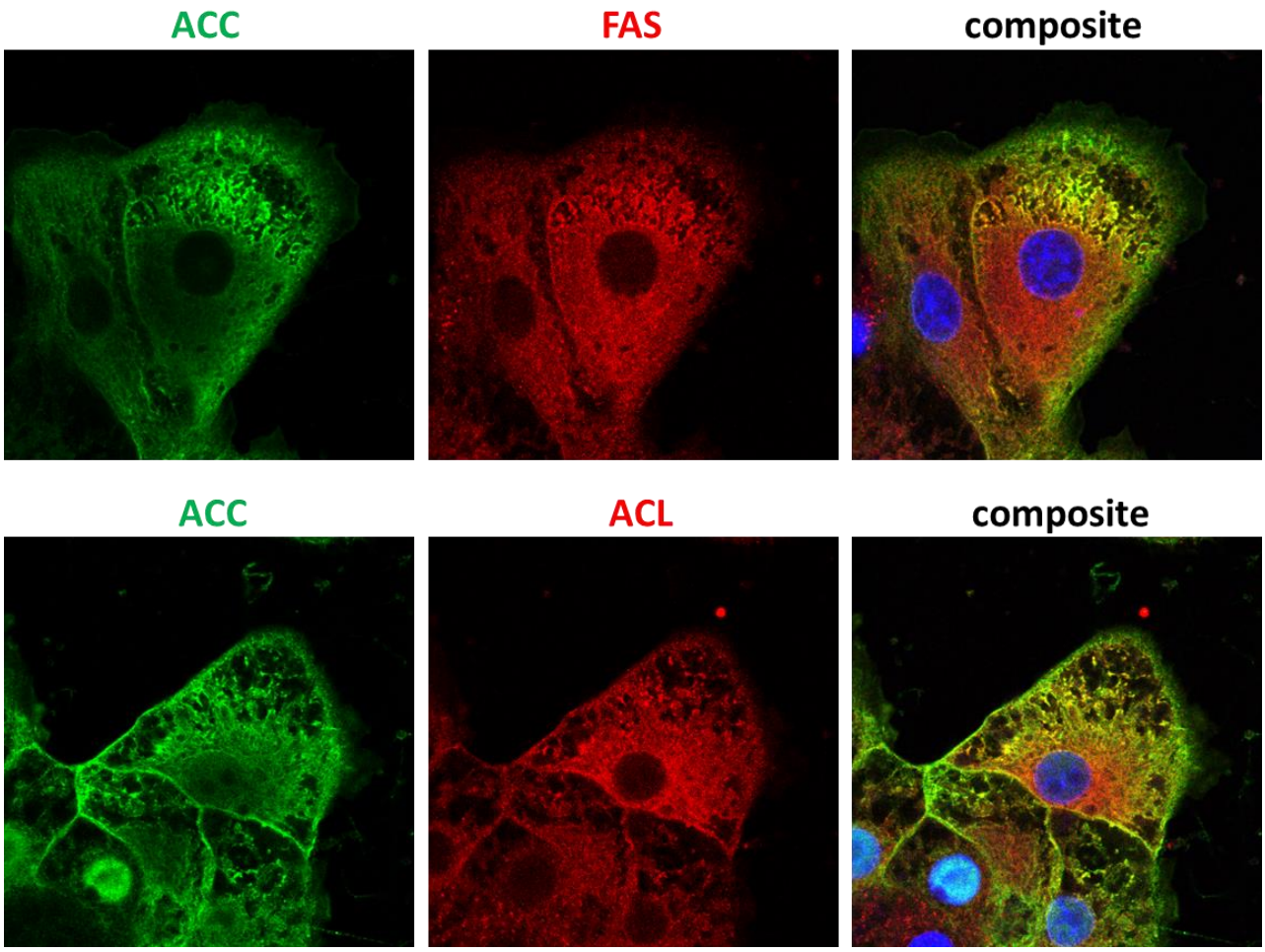

Figure 4-5. ACC co-localizes with FAS and ACL along reticular structures in rat primary hepatocytes.
Primary hepatocytes from rats refed on FFD were cultured for 8 hours in complete M199 at 37 °C and 5% CO_2. Cells were fixed with 4% PFA at room temperature for 30 minutes, then quenched with 1% glycine and permeabilized with 0.2% IGEPAL. Hepatocytes were stained with indicated antibodies for 2 hours at room temperature and washed thoroughly in PBST. Secondary antibody incubation was performed for 1 hour at room temperature. Mounting and imaging was performed as described in *Methods*.

If rats are fed a high carbohydrate/fat-free diet for an extended period of time, accumulation of triglycerides induces significant lipid droplet formation in livers and in isolated hepatocytes. Lipid droplets are triglyceride storage depots, thus upstream association of a fatty acid synthetic complex with these organelles might also occur. When lipid droplet laden hepatocytes were stained with antibodies against ACC, FAS, and ACL, localization of each lipogenic enzyme around lipid droplets was demonstrated **[Figure 4-5]**. These data are consistent with recent reports that the terminal acyltransferase DGAT can be induced to surround lipid droplets with oleate.[81] ACC staining patterns also appear to localize to smaller, more abundant lipid droplets, while FAS and ACL co-stain with larger lipid droplets that are sparser and more variable in size. This suggests that ACC associates with lipid droplets earlier in their morphological development than FAS or ACL. By extension, recruitment of fatty acid synthesis proteins to lipid droplets may require ACC as a foundation. Some experiments also show S14 localization around lipid droplets. Unfortunately, MIG12 immunofluorescence cannot be detected using the fixation methods required to preserve lipid droplet structure . While MIG12 localization around lipid droplets is likely given its close association with ACC, further experimentation is required for more conclusive proof.

For the images shown in **[Figure 4-6]**, Pearson's correlation coefficients for the co-localization of ACC, FAS, or ACL with the lipid droplet marker ADFP are 0.0.3121, 0.3559, and 0.3387, respectively **[Table 4-2]**. Though these data indicate clear positive association, lower PCC values are generated because a significant portion of ACC, FAS, and ACL signal localize to ER structures separate from lipid droplets. Under these circumstances, a better estimation of the relationship between two signals is from normalized Manders' coefficients. The tM2 values for

these data show that 74%, 90%, and 58% of total ADFP overlaps with signal from ACC, FAS, and ACL, respectively.

These findings duplicate previous mass spectrometry analyses that show ACC and FAS are present in various lipid droplet proteomes.[82] However, there are no reports about ACL or S14 association with lipid droplets. Nevertheless, co-localization of fatty acid synthetic enzymes around lipid droplets certainly supports the developing model of a lipogenic metabolon. This is particularly noteworthy given that current understanding of lipid droplet formation places their origins at the ER.

Table 4-2. Pearson's and Manders' coefficients for association of lipogenic enzymes with lipid droplets.

	PCC	tM1	tM2
ACC	0.3121	0.7035	0.7446
FAS	0.3559	0.8189	0.9045
ACL	0.3387	0.4479	0.5757

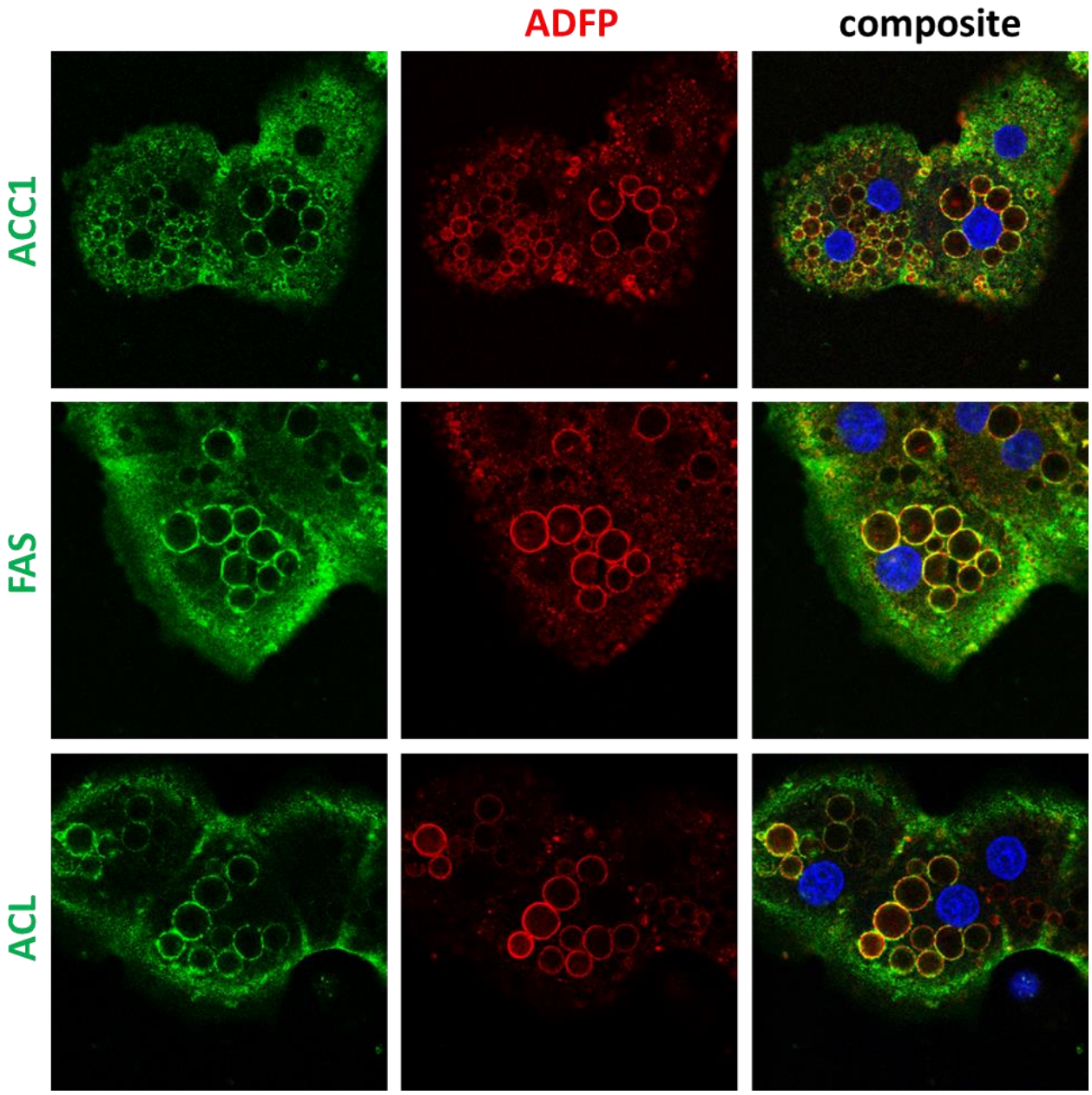

Figure 4-6. ACL, ACC, and FAS co-localize around lipid droplets in primary hepatocytes isolated from rats fed long-term on FFD.
Primary hepatocytes were isolated from FFD fed rats and plated in complete M199 for 8 hours. Cells were fixed in 4% PFA/PHEM and 100% MeOH. Rehydration and blocking were performed at room temperature, and staining with indicated primary and secondary antibodies proceeded for 30 minutes at 37 °C. Mounting and confocal microscopy protocol was followed as outlined in *Methods*.

These data, however, also pose a dilemma for my working hypothesis. Subcellular localization of ACC, FAS, ACL, and S14 around lipid droplets certainly supports the existence of a lipogenic complex that is active at sites of triglyceride synthesis and storage. However, the most accepted model of lipid droplet formation suggests that triglycerides are stored between the bilayers of the ER, and that the morphology of mature lipid droplets consists of only a single membrane layer around the lipid core. This means that the desaturases and elongases, which are integral proteins spanning the entire bilayer of the ER, cannot localize to lipid droplets in this model. This, in turn, would limit the efficiency of palmitate modification and stunt growth of immature lipid droplets. Current developments in lipid droplet morphology, however, are mostly derived from *Drosophila* and yeast data.

To determine whether lipid droplets follow this same model in mammalian cells, rat primary hepatocytes fed long term on a high carbohydrate and fat free diet were isolated, plated, and stained with antibodies against the ER luminal marker PDI. Surprisingly, under these conditions lipid droplets are surrounded by bilayered ER structures, as evidenced by strong PDI staining **[Figure 4-7]**. ACC, FAS, and ACL also localize to the ER around lipid droplets in these experiments. These findings suggest that, at least in insulin-responsive hepatocytes, lipid droplets formed *de novo* are enveloped in complete branches of the ER. Such structure allows for a more direct association of SCD1 and ELOVL6, as well as PAP, AGPAT, and DGAT, with developing and mature lipid droplets.

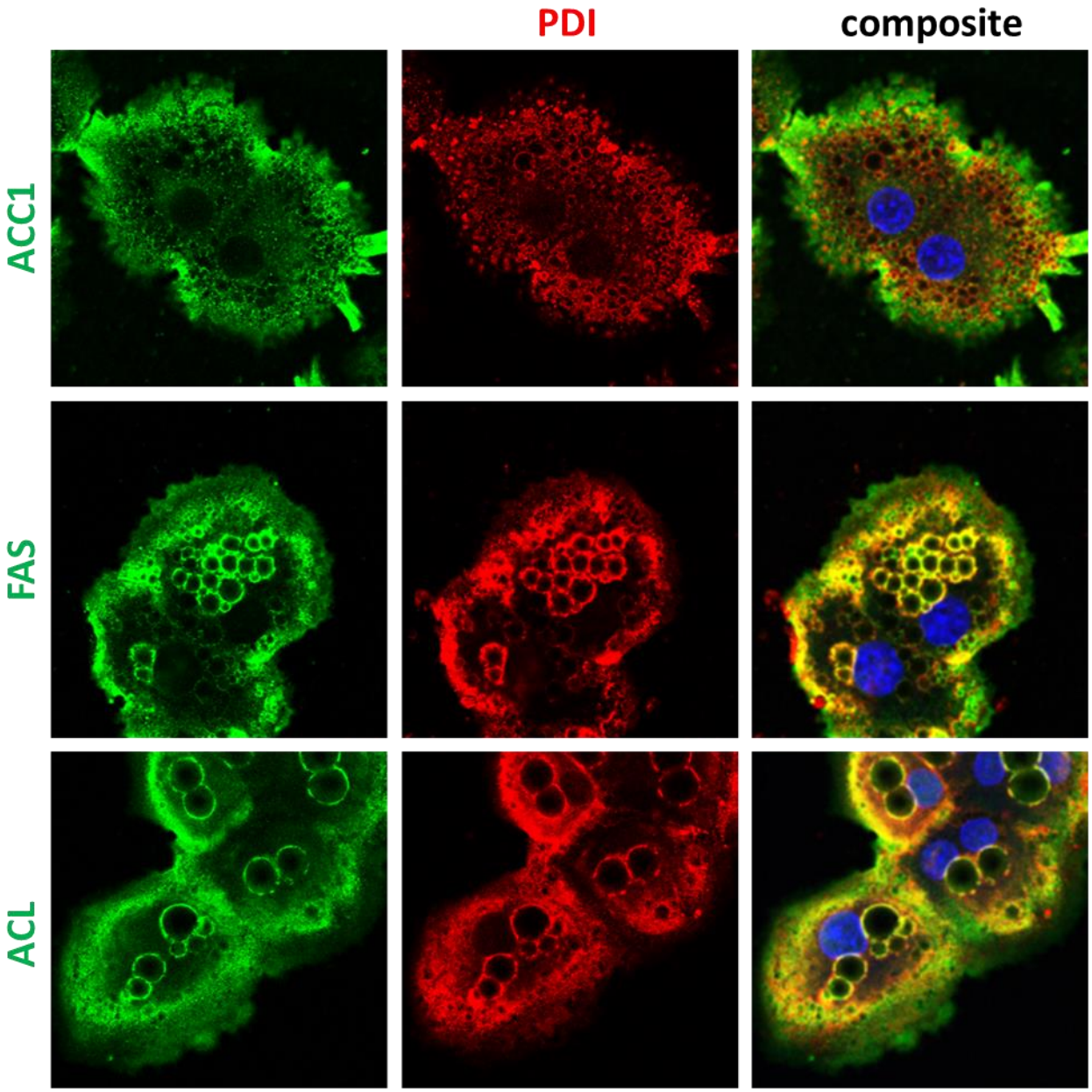

Figure 4-7. Luminal ER marker co-localizes with lipogenic enzymes around lipid droplets in hepatocytes.

Primary hepatocytes from FFD fed rats were isolated and cultured for 4 hours in complete M199 on glass coverslips. Cells were fixed in 4% PFA/PHEM and 100% MeOH. Rehydration and blocking were performed at room temperature, and cells were stained with antibodies against enzymes (green) and ER lumen (red) for 30 minutes at 37 °C. Coverslip mounting and confocal microscopy protocol was followed as described in *Methods*.

Co-Localization of ACC1 and ACC2

To completely coordinate triglyceride production, lipogenic complex formation and localization to the endoplasmic reticulum or lipid droplets is insufficient. Following elongation and desaturation at the ER, fatty acids are further modified and conjugated to glycerol by acyltransferases and lipases. While the terminal steps of triglyceride synthesis are also bound to the ER, recent studies have found that conjugation of fatty acids to the *sn-1* position of glycerol occurs in hepatocytes by GPAT1 – an acyltransferase isoform that localizes to the mitochondria.[83] Other experiments have also shown that the second isoform of DGAT – the terminal acyltransferase that adds a third fatty acid to diglycerides – can localize to the mitochondria. Generally DGAT is targeted to the ER; however, DGAT2 contains a small peptide sequence that also promotes recruitment to mitochondrial membranes.[84] This localization is even present around lipid droplets when cells are supplemented with oleate.

These data suggest that triglyceride synthesis at its most efficient would utilize a juncture between the ER and mitochondria. Such an interface has been shown to exist – mitochondrial associated membranes (MAMs) of the ER are connected to mitochondria by binding of several different integral protein partners that localize to either organelle. MAMs have been shown to have several important cellular functions, including caspace cascade formation, induction of mitochondrial fission, and calcium homeostasis.[85] They have even been implicated in lipid metabolism. Other evidence supports the role of mitochondria in triglyceride production. For example, ACC2, an isozyme of ACC1, binds to the outer leaflet of the mitochondria.[70] Aforementioned data supports that ACC2 is also capable of binding to ACC1 and other lipogenic proteins **[see Chapter 3]**. Immunocytochemistry of ACC2 in hepatocytes derived from CHOW fed rats also shows localization to filamentous structures. Immunocytochemistry of ACC1 and

ACC2 under these same conditions shows that both enzymes completely co-localize with one another along cellular filaments **[Figure 4-8]**. Because subcellular localization of ACC2 has been shown at the mitochondria, and given previous data that shows ACC1filaments localize to the ER, these structures represent a population of proteins likely present at MAMs.

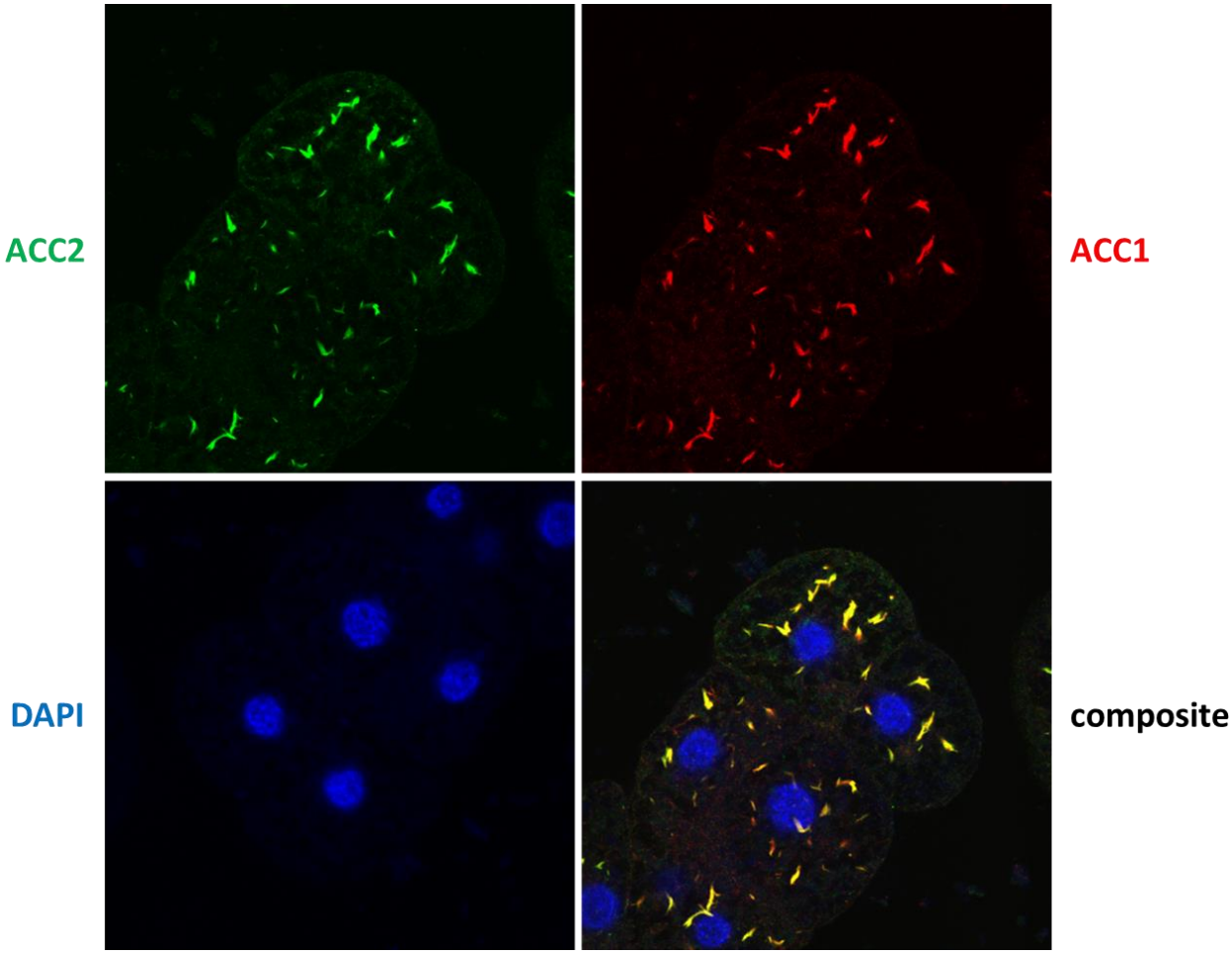

Figure 4-8. **ACC2 co-localizes with ACC1 filaments in rat primary hepatocytes.**
Primary hepatocytes from CHOW fed rats were isolated and cultured on glass coverslips for 8 hours. Cells were fixed in 4% PFA/PBS, quenched in 10% glycine, and permeabilized with 0.2% IGEPAL. Blocking was performed at room temperature, after which hepatocytes were stained with primary antibodies against ACC2 (green) and ACC1 (red) for 2 hours. Samples were incubated with secondary antibodies for 1 hour. Coverslips were mounted using DAPI mounting media and imaged using confocal microscopy.

To further establish an interaction between ACC1 and ACC2, constructs expressing both proteins bound to separate epitope tags were transiently transfected into CHO-K1 cells. Because previous experiments **[Figure 3-6]** showed that co-transfection of ACC1 with ACC2 reduces overall expression of ACC1, ACC1 constructs were used at concentrations 6x higher than ACC2. Cells were cultured for 24 hours and stained with antibodies against HA or Myc. When alone, overexpressed ACC1-3x HA localizes to the cytosol of CHO-K1 cells. This is expected given the lack of insulin sensitivity in these cultures. ACC2-5x-Myc by itself shows complete overlap with mitochondrial marker, consistent with previous reports. When co-transfected with ACC2-5x-Myc, however, a significant portion of ACC1-3x HA signal shifts from the cytosol to mitochondria **[Figure 4-9]**. Since ACC1 is incapable of such localization by itself, these data suggest that a heterodimer between ACC1 and ACC2 forms that is capable of tethering to the outer mitochondrial membrane. It also supports the possibility that ACC filaments represent a junction between the ER and mitochondria. Thus, ACC1 and ACC2, and likely the lipogenic metabolon, is recruited to MAMs during fatty acid synthesis. Furthermore, metabolon targeting to the MAM might require heterodimer formation between ACC1 and ACC2, though further experimentation is required.

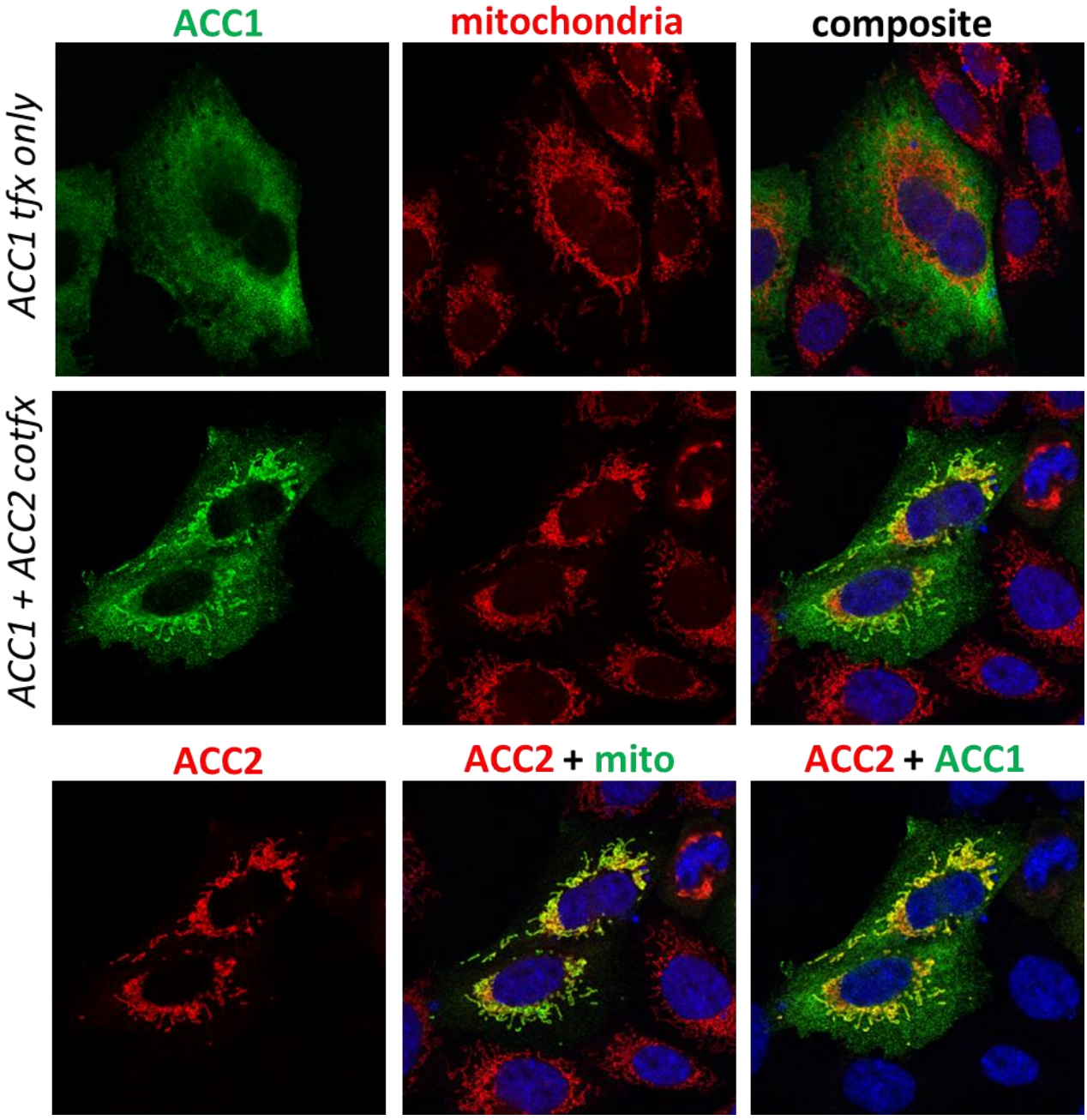

Figure 4-9. Co-transfection of ACC1 with ACC2 induces relocalization of ACC1 from the cytoplasm to mitochondria.
CHO-K1 cells were transfected with ACC1-3x HA (6 μg) and ACC2-5x Myc (1 μg) alone or in combination and cultured for 24 hours at 37 °C and 8.8% CO_2. Prior to fixation, cells were treated with 300 nM mitotracker for 30 minutes. Cells were fixed with 4% PFA/PBS, quenched in 10% glycine, and permeabilized with 0.2% IGEPAL. After blocking at room temperature, cells were stained with antibodies against HA (ACC1) and Myc (ACC2) for 2 hours. Secondary antibodies were incubated with cells for 1 hour, and coverslips were mounted in DAPI mounting media overnight. Confocal microscopy was followed as outlined in *Methods*.

Lipogenic Enzyme Targeting to Mitochondrial Associated Membranes

To conclusively verify that lipogenic proteins co-localize to markers specific for the MAM, plated hepatocytes were stained with mitofusin-2, an integral ER protein essential for tethering with mitochondria. Unfortunately, the antibody had no reactivity in rat tissue. To adjust for this, mouse primary hepatocytes were used instead. Because they show significantly less sensitivity to insulin once plated, mouse primary hepatocytes were fixed immediately after attaching to coverslips (2 hours incubation). Mouse hepatocytes were then blocked and stained with antibodies against mitofusin-2, as well as antibodies against ACC1, ACC2, FAS, and ACL. As shown in **Figure 4-10,** ACC1 and ACC2 completely co-localize with mitofusin-2 in mouse primary hepatocytes, and that certain populations of cells also show co-localization of FAS or ACL and mitofusin-2. Filaments similar to those seen in rat primary hepatocytes could be visualized for ACC1 and ACC2 in mouse tissue. These filaments overlapped mitofusin-2 signal as well. Furthermore, in primary hepatocytes isolated from ACC1 and ACC2 double knockout mice, ACC1 and ACC2 signal was completely absent on immunofluorescence. Knockout of both ACC1 and ACC2 did not influence FAS or ACL localization, indicating that recruitment of these lipogenic enzymes to the MAM occurs independent of one another.

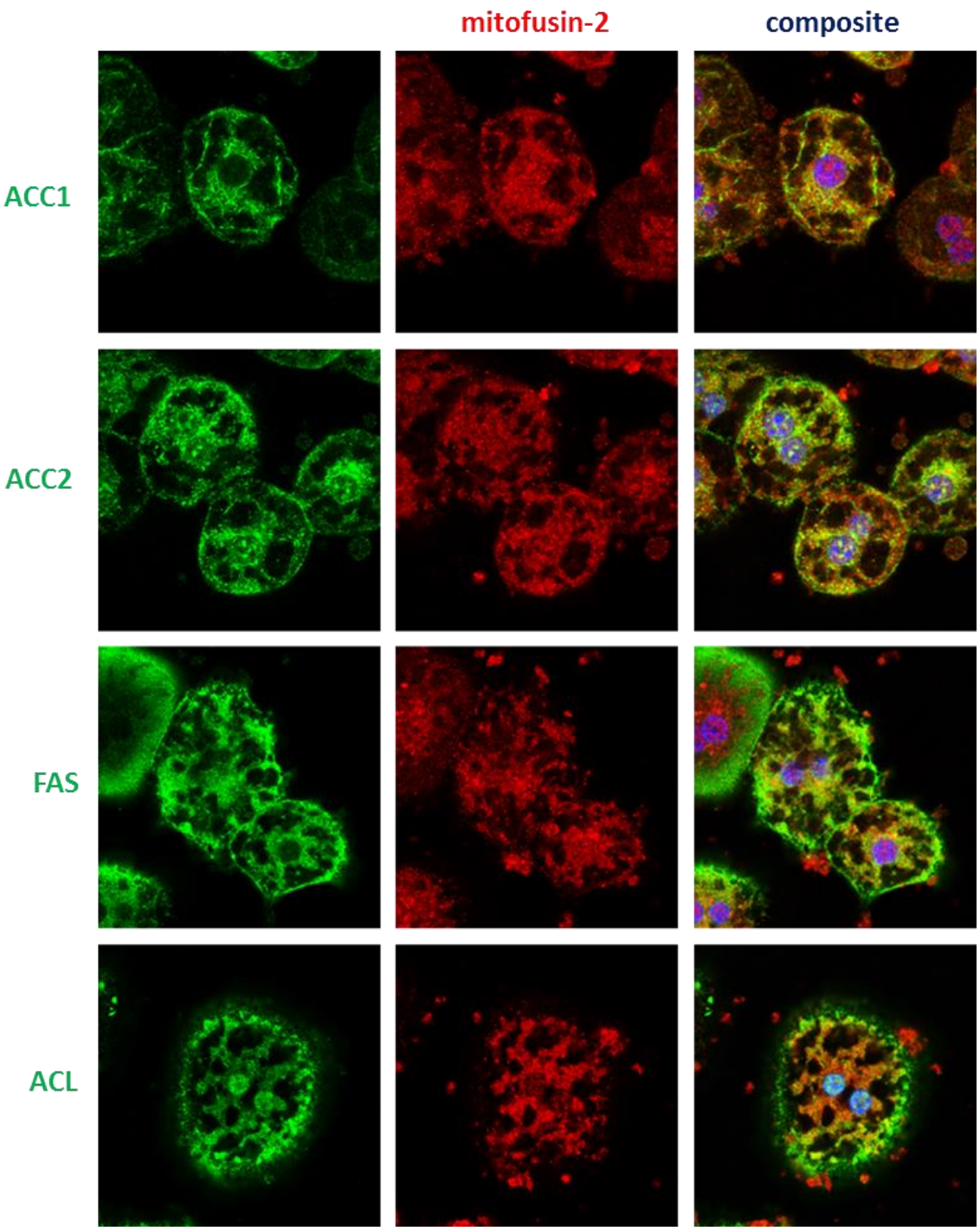

Figure 4-10. Lipogenic enzymes co-localize with the MAM marker mitofusin-2 in mouse primary hepatocytes.
Primary hepatocytes from FFD fed mice were isolated and plated on glass coverslips for 2 hours. Cells were then fixed in 4% PFA/PBS and 100% MeOH. Primary antibodies against lipogenic enzymes (green) or MAM marker mitofusin-2 (red) were bound to hepatocytes for 30 minutes at 37 °C. Cells were also treated with secondary antibodies for 30 minutes and 37 °C. Coverslips were mounted and imaged using confocal microscopy as described in *Methods*.

Summary

Subcellular localization of putative components in the lipogenic metabolon model reinforces biochemical findings. Rather than being exclusively cytosolic as previously held, ACC, FAS, and ACL are significantly enriched along the ER when hepatocytes are treated with glucose and insulin **[Figure 4-4]**. In particular, ACC1 forms subcellular filaments also co-localize with MIG12 **[Figure 4-2]**. These likely represent aggregations of active polymers, though it is uncertain what causes them to target the ER. Importantly, ACC2, which has been demonstrated to bind mitochondria, also co-localizes along these filaments and can induce ACC1 mitochondrial targeting when overexpressed **[Figures 4-8 and 4-9]**. It is possible ACC1:ACC2 heterodimers function to recruit metabolon components to mitochondrial associated membranes. This would allow palmitate production to occur in close proximity with subsequent enzymes involved in triglyceride synthesis. Lipogenic enzymes also surround lipid droplets in hepatocytes isolated from rats on FFD **[Figure 4-6]**. Although these lipid droplets are enveloped by complete ER structure, it remains to be determined whether mitochondria are associated as well. Alternatively, triglyceride synthesis on lipid droplets may use a different GPAT isoform, GPAT4, which has been localized to these structures.[81] Regardless, these data demonstrate that ACC, FAS, ACL, MIG12 and S14 are spatially and temporally capable of binding to one another *in vivo*, and that their co-localization facilitates the transfer of intermediates to each subsequent enzyme.

CHAPTER FIVE: ROLE OF MICROTUBULES IN LIPOGENIC COMPLEX STABILITY AND FUNCTION

Experiments in COS-7 cells have shown that, in addition to static protein interactions, microtubules serve as a substrate for attachment between mitochondria and the endoplasmic reticulum.[86] It has been previously established that microtubules function in the dynamic growth of the endoplasmic reticulum.[87] Microtubules are also important for the structural stability and movement of mitochondria. Friedman and colleagues[86] have recently shown that a subset of microtubules – those that have been post-translationally acetylated – act in the dynamic mobility of MAMs within the cell. Other findings also implicate microtubules as important for fatty acid and triglyceride biosynthesis.

For instance, MIG12 was initially identified as an important microtubule binding protein during midline and neural tube development in embryogenesis.[31,32] Specifically, MIG12 interacts with the protein MID1 to stabilize acetylated microtubules. In addition, studies in hepatocytes to determine subcellular localization of ACC identified significant interactions with cytoskeletal fractions. When hepatocytes are treated with colchicine, a microtubule disrupting reagent, and then permeabilized with digitonin, more ACC is released from the cells upon centrifugation.[88] The opposite is seen if the hepatocytes are treated with paclitaxel, a microtubule stabilizing reagent. Also, colchicine and GTP have been shown to inhibit or enhance the polymerization of ACC – results similar to their effect on tubulin itself.[89] Moreover, knockdown of acetylated microtubules in adipose tissue inhibits cellular differentiation and storage of triglycerides.[90] Glycolytic enzymes also use microtubules as a scaffold to enhance their interaction and activity.[56] Such a model is strikingly similar in form and function to putative lipogenic complexes. Finally, as mentioned previously, when S14 is overexpressed in

rat primary hepatocytes, isoforms of tubulin are significantly enriched in S14 co-immunoprecipitation products **[Table 3-1]**.

Co-Localization of Lipogenic Enzymes and Microtubules

To investigate a possible relationship between lipogenic proteins and microtubules in the cell, I first determined whether co-localization could be visualized using immunofluorescence. Primary hepatocytes were isolated from rats fasted for 24 hours and refed for 48 hours on a high carbohydrate/fat-free diet. The hepatocytes were isolated, fixed, and stained with antibodies directed against β-tubulin and ACC, FAS, or ACL. Confocal imaging revealed extensive overlap in the subcellular localization of lipogenic enzymes and microtubules **[Figure 5-1]**. Pearson's correlation coefficients reinforce these observations. PCC values for ACC, FAS, or ACL with β-tubulin are 0.4158 ± 0.0356, 0.5337 ± 0.0139, and 0.4134 ± 0.0496, respectively **[Table 5-1]**. Presumably this same staining pattern co-localizes with the ER and, at MAM locations, mitochondria. .

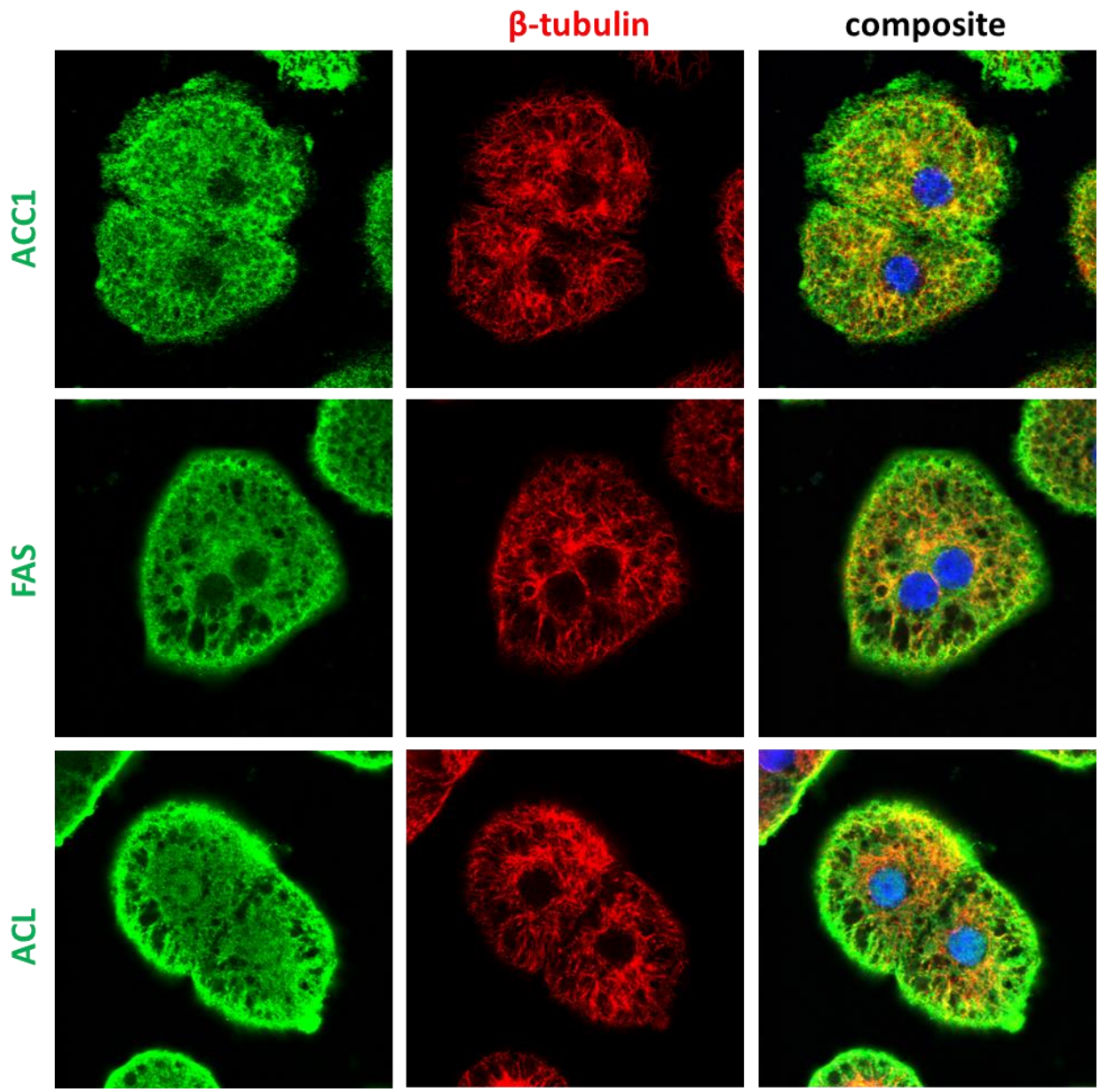

Figure 5-1. Lipogenic enzymes co-localize with microtubules in rat primary hepatocytes. Primary hepatocytes from FFD fed rats were isolated and cultured on glass coverslips for 8 hours at 37 °C and 5% CO_2. Cells were fixed in 4% PFA/PBS and 100% MeOH. Following rehydration and blocking, cells were stained with primary and secondary antibodies against lipogenic enzymes (green) or β-tubulin (red). Mounting and confocal microscopy were followed as outlined in *Methods*.

Table 5-1. Pearson's and Manders' coefficients for association of lipogenic enzymes with microtubules.

	PCC	SEM	tM1	SEM	tM2	SEM
ACC	0.4158	±0.0356	0.9570	±0.0079	0.9441	0.0092
FAS	0.5337	±0.0139	0.9297	±0.0076	0.9500	0.0034
ACL	0.4134	±0.0496	0.9320	±0.0066	0.9462	0.0072

When rats are fed a high carbohydrate/fat-free diet for longer periods of time, microtubules co-localize with ACC1, FAS, ACL, and the ER around lipid droplets. These data reinforce known associations of microtubules with lipid droplets. For instance, Boström and colleagues[91] have shown in 3T3 cells and *in vitro* systems that disrupting microtubules with nocodazole impairs lipid droplet fusion and growth. Given the subcellular co-localization of ACC, FAS, and ACL, microtubules may be involved in regulating these dynamics. Furthermore, in my experiments replacing complete M199 with unsupplemented M199 causes lipid droplets, as well as enzyme and microtubule co-lozalization around them to disappear **[Figure 5-2]**. In addition, total co-localization between ACC1, FAS, or ACL and microtubules decreases once glucose and insulin are removed from culture conditions.

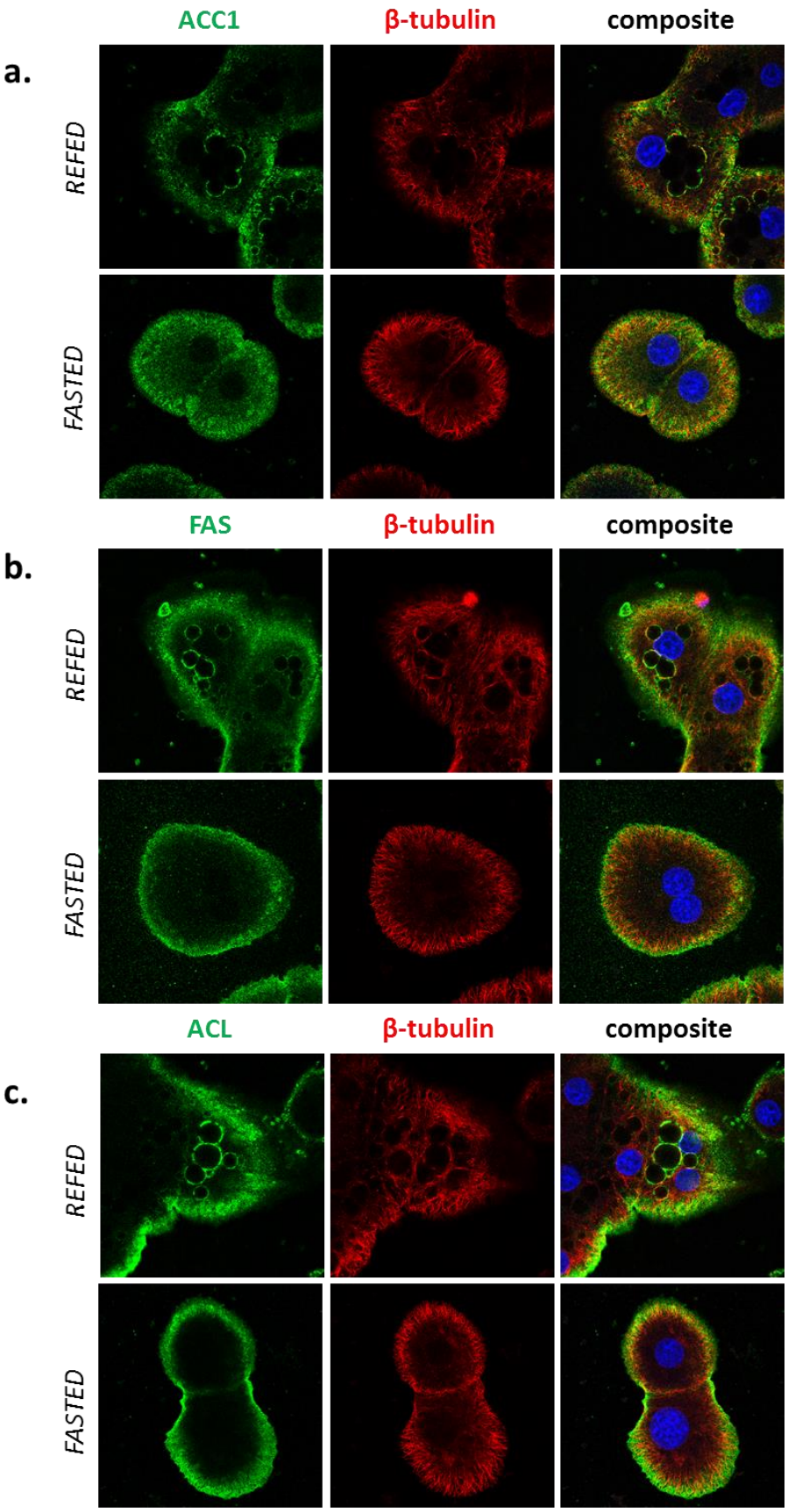
a.
ACC1
β-tubulin
composite
REFED
FASTED
b.
FAS
β-tubulin
composite
REFED
FASTED
c.
ACL
β-tubulin
composite
REFED
FASTED

Figure 5-2. Co-localization of microtubules with ACC, FAS, or ACL around lipid droplets is disrupted under fasting conditions.
Primary hepatocytes from FFD fed rats were isolated and plated in complete M199 or unsupplemented M199 for 8 hours. Coverslips were removed and fixed in 4% PFA/PHEM and 100% MeOH. After rehydration and blocking, cells were stained with primary and secondary antibodies against lipogenic enzymes (green) or β-tubulin (red) for 30 minutes at 37 °C. Mounting and confocal imaging protocol was followed as outlined in *Methods*.

In Vitro Precipitation of Microtubules and Associated Proteins

ACC1, FAS, and ACL subcellular localization overlaps with microtubules. This association appears to be responsive to normal dietary stimuli like carbohydrate and insulin signaling. These data do not, however, establish that physical interaction occurs between components of a putative lipogenic metabolon and the cellular cytoskeleton. To identify whether microtubules directly bind lipogenic proteins, microtubules of a uniform length were prepared from purified bovine tubulin. Microtubules were supplemented with taxol to prevent dynamic collapse at room temperature. Purified recombinant ACC1, FAS, ACL, MIG12, and S14 were combined and incubated with microtubules at room temperature for 30 minutes to facilitate binding. The reaction mixture was centrifuged through a gradient of 60% glycerol to separate microtubules and interacting proteins from recombinant proteins with no affinity. Pellets beneath the glycerol buffer were collected, denatured, and analyzed using SDS-PAGE. Comparison of supernatant and pellet fractions reveal that, while a significant portion of lipogenic proteins precipitate under these conditions, no difference is observed between samples with or without exogenous microtubules.

These data suggest that purified recombinant ACC1, FAS, ACL, MIG12, and S14 do not physically bind microtubules under the conditions tested. However, it is possible that during purification, cofactors or associated proteins necessary for interaction with microtubules are removed. It is also possible that endogenous MAPs removed during the process of bovine

tubulin purification may be necessary for microtubule association with a lipogenic complex. Furthermore, post-translational modifications necessary for interaction with microtubules may not be made on recombinant proteins during production in *sf-9* insect cells. The machinery for modifications like acetylation, methylation, and phosphorylation also differs somewhat between mammalian and insect cells and phosphorylation is a necessary prerequisite for binding of many known microtubule associated proteins (MAPs) to intact microtubules.

Non-specific precipitation observed (particularly with ACC1) might be the effect of instability of purified proteins at room temperature or in PIPES reaction buffers. However, it might also represent the subtle aggregation of protein oligomers in a metabolon. Similar autonomous aggregation was also seen previously in immunoprecipitation experiments of endogenous proteins in refed mouse and rat liver cytosol **[Figure 3-4]**.

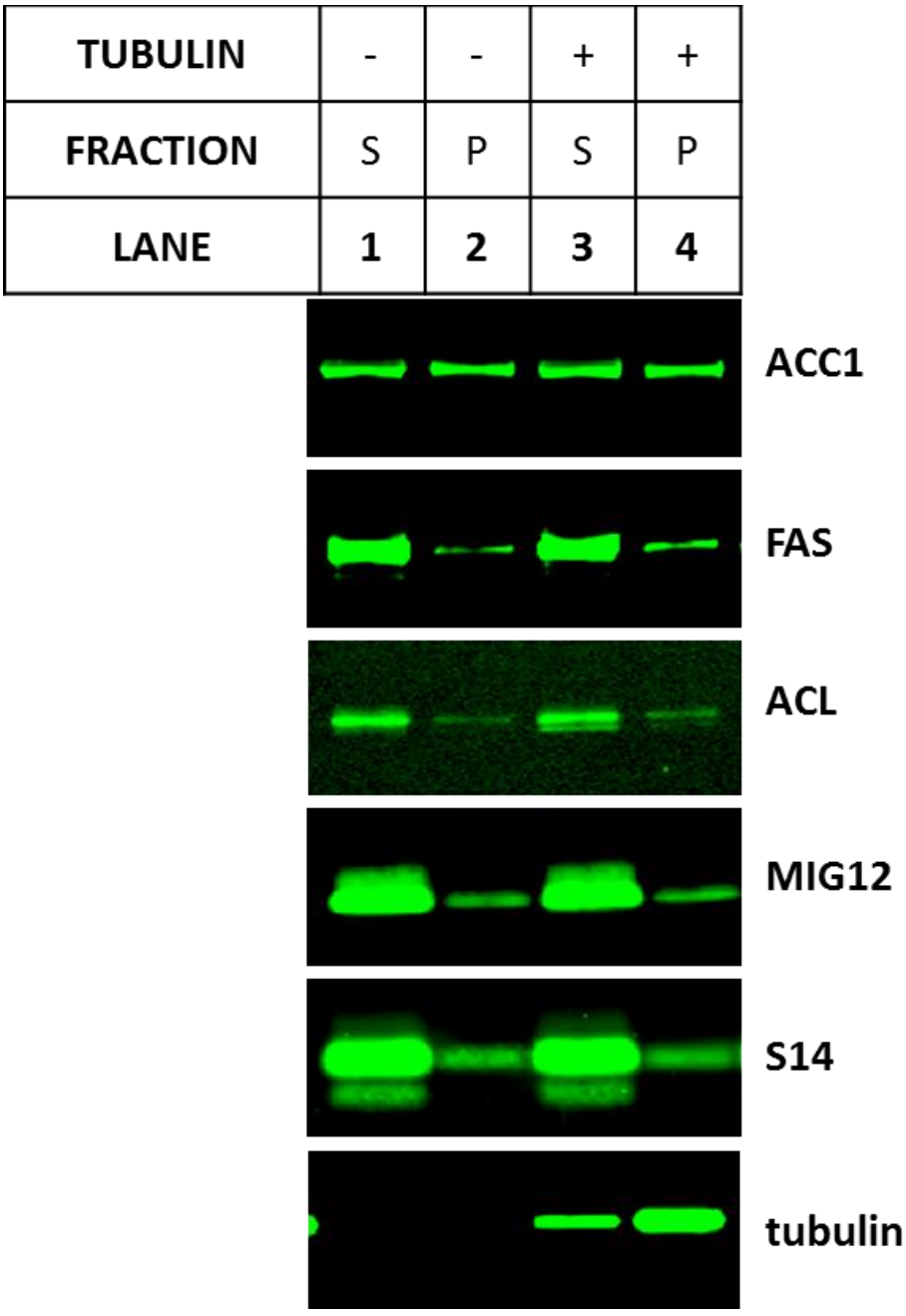

Figure 5-3. Purified recombinant lipogenic proteins do not bind to microtubules.
Purified bovine tubulin was polymerized at 37 °C and made stable by the addition of taxol. Purified recombinant ACC1, FAS, ACL, MIG12, and S14 were equilibrated to room temperature and mixed with stable microtubules for 30 minutes. Mixtures were then ultracentrifuged through a 60% glycerol gradient for 45 minutes at 100,000 x *g*. Pellet and supernatant samples were collected, separated using SDS-PAGE, and immunoblots generated using the rabbit polyclonal antibodies indicated.

To replace potential missing post-translational modifications such as phosphorylation, endogenous proteins in liver cytosol from FFD refed mice were used. Cytosol was generated after adding varying concentrations of digitonin and DTT to liver lysates. This step was performed to dissociate any pre-formed lipogenic aggregates from microsomal and mitochondrial fractions. In addition, purified bovine tubulin prepared to retain native MAPs was polymerized to generate a stable population. Mouse liver cytosol was warmed to 37 °C for 20 minutes to mimic physiologic temperature, then combined at room temperature with stable microtubules + MAPs for 30 minutes. As before, each reaction was centrifuged through a 60% glycerol buffer and the microtubule binding fraction visualized after SDS-PAGE by immunoblotting.

Under these conditions, there is enrichment of the lipogenic proteins ACL, FAS, ACC, and S14 in pellets containing precipitated microtubules + MAPs **[Figure 5-4]**. In addition, amounts of lipogenic proteins in these pellets are significantly greater than those in non-specific precipitates lacking microtubules. This suggests that enzymes involved in fatty acid synthesis physically interact with microtubules. It also suggests that post-translational modifications or yet undefined associations with native MAPs are required for this binding and lipogenic metabolon formation.

	negative control						microtubules + MAPs					
DTT (mM)	0			2			0			2		
digitonin (mg/mL)	0.1	0.6	1.2	0.1	0.6	1.2	0.1	0.6	1.2	0.1	0.6	1.2
LANE	1	2	3	4	5	6	7	8	9	10	11	12

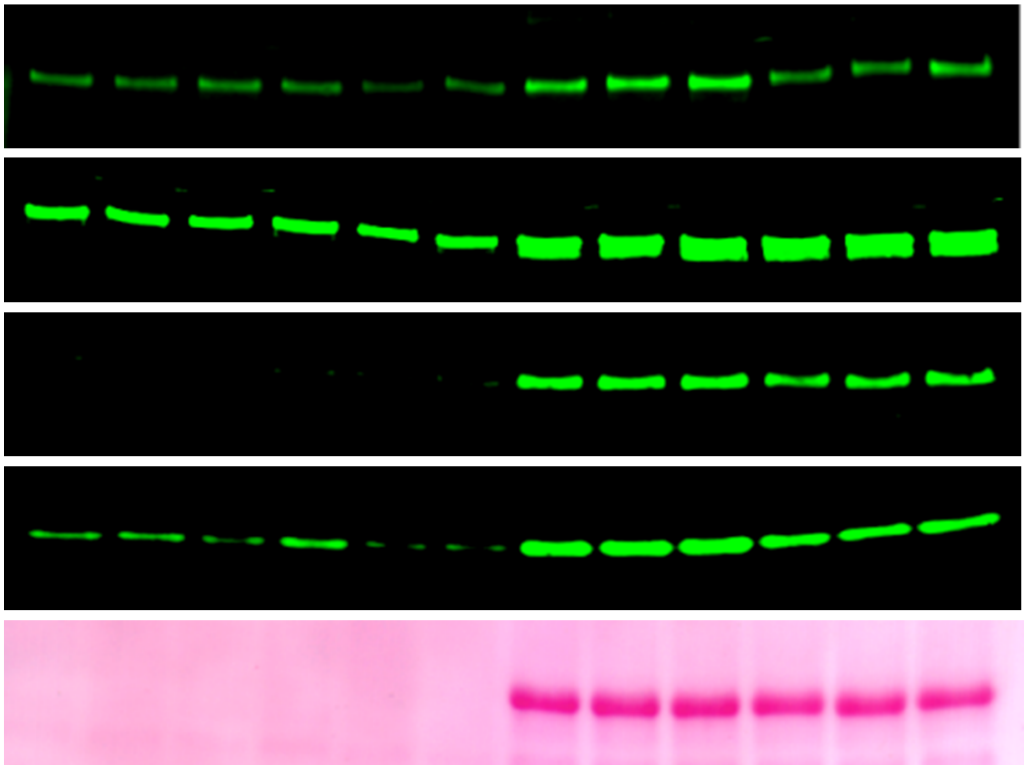

Figure 5-4. Stable polymerized microtubules with MAPs precipitate endogenous lipogenic proteins from mouse liver cytosol.
Liver lysates from FFD fed mice were treated with increasing concentrations of DTT and digitonin. Following short incubation, lysates were clarified by ultracentrifugation at 100,000 x *g* for 30 minutes. Cytosol was collected and warmed to 37 °C for 20 minutes, then combined with stable populations of microtubules and MAPs at room temperature for 30 minutes. Reaction mixtures were overlaid on 60% glycerol buffers and ultracentrifuged at 100,000 x *g* for 40 minutes. Pellets and supernatants were collected and separated using SDS-PAGE, and immunoblots against various lipogenic proteins generated.

Effect of Nocodazole and Taxol on Fatty Acid Synthesis

To confirm the association of lipogenic proteins with microtubules is physiologic and not an *in vitro* artifact, microtubules were stabilized or disrupted and the effect on co-localization patterns in rat primary hepatocytes determined. To accomplish this, primary hepatocytes were isolated from rats fasted for 24 hours and refed for 48 hours with a high carbohydrate/fat-free diet. Hepatocytes were plated and incubated for 4 hours with 20 μM taxol, nocodazole, or DMSO. Taxol acts to stabilize polymerize microtubule structure by binding directly to tubulin polymers and inhibiting dynamic collapse. Nocodazole, on the other hand, binds high affinity sites of tubulin heterodimers to and prevents further polymerization. After treatment with these chemicals, hepatocytes were fixed and stained with antibodies against β-tubulin and ACC1. Confocal imaging of these samples shows depolymerization of microtubules after treatment with nocodazole, and a decrease in overall structure and organization of ACC1 compared to DMSO samples **[Figure 5-5]**. Treatment with taxol also appears to cause a loss of overall co-localization, as microtubules become bunched in parallel aggregates or along the periphery of cells. Overall organization of ACC1, however, is not disrupted following treatment with taxol. This suggests that large structural cytoskeletal branches may not be required for proper subcellular localization of ACC1, but smaller polymers of microtubules might be necessary.

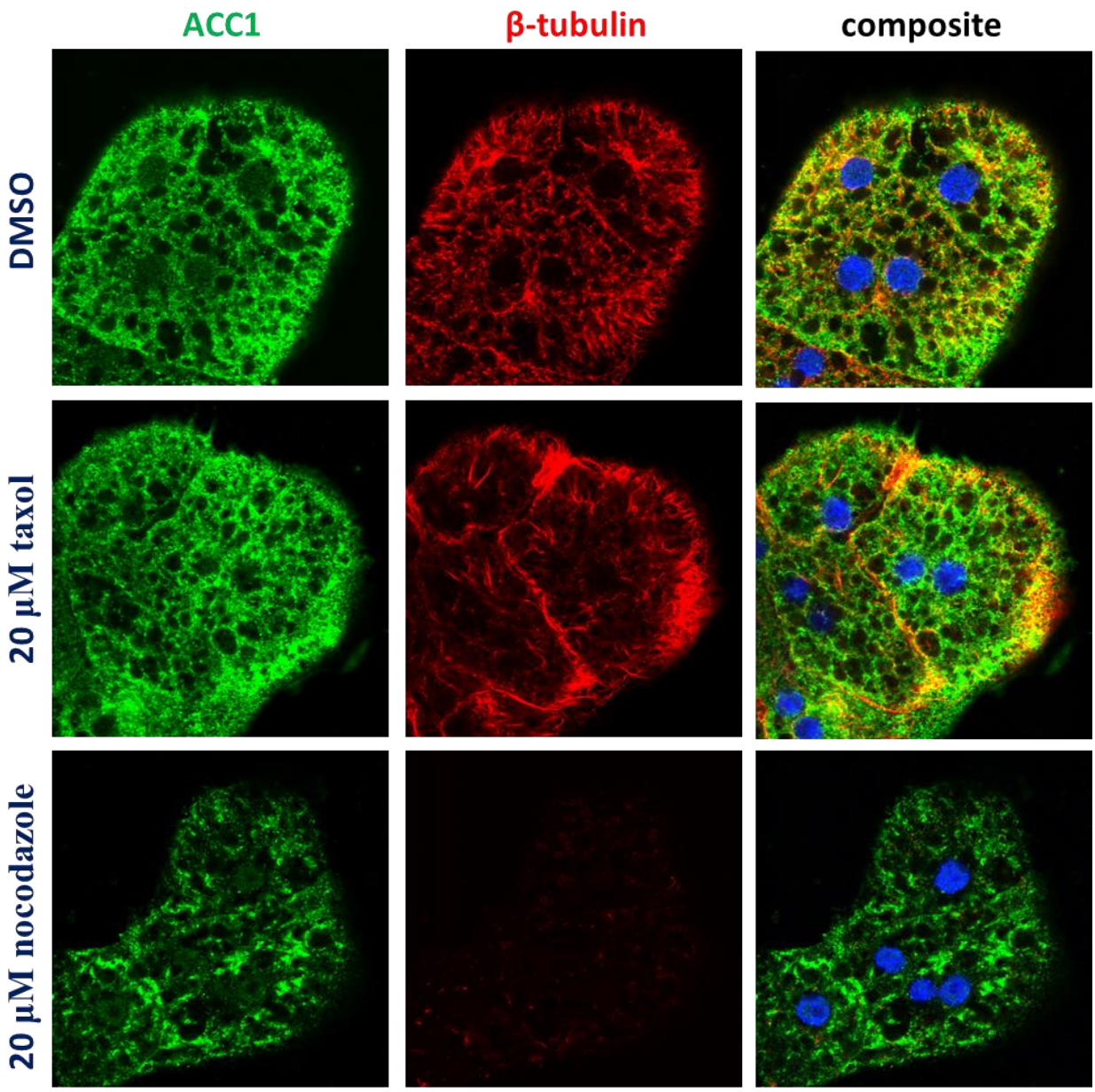

Figure 5-5. Microtubule disruption interferes with proper subcellular localization of ACC1.

Primary hepatocytes isolated from rats fasted for 24 hours and refed on a FFD for 48 hours were plated and incubated for 8 hours in complete M199. 20 µL of nocodazole, taxol, or DMSO was then added and hepatocytes were treated for another for hours at 37 °C and 5% CO_2. Coverslips were collected and fixed in 4% PFA/PBS and 100% MeOH, following which samples were rehydrated, blocked, and stained with antibodies against ACC1 (green) or β-tubulin (red). Mounting and imaging were performed as described in *Methods*.

Subcellular co-localization or association *in vitro* does not ultimately prove a functional interaction exists between lipogenic enzymes and microtubules. Effects of microtubule disruption on fatty acid biosynthesis would further support functionality. To test this, primary hepatocytes were isolated from FFD fed rats as before, cultured in complete M199, and treated again with 20 μM nocodazole, taxol, or DMSO. ^{14}C-labeled citrate was added to hepatocytes 30 minutes after treatment, and cultures were further incubated for 2 or 4 hours. Incorporation of ^{14}C-labeled citrate into fatty acids was then measured. After 2 hours of incubation, no difference in fatty acid synthesis is visible between samples. However, after 4 hours, lipogenesis significantly decreases in hepatocytes treated with nocodazole. There also appears to be a difference in taxol treated cells, although the quantitation did not reach statistical significance. These data mirror immunofluorescence findings under the same conditions and reinforce a model wherein tubulin polymers structurally tether ACL, ACC, and FAS together.

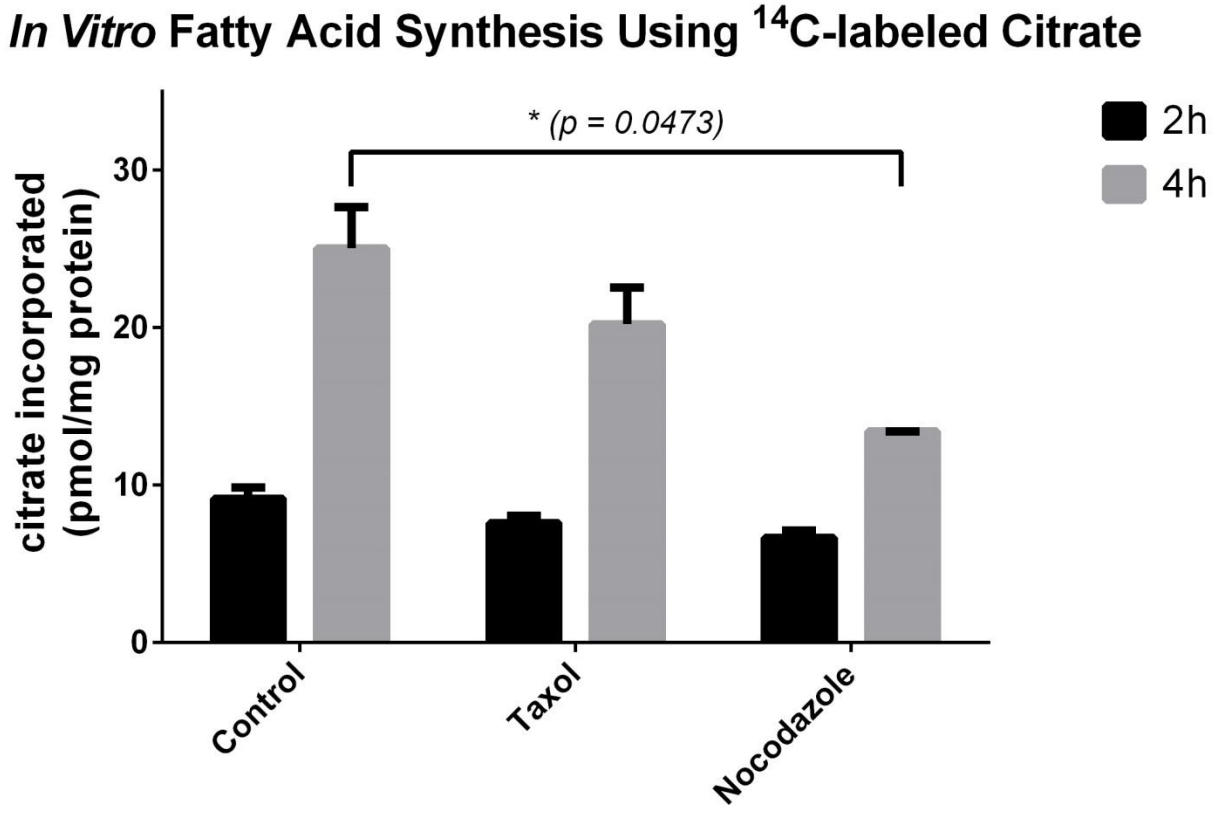

Figure 5-6. Nocodazole treatment significantly inhibits fatty acid synthesis in rat primary hepatocytes.
Primary hepatocytes from FFD fed rats were treated after 8 hours of culture with 20 μM of taxol, nocodazole, or DMSO. Cells were then supplemented with ^{14}C-labeled citrate for 2 or 4 hours. Incorporation of ^{14}C-labeled citrate into fatty acids was measured following treatment. Duplicate measurements were taken and error is reported as SEM.

Summary

Previous studies involving glycolytic enzymes and immunoprecipitation experiments performed here indicate that the cytoskeleton may bind to functional metabolons. Confocal imaging of rat hepatocytes supports this observation, as microtubules and lipogenic enzymes co-localize when hepatocyte lipogenesis is stimulated by high glucose and insulin. **[Figure 5-1]**. Similar precipitation experiments using protein from mouse liver cytosol suggest that endogenous MAPs or native post-translational modifications might be required **[Figures 5-3 and 5-4]**. More importantly, disruption of microtubules using nocodazole has a significant negative impact on both the structure of ACC1 *in vivo* and total fatty acid synthesis in primary rat hepatocytes **[Figure 5-5 and 5-6]**. These data show that microtubules not only associate with lipogenic components but are necessary for maximal rates of palmitate synthase.

CHAPTER SIX: CONCLUSIONS AND FUTURE AVENUES

The demonstration that a functional complex containing ACC, MIG12, S14, FAS, ACL and microtubules provides a fundamental advance in our understanding of the mechanism by which fatty acids are synthesized in liver cells. The direct association of these proteins provides a more efficient transfer of products and reactants allows for regulated production of palmitate. Localized fatty acid synthesis also prevents the unnecessary and toxic accumulation of metabolic intermediates in the cytoplasm.

A more thorough understanding of this lipogenic metabolon might also allow for drug development and targeting of diseases such as NAFLD that are associated with high rates of *de novo* lipogenesis. Though inhibitors of ACL, ACC, and FAS have been tested in various animal models, their method of action and physiologic effect can be broad and produce deleterious off-target effects.[14,74,92–95] For instance, the use of the synthetic FAS inhibitor C75 acts to decrease total body weight and liver accumulation of triglycerides in mice by suppressing food intake. This is accomplished by an accumulation of malonyl-CoA acts upstream of neuropeptide Y (NPY) in the hypothalamus to decrease appetite.[92] While limited caloric restriction might be advantageous in cases of severe obesity, more dramatic drops in food intake could be contraindicated and dangerous for certain patients with heart disease, NAFLD, or cancer. In addition, although the compound SB-204990 directly inhibits ACL activity, it also disrupts mitochondrial membrane potential and induces cell death.[93] This dysregulation is particularly pronounced where glycolysis is high, and likely could not be used on lipogenic tissues. Furthermore, while a variety of ACC inhibitors have been developed, the large majority of them are ineffective in mammalian cells.[14] Drugs that target metabolon structure might allow for

specific downregulation of fatty acid and triglyceride synthesis while preserving individual function of ACL, ACC, and FAS. Such selectivity might prevent development of any adverse reactions.

Investigation of Post-Translational Modifications

Many questions remain, however, prior to the development of a model involving this lipogenic complex in human disease. Among the most significant of these is understanding what post-translational modifications are necessary and/or sufficient to coordinate interaction between ACC, MIG12, S14, FAS, ACL, and microtubules. For instance, phosphorylation is a well-documented PTM that modulates fatty acid synthesis. Furthermore, threonine and serine phosphorylation in ACL is known to stabilize and induce homotetrameric activity. It is also well established that many MAPs require phosphorylation to bind to microtubules.[96] Phosphorylation that positively regulates fatty acid synthesis might facilitate tethering of microtubules as well. Our additional unpublished studies have suggested that MIG12 phosphorylation promotes MIG12:S14 heterodimer formation. Considering that MIG12 has been shown to interact with both ACC and microtubules **[Chapter 2]**, and that S14 interacts with FAS **[Chapter 3]**, perhaps MIG12 phosphorylation is requisite for bridging these complexes through heterodimer formation. Finally, unpublished immunofluorescence data also demonstrate that some ACC present in subcellular filaments or around lipid droplets is phosphorylated at serine-79, a residue known to be modified by AMPK. Perhaps, then, serine-79 phosphorylation is important for complex association under conditions independent of AMPK signaling.

The role of acetylation in protein binding must also be investigated. Other reports indicate that some protein systems might require acetylation prior to interaction. If relevant, acetyl-CoA concentrations might push equilibrium towards this post-translational modification.

For instance, nuclear expression of ACL and high concentrations of glucose in mammalian cells produces acetyl-CoA required for histone protein acetylation.[78] Similarly, double knockouts of ACC1 and ACC2 elicits cytosolic accumulation of acetyl-CoA and induce widespread protein acetylation.[97] By extension, in normal physiology when cellular glucose needs are met and citrate is exported to the cytoplasm, ACC polymerization or subsequent metabolon formation might be triggered through acetylation from the initial build-up of acetyl-CoA. Acetylation is also extremely important in microtubule dynamics. Acetylated microtubules represent an extremely stable and functionally important population that facilitates MAM coordination and lipid droplet expansion.[98] The methods through which acetylated microtubules elicit this change, however, are poorly defined. Perhaps these steady groups of microtubules help initialize ACL, FAS, or ACC polymerization by acting as reliable templates along which monomers and dimers can extend. Alternatively, acetylation of microtubules might act as a method through which phosphorylated residues and proteins recognize binding locations.

Understanding Lipid Droplet and MAM Localization

In addition to post-translational modifications, a more thorough investigation of the association of lipogenic metabolons with lipid droplets and MAMs is warranted. For instance, while ACC, FAS, ACL, and microtubules clearly co-localize with lipid droplet markers **[Chapter 4]**, mechanisms that promote this association have not been resolved. While each protein might be independently recruited, it is also possible that binding of lipogenic enzyme polymers to microtubules is required for targeting to lipid droplets. Such a hypothesis would be consistent with known roles of lipid droplet dependency on microtubules for growth and movement.[91] In addition, immunofluorescence data indicates that ACC associates with smaller lipid droplets than FAS or ACL. This may indicate that ACC is recruited to developing

lipogenic complexes on lipid droplets and is necessary for eventual association with FAS and ACL. Furthermore, previous data **[Chapter 4]** indicates that basic lipid droplet structure in mammalian livers might be different from canonical models developed in *Drosophila* and yeast. A full envelope of ER might be required in tissues of higher organisms that express enzymes like ACC, FAS, and ACL to coordinate the activity of fatty acid synthesis and subsequent triglyceride production. Alternatively, during lipid droplet biogenesis PDI might re-localize to the outside of the ER and help facilitate metabolon formation. Such translocation would explain my immunofluorescence data from rat primary hepatocytes and support current models of lipid droplet development. It should be noted that, in support of this possibility, immunoprecipitation of S14-FLAG in hepatocytes identified several chaperones as putative binding partners.

The role of mitochondrial associated membranes in lipogenic complex development must also be further explored. For example, different subcellular localizations of ACC isozymes and the formation of a putative ACC1:ACC2 heterodimer indicates a functional association in fatty acid synthesis between the ER and mitochondria **[Chapter 3, 4]**. Although studies in ACC1 and ACC2 knockout mice indicate either isozyme can compensate for loss in malonyl-CoA production, it is unclear whether ACC1:ACC2 heterodimer formation is required for lipogenic metabolon formation or normal rates of triglyceride production. It is also uncertain whether ACC1 and ACC2 binding occurs secondary to MAM formation or whether it necessary and/or sufficient to tether mitochondria to the endoplasmic reticulum. In addition, 100% of refed mouse hepatocytes show co-localization of ACC1 and ACC2 with the MAM marker mitofusin-2, whereas only half of cells show this overlap with FAS or ACL. Again, this could indicate that ACC is organized before ACL or FAS during lipogenic complex assembly. Inasmuch as of the deletion of both ACC1 and ACC2 in hepatocytes does not influence the proportion of cells

which show FAS or ACL recruitment to MAM, proteins not yet investigated might be required for metabolon formation. Targeting the lipogenic complex to the MAM allows for close proximity with SCD1, ELOVL6, GPAT1, PAP, AGPAT, and DGAT2 – enzymes integral for production of triglycerides from fatty acids. It is not known, however, whether any physical interaction occurs between lipogenic proteins and these enzymes. It is also unclear whether MAMs are involved in this process in tissues that do not express GPAT1 or DGAT2 – isoforms of acyltransferases that target to the mitochondria.

Evaluating Recombinant Protein Interactions

Perhaps the most conclusive way to validate complex formation between ACC, MIG12, S14, FAS, ACL, and microtubules is through *in vitro* studies using recombinant proteins. For example, I have prepared and purified homologues of each putative component of the metabolon. Data indicates that recombinant S14 and MIG12 significantly changes structure and activity of ACC. Recombinant S14 and MIG12, however, do not appear to influence the activity of purified ACL or FAS. However, the effect of all of these recombinant proteins on fatty acid synthesis has not yet been tested. The next step will be to combine radiolabeled citrate with a mixture of all recombinant proteins to determine rates of total palmitate production. Specific proteins – including microtubules and MAP mixtures – could then be removed or added to assay for the individual effect of each component on lipogenic activity. Mutant recombinant proteins could even be prepared to identify secondary structures or peptide sequences important for complex formation.

Summary and Conclusions

The aims of this dissertation were threefold: to identify physical interactions between a putative complex of lipogenic proteins, to establish the subcellular localization of this metabolon,

and to investigate the role of microtubules in regulating complex interaction and localization. Several advances in current understanding of *de novo* hepatic fatty acid synthesis have been made as a result of this research.

Heterodimer formation between MIG12 and S14 was shown to functionally inhibit the ability of MIG12 to polymerize and activate ACC **[Figure 2-9]**. These data also helped to identify that lipogenesis in tissues containing high levels of MIG12:S14 heterodimer is largely unaffected by knockdown of MIG12 protein **[Figure 2-7]**. Physical interaction was also established between other enzymes of fatty acid synthesis. S14 was shown to form immunocomplexes with FAS and both isozymes of ACC, and MIG12 and S14 both bind ACL when exogenously expressed in cultured cells **[Figures 3-1 and 3-6]**. Moreover, binding between ACC1 and ACC2 was shown *in vivo*, a heterodimeric relationship that has been previously uncharacterized **[Figure 3-5]**. These data provide collective evidence for a large, multimeric complex wherein fatty acid synthesis can be consolidated.

Prior to this research, targeting of ACC, FAS, ACL, MIG12, and S14 was largely considered to be cytosolic. However, immunofluorescence data presented here provides a more complete picture of lipogenic metabolon subcellular localization. For example, ACC and MIG12 were shown to form filaments that localize to the ER in rat primary hepatocytes **[Figure 4-2]**. It was also determined that these filaments were responsive to insulin signaling, as fasting and AICAR treatment disrupted their formation **[Figure 4-3]**. By extension, when hepatocytes were cultured under high glucose and high insulin, ACC filaments extended to incorporate the majority of ER membranes in the cell. This same pattern was shown with FAS and ACL **[Figures 4-4 and 4-5]**. These lipogenic enzymes were even visualized around lipid droplets, indicating a close association with triglyceride synthesis and storage **[Figure 4-6]**. In addition to

the ER, ACC1 was shown to be recruited to the mitochondria when coexpressed with ACC2 **[Figures 4-8 and 4-9]**. These data suggested that the metabolon existed at an interface between the ER and mitochondria, which was confirmed by co-staining with the MAM marker mitofusin-2 **[Figure 4-10]**. Subcellular localization of fatty acid synthetic complexes at the MAM permits a close association between palmitate production and further processing to endogenous triglycerides.

In addition, a relationship between microtubules and fatty acid synthesis has been suggested but never thoroughly established. In these studies, co-localization between microtubules and ACC, FAS, and ACL was shown along the ER and around lipid droplets **[Figures 5-1 and 5-2]**. This was confirmed as a physical relationship by co-precipitation of exogenous microtubules with endogenous lipogenic proteins from mouse liver cytosol **[Figure 5-4]**. Disruption of microtubules using nocodazole had a negative effect on immunofluorescent patterns of ACC in rat primary hepatocytes **[Figure 5-5]**. Nocodazole treatment also inhibited *in vitro* fatty acid synthesis in rat primary hepatocyte culture **[Figure 5-6]**. These results indicate that microtubules are an active component of lipogenic metabolons and are necessary for optimal palmitate production.

I have thus shown that ACC, FAS, ACL, MIG12, and S14 bind to form a large complex capable of streamlining fatty acid synthesis, and that this complex targets to an interface between the ER and mitochondria. I have also shown that microtubules act to maintain the integrity and function of this metabolon.

CHAPTER SEVEN: MATERIALS AND METHODS

Baculovirus construct preparation

Sequences for mouse FAS, ACL, MIG12, or S14 or variant 2 of human ACC1 were cloned and ligated into pAcHLT transfer vectors. These vectors (2 μg) were then combined with BaculoGold viral DNA from BD (0.2 μg) and transfected into *sf-9* insect cells in 6 well dishes using Cellfectin II Rreagent (8 μL, diluted). *sf-9* cells were incubated for 5 hours at 27 °C in unsupplemented Grace's medium, after which culture was replaced in each well with complete Grace's medium (+10% fetal calf serum, ampicillin/penicillin/amphotericin-B) and incubated for another 5 days. After this, the supernatants were collected and clarified as primary viral titers. Primary titers were then diluted 1:100 in complete Grace's medium and added to plated *sf-9* cultures in 100 mm dishes. These cells were again incubated for 5 days at 27 °C, after which the culture medium was collected and clarified as before to generate first viral amplifications. Virus particles were diluted 1:250 from these supernatants and the process of amplification repeated again. Second viral amplifications for each baculovirus construct were then covered with foil and stored at -80 °C until use. Recombinant ACC1, FAS, ACL, and S14 were expressed with His_6 tags, while MIG12 was expressed with a FLAG tag. Each epitope tag was removable with thrombin.

Recombinant protein production

Amplified baculovirus stocks expressing ACC1-His_6, FAS-His_6, ACL-His_6, MIG12-FLAG, or S14-His_6 were diluted 1:100 in 500 mL suspension cultures of *sf-9* insect cells. Dilutions of penicillin, streptomycin, and amphotericin-B were also added to prevent bacterial and fungal contamination. Baculoviral growth cultures were shaken for 3 days at 27 °C and collected by

centrifugation for 10 minutes at 2000 RPM and 4 °C. *sf-9* cell pellets were resuspended in 10 mL of ice-cold 1x DPBS and stored at -80 °C until use.

Established conditions for purification of recombinant ACC were followed for each fusion protein with only slight modifications.[99] Prior to cell lysis, thawed *sf-9* suspensions were supplemented with 2x cOmplete Protease Inhibitor Cocktail (Roche, Florence, SC). Cell pellets were then dounced on ice, ultracentrifuged at 100,000 x *g* for 45 minutes, and the cytosolic supernatants collected. 30 mM imidazole was added post-centrifugation to suspensions of proteins possessing His_6 epitope tags. Individual samples were then added to 4 mL Ni-NTA resin or 2 mL anti-FLAG M2 affinity gel that had been pre-equilibrated with 1x DPBS. Samples were slowly rotated with affinity resins for 2 hours at 4 °C and washed with 5x 10 mL volumes of 1x DPBS. Wash buffer contained 50 mM imidazole for His_6-tagged proteins and 0.1% IGEPAL for MIG12 samples. ACC, FAS, and ACL proteins were eluted by adding 12x 0.5 mL fractions of 1x DPBS and 300 mM imidazole. Rough protein concentrations were determined for fractions by assaying each with Bradford reagent. The five fractions with the highest protein amount were combined for each sample. MIG12 and S14 proteins were eluted off their respective resins by incubation overnight in wash buffer supplemented with 10 units of thrombin. Eluates were then incubated 2x for 1 hour at 4 °C with 1 mL *p*-aminobenzamidine-agarose to remove residual thrombin.

It should be noted that recombinant MIG12-GST was initially used in experiments. However, with the propensity of GST fusion tags to dimerize it became difficult to purify species of MIG12 that were not highly polymerized.[100]

SDS-PAGE

Resolving polyacrylamide gel solutions were prepared by mixing 0.375 M Tris-Cl (pH 8.8) with 13% glycerol, 0.1% sodium dodecyl sulfate (SDS), 0.1% ammonium persulfate (APS), and various concentrations of 37.5:1 bis-acrylamide from a 30% stock (Bio-Rad, Berkeley, CA). Stacking polyacrylamide gel solutions were prepared by combining 0.125 M Tris-Cl (pH 6.8), 0.1% SDS, 0.1% APS, and 4% bis-acrylamide. TEMED was diluted 1:1000 in resolving gel solutions and ~7.5 mL added to casting stands. Resolving gels were overlayed with 100% EtOH until polymerized, after which they were washed 3x with distilled water. Stacking gel solutions were supplemented 1:1000 with TEMED and poured to fill the remainder of each casting stand. Combs were added on top of solutions to act as molds for sample wells. Following stacking gel polymerization, combs were removed and wells washed 3x with distilled water.

Samples of interest were diluted with 5x SDS dye and supplemented with β-mercaptoethanol. Samples were then boiled at 95 °C for 5-10 minutes, allowed to cool, centrifuged, and vortexed to mix. Denatured samples were loaded onto 5.5% polyacrylamide gels for analysis of ACC, FAS, or ACL and 13% polyacrylamide gels for analysis of MIG12 and S14. Gels were run at 120 V for 1.5 hours and the proteins transferred to nitrocellulose membranes using the Trans-Blot Turbo system from Bio-Rad.

Coomassie staining

Gels with protein samples separated using SDS-PAGE were submerged in Imperial Protein Stain (Thermo Scientific, Rockford, IL) and gently rocked for 1-2 hours. Imperial Protein Stain was then discarded and gels washed with distilled water overnight. Following coomassie staining and washing, gels were preserved in cellophane.

Western blotting

Immunoblot data was generated as previously described with slight modifications.[101] Excess nitrocellulose membrane was trimmed following protein transfer. Each membrane was incubated for 1-2 minutes with Ponceau S protein stain and washed briefly with distilled water. Ponceau S stains were scanned and the membranes washed with 1x PBST for 10 minutes. Membranes were then rinsed 3x with distilled water and incubated at room temperature for 30 minutes with Odyssey Blocking Buffer or 1x PBST supplemented with 5% milk. After blocking, membranes were rinsed 3x with distilled water to remove residual buffer and submerged in primary dilutions of rabbit or mouse antibodies. Binding was performed either at room temperature for 2 hours or overnight at 4 °C. Membranes were washed 4x for 10 minutes at room temperature with 1x PBST. Secondary dilutions of goat antibodies against mouse or rabbit antibodies were incubated with membranes for 30 minutes at room temperature. For LiCor analysis, secondary antibodies were conjugated to fluorophores emitting at either 680 or 800 nm. All other experiments were analyzed using ECL HRP-linked secondary antibodies. Membranes were again washed 4x for 10 minutes at room temperature. LiCor Western blots were visualized using the Odyssey Infrared Imaging System (Li-Cor Biosciencess, Lincoln, NE). All other experiments were imaged by washing in SuperSignal West Pico Chemiluminescent Substrate and developing membranes on film.

BN-PAGE

Non-denaturing blue native gels were prepared as described by Wittig and colleagues with slight modification.[102] Briefly, 3.5-10% gradient or 14% polyacrylamide gels solutions were made on ice. Gradient gels were prepared by mixing heavy separating solutions containing ~33 mM Bis-Tris (pH 7.0), ~4.5% (w/v) 6-aminohexanoic acid, 10% bis-acrylamide, 14% glycerol, 0.1% (w/v) ammonium persulfate, and 1:2000 TEMED with light separating solutions containing the

same components without glycerol and only 3.5% bis-acrylamide. This mixture was poured into a casting stand, topped with light separating solution, and solidified with a 15-well comb at room temperature. Non-gradient gels were prepared in a similar manner with solution containing 14% bis-acrylamide and 14% glycerol. Once solidified, combs were removed and wells rinsed 2x with distilled water.

Samples were diluted to 25 µL each with 0.5 mM Bis-Tris (pH 7.0), 6% glycerol, 0.000005% (w/v) coomassie G250, and 0.1% (w/v) 6-aminohexanoic acid and loaded sequentially in wells. These samples were then overlaid with cold 50 mM Bis-Tris (pH 7.0). Gels were run at 4 °C for 2 hours with dark cathode buffer containing 50 mM tricine (pH 7.0), 15 mM Bis-Tris (pH 7.0), and 0.02% (w/v) coomassie G250. This was replaced with light cathode buffer containing 0.002% (w/v) coomassie G250, and the gels run overnight at 4 °C. Anode buffer contained 50 mM Bis-Tris (pH 7.0).

Gels were transferred to 0.2 µm PVDF membranes, after which membranes were rinsed 3x in 100% MeOH to remove coomassie stain. Western blot procedure was then followed as described. Sample loading amounts were as follows: recombinant ACC (6 µg), recombinant MIG12 (1 µg or 5 µg), recombinant S14 (1 µg or 5 µg), recombinant MIG12:S14 heterodimer (2 µg or 10 µg), liver cytosol (30 µg total protein), and CHO-K1 cell cytosol (40 µg total protein).

ACC activity *in vitro*

Measurement of radiolabeled bicarbonate incorporation to acetyl-CoA was performed as described by Wakil and Lane with few modifications.[26,103] Recombinant ACC protein (0.5 µg) was combined alone or in combination with 2 µg of recombinant MIG12 or 0.125 µg of recombinant MIG12, S14, or MIG12:S14 heterodimer. Mixtures were incubated for 5 minutes at 37 °C in 40 mM HEPES (pH 7.6), 10 mM $MgCl_2$, and 2 mM DTT. Reactions were then

supplemented with 5 mM ATP, 8 mM DTT, 0.284 mM acetyl-CoA, and 10 mM $KH^{14}CO_3$ and incubated for 15 minutes longer. Malonyl-CoA synthesis was stopped by adding 6 N HCl to each reaction. Samples were then transferred to scintillation vials and heated for 45 minutes at 80 °C, following which 15 mL scintillation cocktail was added and ^{14}C counts measured. Results were determined as nmol radiolabeled bicarbonate incorporated per μg ACC per minute.

Fatty acid synthesis asssay

Protocol was followed as described by Horton and Shimano with some variation.[104] Wild-type and *Mig12* knockout C57BL/6 mice fed on a high carbohydrate and fat free diet were intraperitoneally injected with 50 mCi of ^3H-labeled water. Mice were incubated for one hour and sacrificed, after which various tissues were removed and saponified in 5 mL alcoholic potassium hydroxide at 65 °C for at least 2 hours. After allowing samples to cool to room temperature, 5 mL distilled water and 15 mL petroleum ether were mixed for 1 minute and allowed to rest for 30 minutes longer to separate aqueous and organic phases. The organic phase was removed by suction, and 1 mL 6 N HCl was added to each aqueous phase. 15 mL hexanes were then added to these suspensions and shaken for 1 minute and allowed to separate for 30 minutes more. The organic phase was transferred to a volumetric flask and a second hexane wash performed on the aqueous phase. The second hexane phase was combined with the first and diluted to 100 mL with hexanes. 10 mL of this mixture was transferred to scintillation vials and evaporated overnight. To ensure all hexanes were evaporated, scintillation vials were then heated at 80 °C for 45 minutes in a vacuum oven. 1 mL methanol and 15 mL scintillation cocktail were then added to each sample and ^3H signal counted. Positive controls from mouse plasma were taken by measuring a 1:100000 dilution in 15 mL scintillation cocktail. Negative controls were determined from 50 μL whole blood samples processed using the same procedure

for tissues as described. Values were determined as μmol fatty acids produced per hour per gram tissue and reported as normalized ratios.

Bimolecular fluorescent complementation

Plasmids expressing the N (pBiFC-VN155) and C (pBiFC-VC155) terminal halves of Venus YFP were obtained from Addgene. These were then used to generate fusion proteins of MIG12 or S14 with either YFP half. Constructs were transiently co-transfected into CHO-K1 cells adherent to coverslips. Expression and subsequent binding between MIG12 and/or S14 caused regeneration of intact Venus YFP. After 18 hours of incubation at 37 °C and 8% CO_2, cells were fixed in 4% paraformaldehyde for 30 minutes, permeabilized with 0.02% IGEPAL CA-630 for 10 minutes, and incubated for 30 minutes with a blocking buffer containing PBS, 10% (v/v) goat serum, and 5% (w/v) BSA. Cells were then stained with mouse monoclonal antibodies (Roche, Indianapolis, IN) against the HA tag present on VN155 proteins. Primary antibodies were visualized by staining with Alexa Fluor 568 secondary dye (Invitrogen, Carlsbad, CA). Coverslips were attached to slides with DAPI mounting media. Anti-mouse Texas Red conjugates, Venus YFP, and DAPI signal were all detected with a Leica TCS SP5 confocal microscope using excitation wavelengths of 578, 514, and 405 nm, respectively.

MIG12:S14 purification

Mouse fusion proteins MIG12-FLAG and S14-His_6 were coexpressed in 2 liters of *sf-9* insect cells following baculovirus infection. Baculovirus preparation was followed as described above. Cell pellets were resuspended and dounced in a 30 mL solution of 1x DPBS, 30 mM imidazole, and protease inhibitor (Roche, Indianapolis, IN), and the supernatant was collected following ultracentrifugation of the lysate at 100,000 x *g* for 45 minutes. The cytosolic fraction was incubated with 6 mL Ni-NTA resin (Qiagen, Valencia, CA) for 2 hours at 4 °C. The resin was

then washed 5 times with 20 mL of 10 mM phosphate buffer pH 7.4, 300 mM NaCl, and 50 mM imidazole. S14 and MIG12:S14 fusion products were eluted from the resin in 0.75 mL fractions using a solution of 10 mM phosphate buffer pH 7.4, 150 mM NaCl, and 300 mM imidazole. Protein positive fractions were pooled and diluted 10x using 1x DPBS and 0.1% IGEPAL.

The dilute Ni-NTA eluate was incubated with 1 mL anti-FLAG M2 affinity gel (Sigma, St. Louis, MO) for 2 hours at 4 °C. Anti-FLAG resin was then washed 5 times with 10 mL of 1x DPBS, 30 mM imidazole, and 0.1% IGEPAL. MIG12:S14 heterodimer was eluted from the affinity gel by cleaving overnight with a 3 mL solution of 1X DPBS, 30 mM imidazole, 0.1% IGEPAL, and 10 units thrombin. Thrombin, excess His_6 tag, and uncleaved fusion heterodimers were removed from the eluate by incubating for 1 hour at 4 °C with 1 mL *p*-aminobenzamidine-agarose (Sigma, St. Louis, MO), 0.25 mL Ni-NTA resin, and 0.25 mL anti-FLAG M2 affinity gel. Purified recombinant heterodimer was concentrated ~4x using Amicon Ultra Centrifugation Filters and then analyzed.

Immunoprecipitation

Livers from refed mice or rats were surgically removed, freeze-clamped, and stored at -80 °C prior to analysis. Liver homogenization and fractionation were followed as previously described with slight modifications.[101,105] Specifically, replicate liver samples were combined in a homogenization buffer containing 20 mM HEPES (pH 7.5), 250 mM sucrose, 2 mM $MgCl_2$, 1 mM DTT, and 2x protease inhibitor (Roche). Liver tissue was homogenized for 20 seconds and then placed immediately on ice, after which nuclear and bulk cellular debris was pelleted by centrifugation at 600 x *g* and 4 °C for 10 minutes. Supernatants from these samples were collected and clarified further via ultracentrifugation at 100,000 x *g* and 4 °C for 30 minutes.

Afterwards, total protein concentrations were determined using BCA analysis and protein amounts were equalized between samples.

Endogenous immunoprecipitation was performed by incubating proteins of interest with liver cytosol for 2 hours at 4 °C. After binding, protein-antibody complexes were captured with equilibrated protein A/G agarose (Pierce) by rotating at 4 °C for 30-60 minutes. Samples were washed 5x in 1x DPBS for 10 mintues at 4 °C. Immunoprecipitated proteins were eluted from resin by boiling in 2x SDS buffer for 10 minutes and vortexing vigorously afterwards.

Recombinant proteins from adenoviral or transfected vectors were purified under the same conditions using resin against the epitope tag of interest, washed, and eluted as before.

Silver staining

Gels were removed from casts and placed in clean plastic containers that had been washed and rinsed with 100% EtOH. Gels were washed 2x for 5 minutes each in filtered, distilled water. Water was decanted and gels were fixed 2x in 30% EtOH and 10% acetic acid for 15 minutes each. Gels were subsequently washed 2x in 10% EtOH for 5 minutes each, and again 2x in filtered, distilled water 2x for 5 minutes each. Wash was decanted and gels were incubated with a 1:500 dilution of Silver Stain Sensitizer for one minute. Gels were immediately washed after incubation 2x with filtered, distilled water. Gels were then incubated with a 1:50 dilution of Silver Stain Enhancer in Silver Stain Solution for 30 minutes at room temperature. Gels were again washed 2x with filtered, distilled water for 20 second each. Bound silver was then detected by incubating gels with a 1:50 dilution of Silver Stain Enhancer in Silver Stain Developer. When bands were sufficiently visible (~3 minutes), gel solution was quickly replaced with 5% acetic acid for at least 10 minutes. Silver stained gels were stored in filtered,

distilled water until further analysis. Silver Staining Kits were obtained from Pierce (Rockford, IL).

Partial protein purification

General protocol for enrichment of lipogenic protein from mouse liver cytosol was followed as outlined by Thampy and colleagues.[106] Mouse liver was homogenized in three volumes of 20 mM HEPES, 250 mM sucrose, 2 mM $MgCl_2$, 1 mM EDTA, 1 mM DTT, and 1x protease inhibitors on ice. Samples were then centrifuged for 10 minutes at 3,500 x *g* and 4 °C, after which supernatants were ultracentrifuged at 100,000 x *g* and 4 °C for 45 minutes. Clarified supernatants were mixed with 2.5% PEG8000 for ACC and 5% PEG8000 for MIG12 and S14 analysis. Slurries were precipitated by centrifugation at 10,000 x *g* for 10 minutes at 4 °C. Supernatants were removed, and pellets resuspended and mixed further with a final concentration of 6.0% PEG8000 for ACC analysis and 15% PEG8000 for MIG12 and S14 analysis. Slurries were centrifuged as before for 15 minutes, after which supernatants were decanted and pellets washed 2x with ice-cold distilled water. Pellets were dissolved in cold 1x DPBS and precipitated again by the addition of 32% ammonium sulfate. Samples were centrifuged at 10,000 x *g* and 4 °C for 15 minutes. Supernatants were again decanted, and protein pellets resuspended on ice in 20 mM HEPES (pH 7.6), 150 mM NaCl, 10% glycerol, 1 mM EDTA, 1 mM DTT, and 1x protease inhibitors. Quantitation of total protein amounts was performed using BCA.

FAS activity assay

Procedure was followed as described by Carey *et* al. with slight modification.[69] Specifically, partially purified or recombinant FAS (4 μg) was diluted with reaction mixture alone or in combination with increasing molar ratios of purified recombinant S14. Where indicated, FAS

protein was also incubated with 250 mM sodium phosphate (pH 7.0), 10% glycerol, 1 mM EDTA, and 1 mM DTT for 1 hour at room temperature. Reaction mixtures contained 200 mM phosphate (pH 6.5), 1 mM DTT, 1 mM EDTA, 0.24 mM NADPH, and 0.030 mM acetyl-CoA. Malonyl –CoA (0.100 mM) or distilled water was then added to separate reaction mixtures for experimental and control measurements. Protein was added individually into 96 well plates and then diluted with either experimental or control reaction mixtures. Plates were immediately analyzed using kinetic spectrophotometry at 25 °C. The decrease in absorbance at 340 nm was directly proportional to NADPH oxidation and total FAS activity. Plates were briefly shaken between each reading interval, and measurements were taken until absorbance changes became non-linear. Readings from samples without malonyl-CoA were subtracted from experimental values to normalize for well-to-well discrepancies.

Transient transfection

pcDNA3 constructs expressing ACC1, ACC2, MIG12, S14, ACL, or FAS were combined with serum free DHG and Fugene-6 (3 µL Fugene-6:1 µg DNA). Mixtures were incubated at room temperature for 15 minutes and added dropwise to cultures containing complete DHG medium. Transfected cells were incubated for 5 hours at 37 °C, after which medium was changed and cells incubated for ~20 hours further prior to analysis.

ACL activity assay

Procedure was followed as described by Srere, *et* al. with slight modification.[107] Specifically, a master reaction mixture containing 100 mM Tris-Cl (pH 8.7), 0.5 mM potassium citrate, 10 mM $MgCl_2$, 5 mM DTT, 0.5 U/mL malate dehydrogenase, 0.1 mM CoASH, 0.14 mM NADH, and 5 mM ATP was prepared on ice. Recombinant or partially purified MIG12, S14, or MIG12:S14 heterodimer were combined with recombinant ACL in 10 µL dilutions in chilled 96 well plates.

190 µL of reaction buffer was then added using a multipipet to all samples and gently mixed. Duplicates of all reactions were simultaneously prepared without ATP as controls. Plates were then immediately transferred to the spectrophotometer and decreases in absorbance at 340 nm kinetically measured for each well. Incubation temperature was 25 °C and plates were briefly shaken between each reading interval. Measurements were run until NADH oxidation changes became non-linear. Readings from samples without ATP were subtracted from experimental values to normalize for well-to-well discrepancies.

2d-gel electrophoresis

Mouse or rat liver cytosol (240 µg total protein) was diluted in 2x Sample Buffer (denatured samples) or distilled water (native samples) to a final volume of 150 µL. IPG buffer (pH 3-10, 4.5 µL) and native or denaturing rehydration buffer (95.5 µL) were also added for a final volume of 250 µL. Samples were thoroughly mixed and incubated on ice for 30 minutes. Individual samples were then loaded into rehydration chambers and overlaid with overturned 13 cm immobiline DryStrip gels. Mineral oil was added to the top of each chamber to prevent evaporation overnight. Denatured and native proteins were rehydrated and resolved using voltage gradients overnight at 15 °C. Rehydration occurred first for 6 hours at a constant 500 V. Proteins were then separated by pI first for 1 hour at a gradient 1000 V followed by 2.5 hours at a gradient 8000 V. Immobiline strips were then kept at 8000 V for another 30 minutes, followed by a constant 500 V until removed to maintain protein position. Overall, samples were incubated for approximately 20 kVh.

Immobiline strips were removed following first dimension separation and loaded on top of 4-15% polyacrylamide gradient gels. When not immediately analyzed, strips were stored in sealed glass bottles at -80 °C. 2x Sample Buffer diluted with agarose was used to seal immobiline

strips to the top of polyacrylamide gels. SDS-PAGE was then performed on samples at 180 V and room temperature for 4 hours for second dimension separation. Proteins were transferred to nitrocellulose membranes at 40 V and 4 °C overnight. Immunoblots were then performed with desired antibodies.

Rat primary hepatocyte production

Male Sprague Dawley rats between one to three months old and weighing approximately 120 grams were fed *ad libitum* on CHOW diet. When necessary, these rats were fasted for 24 hours and then refed on a high carbohydrate fat free diet for 48 hours. For hepatocyte isolation, rats were euthanized by exposure to isofluorane gas. Livers were then surgically exposed and the portal vein cannulated with an 18 gauge catheter. Following cannulation, livers were perfused with warm Liver Perfusion Medium (Invitrogen) and Liver Digest Medium (Invitrogen). After digestion, livers were surgically removed and opened to release hepatocytes. Afterwards, hepatocytes were diluted with Dulbecco's High Glucose Medium or Dulbecco's Low Glucose Medium supplemented with 10% FCS, 10 mM HEPES (pH 7.5), and 1x penicillin/streptomycin. Cells were counted using a hemocytometer and diluted in M199 supplemented with 28 mM glucose, 100 nM insulin, 100 nM T3, and 10 nM dexamethasone. Following dilution, hepatocytes were plated in collagen coated dishes or on collagen coated glass coverslips and incubated for 2 hours at 37 °C and 5% CO_2. Media was then aspirated from attached hepatocytes and replaced with fresh complete or unsupplemented M199.

Immunofluorescence

Hepatocytes were adhered to individual type I collagen coated coverslips (BD) in 6 well dishes at a concentration of 0.75×10^6 cells/well. Hepatocytes were cultured in either complete or unsupplemented M199 at 37 °C and 5% CO_2 between 2 and 12 hours. For certain experiments,

treatment with taxol, nocodazole, or vincristine was carried out at a concentration of 20 uM for 2 hours. When used, mitotracker was incubated with cells at a concentration of 300 nM for 30 minutes. Also, for AICAR treatment, culture media concentrations were kept at 0.5 mM for 1.5 hours. Following hepatocyte culture and treatment, coverslips were removed from each well and transferred to a rack submerged in warmed M199 medium. Once full, racks were immediately transferred to ice-cold 100% MeOH at -20 °C or fixed in 4% PFA/PBS for 15 minutes and then placed in MeOH. In experiments where lipid droplets were observed, PFA fixation was performed in PIPES + HEPES + EGTA + magnesium (PHEM) buffer: 60 mM PIPES (pH 7.0), 25 mM HEPES (pH 7.0), 8 mM $MgCl_2$, and 10 mM EGTA. Coverslips were stored at -20 °C until needed, upon which hepatocytes were rehydrated for 10 minutes at room temperature in 1x DPBS. Coverslips were then blocked in a buffer containing 50 mM Tris-Cl (pH 7.5), 150 mM NaCl, 5% BSA, 10% goat serum, and 0.02% sodium azide for 10 minutes at room temperature. Individual samples were stained with primary antibodies diluted in blocking buffer at 37 °C for 30 minutes, and subsequently rinsed 5x in 1x DPBS. Incubation of individual samples with secondary antibodies was also performed in blocking buffer at 37 °C for 30 minutes, and rinsing was repeated as described. Coverslips were then mounted on slides in Prolong Gold Mounting Medium with DAPI (Invitrogen) overnight at room temperature. After curing, coverslips were sealed to slides with nail polish. DAPI, secondary Alexa Fluor conjugates, and mitotracker were all detected with a Leica TCS SP5 confocal microscope using excitation wavelengths of 405, 488, 561, and 633 nm.

Confocal microscopy

Samples for immunofluorescence were kept covered at room temperature until imaging. Imaging was performed on a Leica TCS SP5 confocal microscope. Low magnification (10X

objective zoom) was used to locate the healthiest and most representative groupings of cells on each coverslip. High magnification under oil immersion (63x objective zoom) was then used for imaging and data collection. Spectral detection was performed with lasers emitting at 405 nm (DAPI), 488 nm (FITC), 561 nm (Texas Red), and 633 (Deep Red). All images and data were collected within one week of antibody staining. Saved files were analyzed using standard ImageJ software. Where applicable, overlap between channels was measured using the Co-localization Analysis plugin. Pearson's correlation coefficients and normalized Manders' coefficients were computed for multiple images within an individual experiment. Mean values were determined for each combination of signal, and error reported as SEM.

Microtubule precipitation

General Tubulin Buffer was prepared by mixing 80 mM PIPES (pH 7.0), 2 mM $MgCl_2$, and 0.5 mM EGTA, and Cushion Buffer was prepared by mixing 80 mM PIPES (pH 7.0), 2 mM $MgCl_2$, 1 mM EGTA, and 60% glycerol. Purified bovine tubulin or purified bovine tubulin + MAPs (Cytoskeleton, Inc., Denver, CO) were diluted on ice with General Tubulin Buffer and 1 mM GTP and snap-frozen. In order to generate stable microtubules, 20 µL of this dilution was combined with 2 µL of Cushion Buffer and immediately incubated at 37 °C for 20 minutes. Following polymerization, reaction mixtures were suspended in 200 µL General Tubulin Buffer and 20 uM taxol. Aliquots (20 µL) of this microtubule preparation were then mixed with 30 µL samples of purified recombinant proteins or warmed mouse liver cytosol and incubated at room temperature for 30 minutes. Individual samples were overlayed on 100 µL Cushion Buffer and ultracentrifuged at 100,000 x *g* for 40 minutes at room temperature. Inert supernatant samples or microtubule pellets and interacting proteins were boiled in 2x SDS buffer and separated using SDS-PAGE. Specific proteins were visualized following transfer using immunoblot.

Hepatocyte fatty acid synthesis

Once plated and treated with 20 μM nocodazole, taxol, or DMSO, hepatocytes were incubated with 1 μCi of ^{14}C-labeled citrate along with 0.5 mM cold citrate. Cells were incubated at 37 °C and 5% CO_2 for 2 or 4 hours. Hepatocytes were then washed 2x with 2 mL of ice-cold 1x DPBS and 1 mL 0.1 N NaOH added to each well at room temperature. Plates were gently rotated for 30 minutes at room temperature and then sealed with parafilm and stored overnight at 4 °C. Total protein from 10 μL aliquots of these lysates were quantitated using BCA, and the remainder transferred to glass tubes containing 1.5 mL ethanol recovery carrier and 0.75 mL 75% KOH. Samples were vortexed thoroughly, covered with foil, and autoclaved for 45 minutes. After cooling, 1.5 mL EtOH was added to samples and mixed completely.

Once phases had separated, aqueous portions were aliquoted and mixed with 1.5 mL 6 N HCl. Each sample was vortexed vigorously and allowed to cool to room temperature. 1.5 mL EtOH was then added and mixed as before. Aqueous phases from each sample were then extracted 3x with 3 mL hexanes, after which organic phases were removed and evaporated. Residual protein was suspended in 30 μL of chloroform and spotted on TLC plates. Proteins were resolved in a 90:30:1 mixture of heptanes, diethyl ether, and acetic acid. Once separated, protein spots were visualized with iodine, cut from filters, and measured for ^{14}C counts.

BIBLIOGRAPHY

1. Ogden, C. L. & Carroll, M. D. Prevalence of overweight, obesity, and extreme obesity among adults: United States, trends 1960 – 1962 through 2007 – 2008. *Div. Heal. Nutr. Exam. Surv.* **1994,** 1–6 (2010).

2. Cohen, J. C., Horton, J. D. & Hobbs, H. H. Human fatty liver disease: old questions and new insights. *Science (80-.).* **332,** 1519–23 (2011).

3. Browning, J. D. *et al.* Prevalence of hepatic steatosis in an urban population in the United States: impact of ethnicity. *Hepatology* **40,** 1387–95 (2004).

4. Bricker, D. K. *et al.* A mitochondrial pyruvate carrier required for pyruvate uptake in yeast, Drosophila, and humans. *Science (80-.).* **337,** 96–100 (2012).

5. Gnoni, G. V, Priore, P., Geelen, M. J. H. & Siculella, L. The mitochondrial citrate carrier: metabolic role and regulation of its activity and expression. *IUBMB Life* **61,** 987–94 (2009).

6. Chypre, M., Zaidi, N. & Smans, K. ATP-citrate lyase: a mini-review. *Biochem. Biophys. Res. Commun.* **422,** 1–4 (2012).

7. Singh, M., Richards, E. G., Mukherjee, A. & Srere, P. A. Structure of ATP citrate lyase from rat liver. Physicochemical studies and proteolytic modification. *J. Biol. Chem.* **251,** 5242–50 (1976).

8. Elshourbagy, N. A. *et al.* Rat ATP citrate-lyase. Molecular cloning and sequence analysis of a full-length cDNA and mRNA abundance as a function of diet, organ, and age. *J. Biol. Chem.* **265,** 1430–5 (1990).

9. Sato, R. *et al.* Transcriptional regulation of the ATP citrate-lyase gene by sterol regulatory element-binding proteins. *J. Biol. Chem.* **275,** 12497–502 (2000).

10. Linn, T. C. & Srere, P. A. Identification of ATP citrate lyase as a phosphoprotein. *J. Biol. Chem.* **254,** 1691–8 (1979).

11. Lord, K. a *et al.* Variant cDNA sequences of human ATP:citrate lyase: cloning, expression, and purification from baculovirus-infected insect cells. *Protein Expr. Purif.* **9,** 133–41 (1997).

12. Migita, T. *et al.* ATP citrate lyase: activation and therapeutic implications in non-small cell lung cancer. *Cancer Res.* **68,** 8547–54 (2008).

13. Lin, R. *et al.* Acetylation stabilizes ATP-citrate lyase to promote lipid biosynthesis and tumor growth. *Mol. Cell* **51,** 506–18 (2013).

14. Tong, L. Acetyl-coenzyme A carboxylase: crucial metabolic enzyme and attractive target for drug discovery. *Cell. Mol. Life Sci.* **62,** 1784–803 (2005).

15. Wakil, S. J., Titchener, E. B. & Gibson, D. M. Evidence for the participation of biotin in the enzymic synthesis of fatty acids. *Biochim. Biophys. Acta* **29,** 225–6 (1958).

16. Waldrop, G. L., Rayment, I. & Holden, H. M. Three-dimensional structure of the biotin carboxylase subunit of acetyl-CoA carboxylase. *Biochemistry* **33,** 10249–56 (1994).

17. Athappilly, F. K. & Hendrickson, W. a. Structure of the biotinyl domain of acetyl-coenzyme A carboxylase determined by MAD phasing. *Structure* **3,** 1407–19 (1995).

18. Zhang, H., Yang, Z., Shen, Y. & Tong, L. Crystal structure of the carboxyltransferase domain of acetyl-coenzyme A carboxylase. *Science (80-.).* **299,** 2064–7 (2003).

19. Cho, Y. S. *et al.* Crystal structure of the biotin carboxylase domain of human acetyl-CoA carboxylase 2. *Proteins* 268–72 (2007). doi:10.1002/prot

20. Madauss, K. P. *et al.* The human ACC2 CT-domain C-terminus is required for full functionality and has a novel twist. *Acta Crystallogr.* **D65,** 449–61 (2009).

21. Horton, J. D., Bashmakov, Y., Shimomura, I. & Shimano, H. Regulation of sterol regulatory element binding proteins in livers. *Proc. Natl. Acad. Sci. U. S. A.* **95,** 5987–92 (1998).

22. Ishii, S., Iizuka, K., Miller, B. C. & Uyeda, K. Carbohydrate response element binding protein directly promotes lipogenic enzyme gene transcription. *Proc. Natl. Acad. Sci. U. S. A.* **101,** 15597–602 (2004).

23. Ma, L., Tsatsos, N. G. & Towle, H. C. Direct role of ChREBP-Mlx in regulating hepatic glucose-responsive genes. *J. Biol. Chem.* **280,** 12019–27 (2005).

24. Hardie, D. G. Regulation of fatty acid and cholesterol metabolism by the AMP-activated protein kinase. *Biochim. Biophys. Acta* **1123,** 231–8 (1992).

25. Witters, L. a, Watts, T. D., Daniels, D. L. & Evans, J. L. Insulin stimulates the dephosphorylation and activation of acetyl-CoA carboxylase. *Proc. Natl. Acad. Sci. U. S. A.* **85,** 5473–7 (1988).

26. Gregolin, C., Ryder, E., Kleinschmidt, A. K., Warner, R. C. & Lane, M. D. Molecular characteristics of liver acetyl-CoA carboxylase. *Biochemistry* **56,** 148–155 (1966).

27. Beaty, N. B. & Lane, M. D. Kinetics of activation of acetyl-CoA carboxylase by citrate. *J. Biol. Chem.* **258,** 13043–50 (1983).

28. Bianchi, a *et al.* Identification of an isozymic form of acetyl-CoA carboxylase. *J. Biol. Chem.* **265,** 1502–9 (1990).

29. Thampy, K. G. Formation of malonyl Coenzyme A in rat heart. *J. Biol. Chem.* **264,** 17631–4 (1989).

30. Kim, C.-W. *et al.* Induced polymerization of mammalian acetyl-CoA carboxylase by MIG12 provides a tertiary level of regulation of fatty acid synthesis. *Proc. Natl. Acad. Sci. U. S. A.* **107,** 9626–31 (2010).

31. Berti, C., Fontanella, B., Ferrentino, R. & Meroni, G. Mig12, a novel Opitz syndrome gene product partner, is expressed in the embryonic ventral midline and co-operates with Mid1 to bundle and stabilize microtubules. *BMC Cell Biol.* **5,** 1–12 (2004).

32. Suzuki, M., Hara, Y., Takagi, C., Yamamoto, T. S. & Ueno, N. MID1 and MID2 are required for Xenopus neural tube closure through the regulation of microtubule organization. *Development* **137,** 2329–39 (2010).

33. Horton, J. D. *et al.* Combined analysis of oligonucleotide microarray data from transgenic and knockout mice identifies direct SREBP target genes. *Proc. Natl. Acad. Sci. U. S. A.* **100,** 12027–32 (2003).

34. Inoue, J. *et al.* Identification of MIG12 as a mediator for stimulation of lipogenesis by LXR activation. *Mol. Endocrinol.* **25,** 995–1005 (2011).

35. Colbert, C. L. *et al.* Crystal structure of Spot 14, a modulator of fatty acid synthesis. *Proc. Natl. Acad. Sci. U. S. A.* **107,** 18820–25 (2010).

36. Seelig, S., Liuw, C., Towle, H. C. & Oppenheimer, J. H. Thyroid hormone attenuates and augments hepatic gene expression at a pretranslational level. *Proc. Natl. Acad. Sci. U. S. A.* **78,** 4733–37 (1981).

37. Tsatsos, N. G., Augustin, L. B., Anderson, G. W., Towle, H. C. & Mariash, C. N. Hepatic expression of the SPOT 14 (S14) paralog S14-related (Mid1 interacting protein) is regulated by dietary carbohydrate. *Endocrinology* **149,** 5155–61 (2008).

38. Cunningham, B. A., Maloney, M. & Kinlaw, W. B. Spot 14 protein-protein interactions: evidence for both homo- and heterodimer formation in vivo. *Endocrinology* **138,** 5184–88 (1997).

39. Jensen-Urstad, A. P. L. & Semenkovich, C. F. Fatty acid synthase and liver triglyceride metabolism: housekeeper or messenger? *Biochim. Biophys. Acta* **1821,** 747–53 (2012).

40. Maier, T., Leibundgut, M. & Ban, N. The crystal structure of a mammalian fatty acid synthase. *Science (80-.).* **321,** 1315–22 (2008).

41. Qureshi, A. A., Jenik, R. A., Kim, M., Lornitzo, F. A. & Porter, J. W. Separation of two active forms (holo-a and holo-b) of pigeon liver fatty acid synthetase and their interconversion by phosphorylation and dephosphorylation. *Biochem. Biophys. Res. Commun.* **66,** 344–51 (1975).

42. An, Z. *et al.* Nicotine-induced activation of AMP-activated protein kinase inhibits fatty acid synthase in 3T3L1 adipocytes: a role for oxidant stress. *J. Biol. Chem.* **282,** 26793–801 (2007).

43. Hennigar, R. a *et al.* Characterization of fatty acid synthase in cell lines derived from experimental mammary tumors. *Biochim. Biophys. Acta* **1392,** 85–100 (1998).

44. Jin, Q. *et al.* Fatty acid synthase phosphorylation: a novel therapeutic target in HER2-overexpressing breast cancer cells. *Breast Cancer Res.* **12,** R96–110 (2010).

45. Zhao, S. *et al.* Regulation of cellular metabolism by protein lysine acetylation. *Science (80-.).* **327,** 1000–4 (2010).

46. Flowers, M. T. & Ntambi, J. M. Stearoyl-CoA desaturase and its relation to high-carbohydrate diets and obesity. *Biochim. Biophys. Acta* **1791,** 85–91 (2009).

47. Jakobsson, A., Westerberg, R. & Jacobsson, A. Fatty acid elongases in mammals: their regulation and roles in metabolism. *Prog. Lipid Res.* **45,** 237–49 (2006).

48. Xu, H. *et al.* Hepatic knockdown of mitochondrial GPAT1 in ob/ob mice improves metabolic profile. *Biochem. Biophys. Res. Commun.* **349,** 439–48 (2006).

49. Lu, Y. *et al.* Citrate induces apoptotic cell death: a promising way to treat gastric carcinoma? *Anticancer Res.* **31,** 797–805 (2011).

50. Pizer, E. S. *et al.* Malonyl-Coenzyme-A is a potential mediator of cytotoxicity induced by fatty-acid synthase inhibition in human breast cancer cells and xenografts. **60,** 213–218 (2000).

51. Monné, M., Gafvelin, G., Nilsson, R. & von Heijne, G. N-tail translocation in a eukaryotic polytopic membrane protein: synergy between neighboring transmembrane segments. *Eur. J. Biochem.* **263,** 264–9 (1999).

52. Man, W. C., Miyazaki, M., Chu, K. & Ntambi, J. M. Membrane topology of mouse stearoyl-CoA desaturase 1. *J. Biol. Chem.* **281,** 1251–60 (2006).

53. Pellon-Maison, M., Montanaro, M. a, Coleman, R. a & Gonzalez-Baró, M. R. Mitochondrial glycerol-3-P acyltransferase 1 is most active in outer mitochondrial membrane but not in mitochondrial associated vesicles (MAV). *Biochim. Biophys. Acta* **1771,** 830–8 (2007).

54. Robinson, J. B., Inman, L., Sumegi, B. & Srere, P. A. Further characterization of the Krebs tricarboxylic acid cycle metabolon. *J. Biol. Chem.* **262,** 1786–90 (1987).

55. Kurganov, B. I. The role of multienzyme complexes in integration of cellular metabolism. *J. Theor. Biol.* **119,** 445–455 (1986).

56. Walsh, J. L., Keith, T. J. & Knull, H. R. Glycolytic enzyme interactions with tubulin and microtubules. *Biochim. Biophys. Acta* **999,** 64–70 (1989).

57. Volker, K. W., Reinitz, C. A. & Knull, H. R. Glycolytic enzymes and assembly of microtubule networks. *Comp. Biochem. Physiol.* **112,** 503–514 (1995).

58. Vertessy, B. G., Orosz, F., Kovacs, J. & Ovadi, J. Alternative binding of two sequential glycolytic enzymes to microtubules: molecular studies in the phosphofructokinase/aldolase/microtubule system. *J. Biol. Chem.* **272,** 25542–6 (1997).

59. Aipoalani, D. L., O'Callaghan, B. L., Mashek, D. G., Mariash, C. N. & Towle, H. C. Overlapping roles of the glucose-responsive genes, S14 and S14R, in hepatic lipogenesis. *Endocrinology* **151,** 2071–7 (2010).

60. Zhu, Q. *et al.* Spot 14 gene deletion increases hepatic de novo lipogenesis. *Endocrinology* **142,** 4363–70 (2001).

61. Oppenheimer, J. H. High basal expression and 3,5,3'-triiodothyronine regulation of messenger ribonucleic acid S14 in lipogenic tissues. *Endocrinology* **117,** 6–13 (1985).

62. Nishi, N., Shoji, H., Miyanaka, H. & Nakamura, T. Transient up-regulation of a novel member of Spot 14 family in androgen-stimulated rat prostate. *Biochim. Biophys. Acta* **1780,** 1004–9 (2008).

63. Park, S. *et al.* Spot14/Mig12 heterocomplex sequesters polymerization and restrains catalytic function of human acetyl-CoA carboxylase 2. *J. Mol. Recognit.* **26,** 679–88 (2013).

64. Zhu, Q. *et al.* The Spot 14 protein is required for de novo lipid synthesis in the lactating mammary gland. *Endocrinology* **146,** 3343–50 (2005).

65. Smith, S. & Abraham, S. Fatty acid synthase from lactating rat mammary gland. *Methods Enzymol.* **35,** 65–74 (1975).

66. Cox, B. G. & Hammes, G. G. Steady-state kinetic study of fatty acid synthase from chicken liver. *Proc. Natl. Acad. Sci. U. S. A.* **80,** 4233–7 (1983).

67. Rudolph, M. C. *et al.* Mammalian fatty acid synthase activity from crude tissue lysates tracing ^{13}C-labeled substrates using gas chromatography-mass spectrometry. *Anal. Biochem.* **428,** 158–66 (2012).

68. Smith, S. & Abraham, S. Fatty acid synthetase from lactating rat mammary gland: III. Dissociation and reassociation. *J. Biol. Chem.* **246,** 6428–35 (1971).

69. Carey, E. M. & Dils, R. Fatty acid biosynthesis. V. Purification and characterisation of fatty acid synthetase from lactating-rabbit mammary gland. *Biochim. Biophys. Acta* **210,** 371–387 (1970).

70. Abu-Elheiga, L. *et al.* The subcellular localization of acetyl-CoA carboxylase 2. *Proc. Natl. Acad. Sci. U. S. A.* **97,** 1444–9 (2000).

71. Ishii, M., Igarashi, Y. & Kodama, T. Purification and characterization of ATP:Citrate Lyase from Hydrogenobacter thermophilus TK-6. *J. Bacteriol.* **171,** 1788–92 (1989).

72. Pierce, M. W. & Palmers, J. L. ATP-citrate lyase. Structure of a tryptic peptide containing the phosphorylation site directed by glucagon and the cAMP-dependent protein kinase. *J. Biol. Chem.* **256,** 8867–70 (1981).

73. Wagner, P. D. & Vu, N.-D. Phosphorylation of ATP-citrate lyase by nucleoside diphosphate kinase. *J. Biol. Chem.* **270,** 21758–64 (1995).

74. Shi, Y. & Burn, P. Lipid metabolic enzymes: emerging drug targets for the treatment of obesity. *Nat. Rev.* **3,** 695–710 (2004).

75. Witters, L. a, Friedman, S. a & Bacon, G. W. Microsomal acetyl-CoA carboxylase: evidence for association of enzyme polymer with liver microsomes. *Proc. Natl. Acad. Sci. U. S. A.* **78,** 3639–43 (1981).

76. Lin, D. I. *et al.* Phosphorylation-dependent ubiquitination of cyclin D1 by the SCF (FBX4-alphaB crystallin) complex. *Mol. Cell* **24,** 355–66 (2006).

77. Dunn, K. W., Kamocka, M. M. & McDonald, J. H. A practical guide to evaluating colocalization in biological microscopy. *Am. J. Physiol.* **300,** C723–42 (2011).

78. Wellen, K. E. *et al.* ATP-citrate lyase links cellular metabolism to histone acetylation. *Science (80-.).* **324,** 1076–80 (2009).

79. Roche, R. *et al.* Spot 14 protein interacts and co-operates with chicken ovalbumin upstream promoter-transcription factor 1 in the transcription of the L-type pyruvate kinase gene through a specificity protein 1 (Sp1) binding site. *J. Biochem.* **183,** 175–83 (2001).

80. Kinlaw, W. B., Church, J. L., Harmon, J. & Mariash, C. N. Direct evidence for a role of the “Spot 14” protein in the regulation of lipid synthesis. *J. Biol. Chem.* **270,** 16615–8 (1995).

81. Wilfling, F. *et al.* Triacylglycerol synthesis enzymes mediate lipid droplet growth by relocalizing from the ER to lipid droplets. *Dev. Cell* **24,** 384–99 (2013).

82. Ding, Y., Wu, Y., Zeng, R. & Liao, K. Proteomic profiling of lipid droplet-associated proteins in primary adipocytes of normal and obese mouse. *Acta Biochim. Biophys. Sin. (Shanghai).* **20,** 1–13 (2012).

83. Wendel, A. a, Cooper, D. E., Ilkayeva, O. R., Muoio, D. M. & Coleman, R. a. Glycerol-3-phosphate acyltransferase (GPAT)-1, but not GPAT4, incorporates newly synthesized fatty acids into triacylglycerol and diminishes fatty acid oxidation. *J. Biol. Chem.* **288,** 27299–306 (2013).

84. Stone, S. J. *et al.* The endoplasmic reticulum enzyme DGAT2 is found in mitochondria-associated membranes and has a mitochondrial targeting signal that promotes its association with mitochondria. *J. Biol. Chem.* **284,** 5352–61 (2009).

85. Raturi, A. & Simmen, T. Where the endoplasmic reticulum and the mitochondrion tie the knot: the mitochondria-associated membrane (MAM). *Biochim. Biophys. Acta* **1833,** 213–24 (2013).

86. Friedman, J. R., Webster, B. M., Mastronarde, D. N., Verhey, K. J. & Voeltz, G. K. ER sliding dynamics and ER-mitochondrial contacts occur on acetylated microtubules. *J. Cell Biol.* **190,** 363–75 (2010).

87. Terasaki, M., Chen, L. B. & Fujiwara, K. Microtubules and the endoplasmic reticulum are highly interdependent structures. *J. Cell Biol.* **103,** 1557–68 (1986).

88. Geelen, M. J., Bijleveld, C., Velasco, G., Wanders, R. J. & Guzmán, M. Studies on the intracellular localization of acetyl-CoA carboxylase. *Biochem. Biophys. Res. Commun.* **233,** 253–7 (1997).

89. Buechler, K. F. & Gibson, D. M. Guanosine triphosphate and colchicine affect the activity and the polymeric state of acetyl-CoA carboxylase. *Arch. Biochem. Biophys.* **233,** 698–707 (1984).

90. Yang, W. *et al.* Regulation of adipogenesis by cytoskeleton remodelling is facilitated by acetyltransferase MEC-17-dependent acetylation of α-tubulin. *Biochem. J.* **449,** 605–12 (2013).

91. Boström, P. *et al.* Cytosolic lipid droplets increase in size by microtubule-dependent complex formation. *Arterioscler. Thromb. Vasc. Biol.* **25,** 1945–51 (2005).

92. Loftus, T. M. Reduced food intake and body weight in mice treated with fatty acid synthase inhibitors. *Science (80-.).* **288,** 2379–81 (2000).

93. Hatzivassiliou, G. *et al.* ATP citrate lyase inhibition can suppress tumor cell growth. *Cancer Cell* **8,** 311–21 (2005).

94. Wu, M. *et al.* Antidiabetic and antisteatotic effects of the selective fatty acid synthase (FAS) inhibitor platensimycin in mouse models of diabetes. *Proc. Natl. Acad. Sci. U. S. A.* **108,** 5378–83 (2011).

95. Levert, K. L., Waldrop, G. L. & Stephens, J. M. A biotin analog inhibits acetyl-CoA carboxylase activity and adipogenesis. *J. Biol. Chem.* **277,** 16347–50 (2002).

96. Brugg, B. & Matus, A. Phosphorylation determines the binding of microtubule-associated protein 2 (MAP2) to microtubules in living cells. *J. Cell Biol.* **114,** 735–43 (1991).

97. Chow, J. D. Y. *et al.* Genetic inhibition of hepatic acetyl-CoA carboxylase activity increases liver fat and alters global protein acetylation. *Mol. Metab.* **3,** 419–431 (2014).

98. Piperno, G., Ledizet, M. & Chang, X. Microtubules containing acetylated alpha-tubulin in mammalian cells in culture. *J. Cell Biol.* **104,** 289–302 (1987).

99. Cheng, D. *et al.* Expression, purification, and characterization of human and rat acetyl coenzyme A carboxylase (ACC) isozymes. *Protein Expr. Purif.* **51,** 11–21 (2007).

100. Waugh, D. S. Making the most of affinity tags. *Trends Biotechnol.* **23,** 316–20 (2005).

101. Engelking, L. J. *et al.* Overexpression of Insig-1 in the livers of transgenic mice inhibits SREBP processing and reduces insulin-stimulated lipogenesis. *J. Clin. Invest.* **113,** 1168–75 (2004).

102. Wittig, I., Braun, H.-P. & Schägger, H. Blue native PAGE. *Nat. Protoc.* **1,** 418–428 (2006).

103. Thampy, K. G. & Wakil, J. Activation of Acetyl-CoA carboxylase. *J. Biol. Chem.* **260,** 6318–23 (1985).

104. Shimano, H. *et al.* Overproduction of cholesterol and fatty acids causes massive liver enlargement in transgenic mice expressing truncated SREBP-1a. *J. Clin. Invest.* **98,** 1575–84 (1996).

105. Simpson, R. J. Homogenization of mammalian tissue. *Cold Spring Harb. Protoc.* 1–4 (2010). doi:10.1101/pdb.prot5455

106. Thampy, K. G. & Wakil, J. Regulation of Acetyl-Coenzyme A carboxylase. *J. Biol. Chem.* **263,** 6447–53 (1988).

107. Srere, P. A. The citrate cleavage enzyme: I. Distribution and purification. *J. Biol. Chem.* **234,** 2544–47 (1959).